DEVELOPING A SEAWALL ALGORITHM FOR THE DNR MODEL WITH APPLICATION TO THE OCEANSIDE, CALIFORNIA, COASTLINE

By

GABRIEL A. PERDOMO

A THESIS PRESENTED TO THE GRADUATE SCHOOL
OF THE UNIVERSITY OF FLORIDA IN PARTIAL FULFILLMENT
OF THE REQUIREMENTS FOR THE DEGREE OF
MASTER OF SCIENCE

UNIVERSITY OF FLORIDA

2004

ACKNOWLEDGMENTS

I thank my wife for giving me her indispensable and unconditional support in every goal that I have strived to accomplish. I thank my daughter for giving me the inspiration to be a better person. I thank my parents for providing me with the morals, commitment, and attitude for excellence that has led me to achieve my childhood dreams. I thank my two sisters for making me a proud older brother. I also thank everyone who offered me assistance, guidance, and their friendship (both inside and outside the classroom) throughout my years at the University of Florida. Most of all, I would like to thank God, for He has given me all who I have mentioned above, and all the other gifts that I am so blessed to have in my life.

TABLE OF CONTENTS

LIST OF TABLES

LIST OF FIGURES

Abstract of Thesis Presented to the Graduate School
of the University of Florida in Partial Fulfillment of the
Requirements for the Degree of Master of Science

DEVELOPING A SEAWALL ALGORITHM FOR THE DNR MODEL WITH APPLICATION TO THE OCEANSIDE, CALIFORNIA, COASTLINE

By

Gabriel A. Perdomo

May 2004

Chair: William G. McDougal
Cochair: Robert G. Dean
Major Department: Civil and Coastal Engineering

The Oceanside Littoral Cell spans the southern coast of California from La Jolla Canyon to Dana Point. Our study examined the portion of the Oceanside Littoral Cell from Agua Hedionda Lagoon in Carlsbad, to a point 14.5 km (9.0 mi) north of the Oceanside Harbor along the Camp Pendleton shoreline. The coastline along this reach has historically experienced a variety of changes (including construction of the Oceanside Harbor, urbanization of coastal lands, changes in sediment supply, coastal stabilization structures, and sand removal and placement) that have significantly influenced the shoreline position. Our objective was to estimate the shoreline impacts attributable to Oceanside Harbor by applying the DNR model. To accomplish this, shoreline characteristics within the project area were defined. A seawall algorithm (that tracks volume change and then solves for the shoreline position) was added to the DNR model. Verification results for the seawall algorithm are given. Wave run-up, bore propagation, and force calculations were also added to the DNR model. Shoreline evolution and

damage results were examined for 50 different wave cases for two 60-year forecast simulations with and without breakwaters. Results for the with-breakwater case show that if current natural processes and human practices continue into the future, the shoreline will erode back to the seawall, causing progressively more overtopping and damage events along the Oceanside coastline. Results for the no-breakwater forecast case give significantly less damage, and show the shoreline stabilizing to a future equilibrium position that is shaped somewhat like the 1934 measured shoreline.

CHAPTER 1
INTRODUCTION

Overview

The Oceanside littoral cell spans the southern coast of California from La Jolla Canyon to Dana Point. This cell is 86.1 km (53.5 mi) long, and is defined by natural coastal features such as rivers, creeks, lagoons, and cliffs; as well as man-made features including beach nourishments, seawalls, groins, jetties, and breakwaters. This study examines only a portion of the Oceanside Littoral Cell. The project area includes the shorelines of Carlsbad, Oceanside, and Camp Pendleton. The southern boundary is the north Agua Hedionda Lagoon discharge jetty, in Carlsbad. This structure is approximately 8.5 km (5.3 mi) south of Oceanside Harbor. The northern boundary is approximately 14.5 km (9.0 mi) north of the Oceanside Harbor, along the Camp Pendleton shoreline.

Over the past 60 years, the coastline along this reach has experienced a variety of changes. The most significant change was the construction of the Del Mar Boat Basin in 1942, and the subsequent expansions to form what is now Oceanside Harbor. Other factors that contributed to shoreline change include a decrease in sediment supply, coastal stabilization structures, and sand removal and placement.

Oceanside Harbor and its protecting structures have had a significant influence on the shoreline. Construction of the Del Mar Boat Basin in 1942 was a major littoral barrier to the downdrift beaches. The updrift breakwater of the Del Mar Boat Basin began trapping sediment, and a fillet developed north of the harbor. The fillet increased

in size, and sediment attempted to bypass the harbor. Meanwhile, urbanization of coastal lands and construction of flood control structures decreased the sediment discharge from the Santa Margarita and San Luis Rey rivers into the Oceanside littoral system. The trapping of littoral material by the harbor and the reduction of river sediment supply have been attributed to severe erosion on the beaches downcoast of Oceanside Harbor. To reduce erosion damage, shoreline stabilization structures were constructed along the Oceanside and Carlsbad coastlines (USACE, 1991c).

Aerial photography of the Oceanside area is available before 1942. These historical photographs show the shoreline before significant human intervention. Figure 1-2 shows the Oceanside Pier in June 1938 and January 1953 (11 years after the initial construction of the Del Mar Boat Basin). The two photographs are shown at a similar scale. The pier is longer in 1953 than in 1938 because of the reconstruction and lengthening of the pier in 1947 after its partial destruction by a storm in 1942. Comparison of the two photographs indicates significant shoreline recession.

Project Scope

Our general objective was to estimate the shoreline impacts attributable to Oceanside Harbor. The historical influence of the breakwaters was examined with the DNR model to estimate harbor impact on the coastline relative to a no breakwater condition. Results yield the influence of sediment volume trapped by the north breakwater and long-term shoreline position changes. For lack of necessary data over the past 70 years, certain historical conditions and their components (including wave height and direction, river contributions, dredging, bypassing, beach nourishments, bluff erosion, and water levels) had to be synthesized. As a result, the model predicts the

relative long-term results for conditions with and without breakwaters, as opposed to a detailed outcome.

Damage attributable to the harbor can then be determined by comparing damage results with and without harbor processes. Shoreline modeling determined the historical influence of the breakwaters and estimated the damage events 50 years into the future with and without the harbor present. Completion of these objectives involved the following tasks:

- Determining wave and water-level conditions for the period of simulation
- Determining sediment sources, sinks, dredging, bypassing, and nourishments
- Developing information on initial shoreline configuration, description of structures, beach profiles, and sediment characteristics
- Specifying a damage-cost function related to calculated hydrodynamic responses
- Using a Monte Carlo simulation to determine the statistical estimates of responses.

Enhancements to the DNR Model

To accomplish these goals, the DNR model had to be modified to allow for the inclusion of seawalls and revetments in the study area. The seawall routine allowed the DNR model to more realistically model shoreline responses for armored beaches. Development of the seawall algorithm was a major component of our study. Therefore, development and verification of the seawall routine is described in detail. A subroutine was also added to the DNR model to quantify the damage resulting from overtopping events at seawalls. This routine calculated run-up, bore propagation behind the seawall, and the forces on a vertical-faced structure.

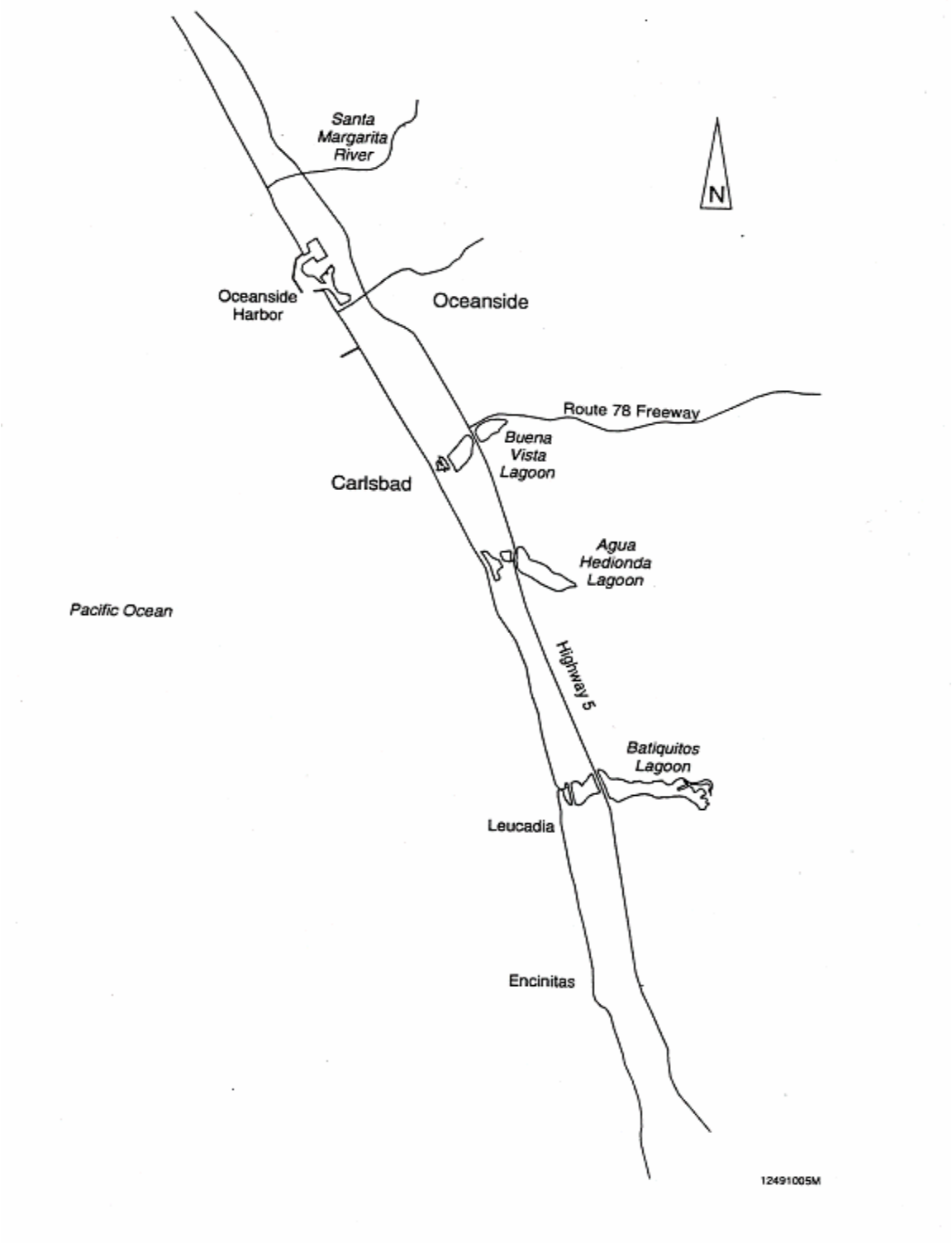

Figure 1-1. Overview of site. U.S. Army Corps of Engineers (USACE), Los Angeles District (1994), "Oceanside Shoreline, Oceanside, San Diego County California: Chapter 2.0 The Study Area", Reconnaissance Report, Main Report, pp. 2-2.

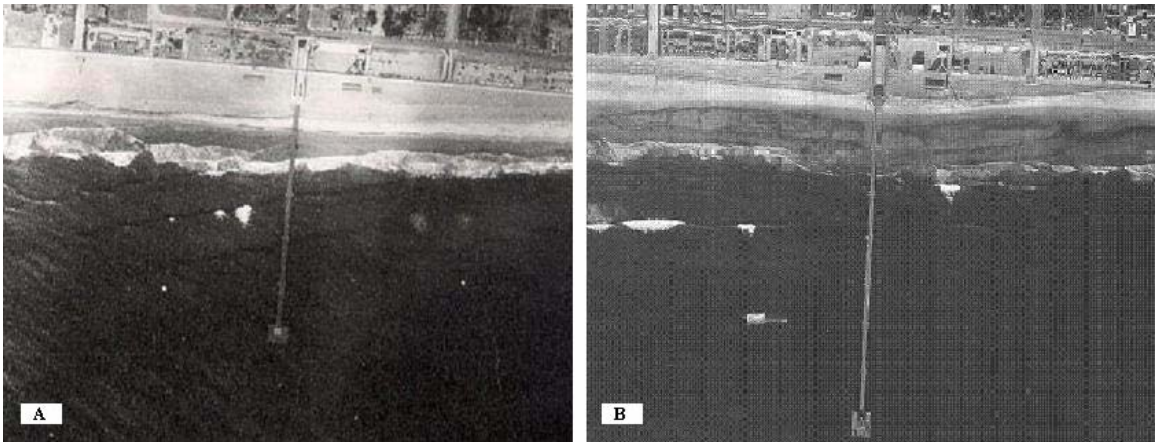

Figure 1-2. Oceanside Beach at the Oceanside Municipal Pier. A) June 1938. B) January 1953.

CHAPTER 2
SITE CHARACTERIZATION

This chapter discusses the physical characteristics of the study area (including shoreline position; beach profiles; wave climate; tides; El Nino; Oceanside Harbor breakwaters and groins; dredging, by-passing, and nourishment events; sources and sinks; background erosion; north breakwater fillet formation; historical volume changes; and seawalls). This chapter presents findings from previous studies performed along this coastline, and procedures used to define these characteristics for use in the DNR model.

Shorelines

The U.S. Army Corp of Engineers, Los Angeles District, provided three measured shorelines for the study area: 1) 1934 pre-harbor shoreline, 2) 1972 shoreline, and 3) 1998 shoreline (Ryan, 2002). These shorelines were referenced to a baseline located approximately 650 m (2,100 ft) inland of the shoreline at the Agua Hedionda discharge jetties in Carlsbad. The baseline has a bearing of 325º08'38".

The 1934 shoreline was digitized from three U.S. Coast and Geodetic Survey sheets. The surveys were performed between March 1934 and May 1934 in three sections from Carlsbad to San Mateo Point:

- Carlsbad to Santa Margarita River; March to April 1934. Hydrographic Survey #5648.
- Santa Margarita River to Las Flores; April to July 1934. Hydrographic Survey #5606.
- Horno Canyon to San Mateo Point; May 1934. Hydrographic Survey #5605

This shoreline is assumed to be Mean Tide Level (MTL). The USACE (Ryan, 2003) provided the 1972 shoreline, which was with respect to mean sea level (MSL). Plan views of survey plots were scanned and analyzed. The 1998 shoreline was taken from a LIDAR survey conducted in April 1998 and represents the shoreline referenced to MTL.

The southern boundary of the study area is located the north Agua Hedionda discharge jetty. The northern boundary is located 24.1 km (15.0 mi) upcoast of the Agua Hedionda discharge jetty, which is approximately 14.5 km (9.0 mi) north of the Oceanside Harbor Complex in Camp Pendleton. The 1934 and 1998 shorelines surveys extended past the northern boundary. However, the 1972 shoreline survey stopped approximately 4 km (2.5 mi) short of the upper boundary. Figure 2-1 shows the three shorelines. These will be discussed later in greater detail.

Beach Profiles

In the DNR model, the beach profile is defined by the Brunn/Dean equilibrium beach profile. The equilibrium profile is based on constant wave energy dissipation per unit volume of surf zone. This profile definition has been well documented and widely used in coastal engineering, and is given as

$$h = Ay^{2/3} \tag{2.1}$$

where h is the still water depth along the profile, A is the profile coefficient related to the sediment diameter, and y is the cross-shore distance along the profile (Dean and Dalrymple, 2002). Figure 2-2 shows a comparison between a SANDAG profile representative of the Oceanside coastline and the Brunn/Dean equilibrium profile. The figure shows that the equilibrium beach profile provides a good fit to the SANDAG profile.

Development of Wave Conditions

O'Reilly (2004) developed the wave conditions. The waves were estimated from statistical analyses of historical wave data. The primary source of these data was the Coastal Data Information Program (CDIP) buoy located offshore of Oceanside. The wave records only spanned five years of measurements, which is short for the development of 50-year wave records. The data were subdivided into three wave groups: 1) north swell, 2) south swell, and 3) local seas. Each of these was analyzed as an independent population and then further categorized by the season (fall, winter, spring, or summer) and whether the event was during an El Nino year. For each of these groups, typical storm hydrographs were developed. The magnitude of the hydrograph was changed to correspond to different magnitude events. The magnitudes of the events were selected in accordance with the extreme value statistics for the specific population. The wave simulations algorithm proceeded in the following order and repeated every hour for 50 years to generate a 50-year wave record:

- Determining if an El Nino year
- Determining season.
- Making a Monte Carlo selection of the event magnitudes for each population.
- Generating the wave hydrographs.
- Superimposing the hydrographs into a single wave time series.
- Transforming the waves to the -12-m (-40-ft) contour.

The initial plan for the shoreline model was to use predicted waves at a number of locations along the study area to drive the longshore sediment transport (LST). Nine stations, determined by taking the average of ten alongshore locations near the stations

along the -12-m (-40-ft) contour, were selected that spanned the study area. The locations of the nine wave stations and the 90 computation sites are shown in Figure 2-3.

Figure 2-4 shows the mean values of each of the 50-year wave records (438,000 individual wave conditions) for the nine wave stations. The study area is located from alongshore distance x = 0 to 24,100 m (0 to 79,000 ft) in Figure 2-4. The two heavy, vertical, black lines mark the location of the Oceanside Harbor breakwaters. The mean significant wave heights and mean peak periods are nearly constant along the study area. The average significant wave height is 0.66 m (2.2 ft) and the average peak period is 10.7 s. South of the Agua Hedionda discharge jetty, the wave heights and periods decrease because of the Carlsbad Canyon. However, these decreases are only 8% of the mean significant wave height and 7% of the average peak period. The maximum wave heights for each 50-year time series are shown in Figure 2-5. The average maximum is 6.2 m (20.3 ft) with little variation in the alongshore direction.

Figure 2-6 shows the mean local wave angle with respect to the local shoreline orientation. This figure shows that significant variations exist in the local wave angle. North of the harbor, the local wave angle varies from -2º to -11º. Local wave angles are defined such that negative angles drive the LST to the south. The LST is approximately linear with respect to the wave angle for small wave angles with a constant wave height. A wave angle change from -2º to -11º results in a variation in LST by more than a factor of five. The historical shorelines north of the harbor do not support this large variation in longshore transport. South of the harbor there is a 6º variation in the local wave angle. This variation south of the harbor is more probable and could be associated with the Carlsbad Canyon.

Using the wave time series with the wave heights, periods, and local wave angles characterized in Figures 2-4 and 2-6 does not lead to reasonable shoreline predictions. The waves have a significant amount of longshore variation that can result in local convergences and divergences in the LST. As a result, necessary modifications were made to the wave data to achieve realistic shoreline modeling results. These modifications are discussed in Chapter 5.

Tides

Tides along the southern California coastline are of the mixed semi-diurnal type, consisting of two high and two low tides each of different magnitude (USACE, 1994a). The tidal characteristics for La Jolla (Latitude: 32° 52.0' N, Longitude: 117° 15.5' W), referenced to mean lower low water, are shown in Table 2.1. These data are a result of 18 years of measurements at La Jolla by the National Oceanic and Atmospheric Administration (NOAA). At La Jolla, a difference of 0.02 ft exists between MTL and MSL. Therefore, MSL and MTL will be assumed equal for this project.

NOAA[1] provides the harmonic constituents to calculate the tide. These are the amplitude, epoch, and the speed for each component. Amplitude is one-half the range of a tidal constituent in meters, epoch is the phase lag of the observed tidal constituent relative to the theoretical equilibrium tide in degrees referenced to UTC (GMT), and speed is the rate change in the phase of a constituent, expressed in °/hr. The speed is equal to 360° divided by the constituent period expressed in hours. The tide is then computed as follows,

[1] NOAA/NOS/CO-OPS Water Level Data Retrieval Page (http://co-ops.nos.noaa.gov/cgi-bin/co-ops_qry_direct.cgi?stn=9410230+LA+JOLLA%2C+PACIFIC+OCEAN+%2C+CA&dcp=1&ssid=WL&pc=P2&datum=NULL&unit=0&bdate=20030201&edate=20030201&date=1&shift=0&level=-4&form=0&host=&addr=68.18.240.2&data_type=har&format=View+Data)

$$\text{Tide} = \sum_{i=1}^{I} A_i \{\cos[(s_i)(t) + E_i]\} \quad (2.2)$$

where A_i is the amplitude (m), s_i is the speed (°/hr), t is the time (hrs), and E_i is the epoch (°). These values are given for each tidal component.

El Nino Southern Oscillation

The El Nino Southern Oscillation (ENSO) episodes are inter-annual large-scale oscillations in circulation and temperature distribution occurring in the Pacific Ocean. El Nino occurrences last from one to three years and occurred approximately every 14 years on average for the past century. Analyses suggest that ENSO episodes create a +0.3 m (+1 ft) tidal departure. ENSO periods increase the probability of experiencing more severe winter storms, and as a result, increase the likelihood of coincident storm waves and higher storm surge (USACE, 1994a). In the model, the MSL is increased +0.3 m (+1 ft) during ENSO episodes.

Development of Oceanside Harbor Breakwaters and Groins

The Oceanside coastline features several jetties, groins, and breakwaters. Initial construction of the harbor included two converging breakwaters extending offshore to the -6-m (-20-ft) contour. The north breakwater was 640 m (2,100 ft) long and the south breakwater was 396 m (1,300 ft) long. In 1957, these two breakwaters were extended to reduce the rate of sediment accumulation within the harbor. The upcoast breakwater was extended approximately 274 m (900 ft) on the same alignment and another 427 m (1,400 ft) in the down coast direction bringing its total length to 1,325 m (4,350 ft). The downcoast breakwater had 76 m (250 ft) removed from its seaward end and was then rebuilt 115 m (380 ft) bringing the total length to 433 m (1,420 ft) (Clancy, 1972).

After 1960, shore-perpendicular structures downcoast of the Del Mar Boat Basin were built to control the flow of sediment near the harbor. In 1961, a 120 m (400 ft) long groin extending 90 m (300 ft) into the ocean at the upcoast side of the San Luis Rey River was built. From March to June of the same year, the "south jetty" of the recently constructed Oceanside Small-Craft Harbor complex was constructed to a length of 266 m (873 ft); and in 1962, the south jetty was lengthened on the shoreward end 39 m (127 ft). Also in 1962, the 216 m (710 ft) north groin was built. This structure was a submerged groin that formed the upcoast side of the entrance channel to the Small Craft Harbor. In July 1968, the south groin at the San Luis Rey River was extended approximately 158 m (518 ft) bringing its total length to 280 m (918 ft) (Clancy, 1972). In 1973, the south jetty was extended 114 m (375 ft) seaward bringing its total length to 419 m (1,375 ft). Figure 2-7 shows a chronological summary of the harbor development.

Structures were also constructed on Oceanside Beach. In 1952, two 76-m (250-ft) long groins were built on Oceanside Beach extending out to the mean sea level. One was located at the south property line of Wisconsin Avenue and the other was located 305 m (1,000 ft) downcoast of Wisconsin Avenue (Clancy, 1972). The rubble rip-rap base of the Oceanside Municipal Pier may also act as a groin during high-energy storm events.

Presently, the only structures having a significant effect on the longshore littoral transport in the Oceanside area are the north breakwater and south breakwater (the new south jetty) at Oceanside Harbor, the south groin just north of the San Luis Rey River, and potentially the base of the Oceanside Municipal Pier during significant storm events (USACE, 1994b). These structures are all rock rubble mound structures.

Dredging, By-passing, and Nourishment Events

The years immediately after the initial construction of the Del Mar Boat Basin were characterized by drastic changes in shoreline position north and south of the harbor. Sediment accumulated in a fillet north of the north breakwater. On the beaches south of the harbor, erosion became a problem. Furthermore, a shoal developed across the entrance channel to the harbor decreasing its depth and width. With time, it became apparent that to maintain the channel at its design dimensions and to prevent erosion damage to the beaches downcoast, sand would have to be artificially by-passed around the harbor (Clancy, 1972).

The construction of the Del Mar Boat Basin began in 1942 and marked the beginning of a number of dredgings that would occur at this site. The initial cutting of the harbor required the removal of 1,150,000 m^3 (1,500,000 yd^3) of sediment. The U.S. Navy conducted a second dredging in 1945, removing 167,000 m^3 (219,000 yd^3) of sediment from the entrance channel. The material from these two dredgings was taken to an inland disposal site. In 1957, the U.S. Navy once again dredged material from the harbor entrance. The 612,000 m^3 (800,000 yd^3) of removed sediment was placed on the downcoast beaches from approximately 9^{th} Street to 6^{th} Street to alleviate some severe erosion problems that were threatening the street and sewer line (Clancy, 1972). This marked the first by-passing of sediment from the harbor to Oceanside Beach. Table 2-2 summarizes the nourishment dates, locations, and volumes for beaches downcoast of the harbor. Figure 2-8 shows the location and times of all nourishments in the project area.

Starting in 1960, sediment was regularly by-passed to beaches south of the harbor. In 1963, the Army Corp of Engineers completed the construction of the Oceanside Small-

Craft Harbor. The total material dredged from the site was approximately 2,900,000 m^3 (3,800,000 yd^3), which was placed on the downcoast beaches.

Nourishment placement patterns along Oceanside beach have varied since they began in 1957. The source of sediment for the following nourishments was Oceanside harbor. Before 1971, the center of gravity of by-passed sediment was located about 2.1 km (7,000 ft) downcoast the south breakwater near the Oceanside Municipal Pier (USACE, 1991b). These are shown in red in Figure 2-8. From 1971 to 1990, the center of gravity of the beach nourishments was positioned approximately 3.4 km (11,000 ft) downcoast of the south breakwater seaward of Hayes Street (USACE, 1991b). These are shown in blue in Figure 2-8.

In 1992 and 1993, two nourishments were placed seaward of Tyson Avenue, which is approximately 2.4 km (8,000 ft) downcoast from the south jetty. From 1995 to 1998, the dredged material was placed "nearshore" in -4.6 to -7.6 m (-15 to -25 ft) of water depth seaward of Oceanside Boulevard, which is approximately 4.0 km (13,000 ft) south of the south jetty. Sediment dredged from the harbor and placed on the beaches from 1999 to 2003 was again placed seaward of Tyson Avenue on Oceanside Beach (Ryan, 2003). The Tyson Avenue nourishments are shown in green and the nearshore Oceanside Boulevard nourishments are shown in orange in Figure 2-8.

From 1995 to 2001, several nourishments took place on the beaches within the project area where the sediment source was not from Oceanside Harbor. In June 1995, sediment was taken from the Santa Margarita River Desiltation project and placed seaward of Oceanside Boulevard. In March 1997, sand was taken from an inland source as part of the Sand-for-Trash project and placed seaward of Oceanside Boulevard. In

September 1997, the US Navy Homeporting project took sand from North Island and nourished the beach seaward of Oceanside Boulevard (Coastal Frontiers Corporation, 2003). These three nourishments are shown in black in Figure 2-8.

In 2001 sediment was taken from an offshore borrow pit and placed along Carlsbad and Oceanside beaches for the SANDAG nourishment project. These were the only two SANDAG beach nourishments that occurred in our project area, and they are shown in gray in Figure 2-8. From 1988 to 1999, six nourishments were placed on Carlsbad State Beach as sediment was back-passed from the Agua Hedionda discharge channel (Coastal Frontiers Corporation, 2003). These nourishments were placed from Acacia Avenue to Oak Avenue and are shown in purple in Figure 2-8.

Sources/Sinks

Rivers, Creeks, and Lagoons

During the period before the construction of the Del Mar Boat Basin, rivers, streams, and lagoons served as significant sources of sand to the littoral system after major storm and flood events (USACE, 1991a). However, urbanization of the upper watersheds and the implementation of flood control systems reduced the amount of sediment carried into the littoral system from these potential sources. The two major rivers in the project area are the San Luis Rey River and the Santa Margarita River. During the time period between 1900 and 1938, the deltas of the Santa Margarita and the San Luis Rey Rivers built the beach seaward (USACE, 1991a). Recently, these rivers have not contributed significant amounts of sediment to the littoral system.

Other smaller potential sediment sources within the project area are Loma Alta Creek and Buena Vista Lagoon. As with the Santa Margarita and the San Luis Rey Rivers, these other contributors have seen a dramatic decrease in their discharge rates

since the construction of the harbor because of urbanization and a reduction in major storm events. Table 2-3 provides a summary of sediment contribution estimates from several studies performed on the Oceanside littoral cell.

The river sources used in the DNR simulations include the Santa Margarita River, San Luis Rey River, and Loma Alta Creek. The values listed in Table 2-3 from the various studies were averaged to determine the representative sediment contribution to the littoral system from the Santa Margarita River and the Loma Alta Creek. However, for the San Luis Rey River, the two studies that concluded a sediment contribution of 268,000 m^3/yr (351,000 yd^3/yr), which seems excessively disproportionate to the values used in previous studies of the Oceanside coastline, were discarded and the remaining values were averaged. Buena Vista Lagoon was not considered a sediment source, as it does not contribute sediment into the littoral system because of the weir that was constructed at its discharge point to artificially maintain the lagoon at 1.8 m (5.8 ft) above mean sea level (USACE, 1994a). The locations and final values used for the three sediment sources are listed in Table 2-4.

Background Erosion

Background erosion is a long-term coastal phenomena resulting in chronic shoreline retreat. The coastline at Oceanside has experienced background erosion over the past 70 years. This section discusses methods for quantifying background erosion and shoreline recession for use in the DNR model.

Even-odd analysis

The analyses are based on the three shorelines discussed above in the "Shoreline Position" section of this chapter. Figure 2-10 shows the measured shorelines for 1934 and 1998 north and south of the harbor at Oceanside where two things become evident.

First, the breakwaters at the harbor act as a littoral barrier to the longshore sediment transport. The net transport is to the south causing impoundment of sand north of the harbor and erosion to the south beaches. Second is that north of the harbor in Camp Pendleton, the shoreline has retreated in the past 60 years in spite of the fillet that has formed because of the north breakwater (Figure 2-11). The recession that has occurred north of the harbor shows that the coastline within the project area (north and south of the harbor) has experienced background erosion. An even-odd analysis is used to separate the effects of the harbor and the background erosion (Dean and Dalrymple, 2002).

The purpose of the even-odd analysis is to separate out those shoreline changes that are symmetric about a point on the coastline (and probably not attributable to the structure) and those that are attributable the presence of the coastal structure (Dean and Dalrymple, 2002). The analysis separates shoreline changes, Δy_s, into an even and an odd function, $\Delta y_e(x)$ and $\Delta y_o(x)$ respectively, where the x-axis is the alongshore axis. For a specific distance north of the north breakwater, $+x$, and the same distance to the south of the south breakwater, $-x$, the even values of shoreline position change are the same, $y_e(+x) = y_e(-x)$. For the odd component, $y_o(+x) = -y_o(-x)$. The even function approximately represents the ongoing changes in shoreline position in the absence of a coastal feature, and the odd function approximates the change in shoreline associated with the coastal feature. The total change in shoreline position at any location along the coast is the sum of the even and the odd functions:

$$\Delta y_s(x) = \Delta y_e(x) + \Delta y_o(x) \tag{2.3}$$

Results for the even-odd analysis using the changes in shoreline position from 1934 to 1998 are shown in Figure 2-12. The even function (shown in red) shows that erosion,

not attributable to the structures, occurred during this time period along the natural shoreline north of the harbor and along Oceanside beach. The shoreline changes attributable to the harbor are seen in the odd function (shown in blue) with accretion north of the harbor and erosion south of the harbor. In conclusion, the coastline within the study area has experienced background erosion.

Incorporating the intermediate 1972 shoreline into the even-odd analysis allows for a comparison of background erosion from 1934 to 1972 and then from 1972 to 1998. To make a direct comparison, the total background erosion for each time period was converted into annual recession rates. Figures 2-13 and 2-14 show results for the even-odd analysis and the recession rates for the two time periods. These two figures show that most of the background erosion that occurred from 1934 to 1998 actually occurred from 1934 to 1972.

Historic shoreline change

The Camp Pendleton shoreline north of the harbor, beyond the range of influence of the north breakwater, has experienced minor human intervention. This section of the coast provides an indication of the historical natural shoreline response for the project area. Figure 2-15 shows the historical shoreline positions in 1934, 1972, and 1998. The survey for the 1972 shoreline ended approximately 4 km (2.5 mi) downcoast of the northern project boundary. The total average change between 1934 and 1998 for the shoreline north of the Oceanside Harbor was -26.2 m (-86.0 ft). This means that a net recession occurred in spite of the fillet that formed in response to the north breakwater. Table 2-5 shows the historical shoreline change rates between surveys for the Camp Pendleton shoreline. Notice that most of the erosion occurred before 1972. Table 2-5 also seems to show a discrepancy in conservation of sand since the changes from 1937 to

1972 and 1972 to 1998 do not sum to the change from 1934 to 1998. The reason for this is the lack of survey data for the 1972 shoreline for the upcoast 4 km (2.5 mi) of the project area.

Toward the northern boundary of the project area (Figure 2-10), the 1934 and the 1998 shorelines are almost parallel. This suggests that the historical rate of shoreline retreat has been uniform along this section of the coast. Figure 2-16, which is the average rate of shoreline change, shows that the average annual rate of shoreline recession between 1934 and 1998 was about 0.6m/yr (2 ft/yr). As previously mentioned, most of this shoreline retreat occurred between 1934 and 1972, with a small amount of accretion from 1972 to 1998. If this accretion is neglected, then the average rate of recession for 1934 to 1972 is linearly approximated as

$$\frac{dy_{1934-1972}}{dt} \approx \frac{dy_{1934-1998}}{dt}\frac{(1998-1934)}{(1972-1934)} = \text{-1.0m/yr (-3.4ft/yr)} \qquad (2.4)$$

This result is in agreement with the even-odd analysis for the 1934 to 1972 time period (Figure 2-13).

Figure 2-16 shows that most of the erosion south of the harbor also occurred between 1934 and 1972. Table 2-6 shows the shoreline change rates for the coastline south of the harbor. By comparing Table 2-6 to Table 2-5, it is apparent that the recession rates were significantly higher to the south of the harbor. Figure 2-16 shows that the annual recession rate for the entire coast south of the harbor from 1934 to 1972 was 1.4 m/yr (4.6ft/yr). For the 5.5 km (3.4 mi) immediately south of the harbor, the shoreline recession rate was much greater at 2 m/yr (6.6 ft/yr). The recession rate decreased significantly from 1972 to 1998 because of the routine Oceanside Harbor by-passing/nourishment projects that took place during this time period. However, although

the recession rates decreased from 2 m/yr (6.6 ft/yr) to 0.5 m/yr (1.6 ft/yr), the shoreline continued to retreat despite the nourishment efforts. If present practices are continued, shoreline recession will continue into the future; and the seawalls and properties along the Oceanside coastline will progressively experience more overtopping events, and consequently, greater damage.

In the DNR model runs, a uniform background erosion of -1.1 m/yr (-3.5 ft/yr) was assumed over the entire open coastline from 1934 to 1972 and no background erosion after 1972. This rather simplistic assumption follows from the three shoreline surveys and results from the even-odd analysis.

Longshore Sediment Transport

The net longshore sediment transport for the Oceanside coast is approximately 153,000 m^3/yr (200,000 yd^3/yr) to the south. However, published values of LST from various studies--which include both analyses of historical wave statistics (north swell, south swell, and local seas) and analyses of sediment accumulation rates in the fillet north of the harbor and in the harbor itself--yielded varying results. Furthermore, several studies suggested long-term variations in LST over the past 90 years.

Hales (1978) determined a net LST rate for the Oceanside Littoral Cell of 76,000 m^3/yr (100,000 yd^3/yr) to the south based on wave statistics. Marine Advisors (1960) and Inman and Jenkins (1983) also employed wave statistics to determine the LST rates in this area. Marine Advisors found a net southerly transport of 165,000 m^3/yr (216,000 yd^3/yr), and Inman and Jenkins found a net southerly transport of 194,000 m^3/yr (254,000 yd^3/yr). A study by Tekmarine, Inc. (1987) gave a net southerly LST of 81,000 m^3/yr (106,000 yd^3/yr) at Oceanside Harbor. Moffat and Nichol (1990) performed the most comprehensive determination of LST in the Oceanside Littoral Cell. This study predicted

a net southerly LST rate of 76, 000 to 191,000 m^3/yr (100,000 to 250,000 yd^3/yr) from 1945-1977. From 1978-1987, data analysis gave the net southerly transport rate to be from 0 to 31,000 m^3/yr (0 to 40,000 yd^3/yr), which is a substantial decrease form the pervious time period.

North Breakwater Fillet

As previously mentioned, a fillet developed to the north of the north breakwater. This fillet began forming immediately after the initial construction of the north breakwater in 1942 and extends 8.9 km (5.5 mi) north of the harbor. The sediment rate of retention has been quantified as approximately 38,000 m^3/yr (50,000 yd^3/yr) (USACE, 1994a).

The volume of the sediment in the north fillet can be estimated from the 1934, 1972, and 1998 shorelines. The volume estimates are based on a closure depth of 7.6 m (25 ft) and a berm elevation of 4.3 m (14 ft). These volumes are converted to annual rates of accumulation, noting that the fillet began forming after the north breakwater was constructed in 1942 (Table 2-7). The net longshore transport significantly exceeds these accumulation rates. Since the placement of the north breakwater in 1942, only a portion of the transport has been impounded. The rest of the transport is carried into the harbor, by-passed around the harbor, or lost offshore.

The values in Table 2-7 are lower than the estimate of 38,000 m^3/yr (50,000 yd^3/yr) published by the U.S. Army Corps of Engineers. Also, it is surprising that the accumulation rates are higher in more recent times. Based on the above discussion, an average accumulation rate of 31,000 m^3/yr (40,000 yd^3/yr) is used for the north fillet.

Immediately to the south of the south breakwater, the shorelines in the 1934, 1972, and 1998 surveys do not show the development of a fillet or an eroded area. This is a

result of sheltering behind the breakwater, longshore transport reversals, and sediment retention between the breakwater and the San Luis Rey groin.

Historic Volume Changes

The measured shorelines from Figure 2-10 provide an opportunity to estimate the total changes in sediment volume north and south of the harbor. For these estimates, the closure depth is defined as 7.6 m (25 ft) and the berm elevation is defined at 4.3 m (14 ft). The resulting volume change rates are summarized in Table 2-6. For the full reach north of the harbor including the fillet, the average shoreline recession, as previously mentioned, from 1932 to 1998 was -0.4 m/yr (-1.3 ft/yr). North of the harbor, there was an annual loss of –3.5 m^3/m/yr (-1.4 yd^3/ft/yr) from 1934 to 1998. This volume change rate includes the fillet accretion updrift of the north breakwater. Moving farther north out of the fillet, the recession rate over this period was approximately -0.6 m/yr (-2 ft/yr), which is a removal of -8.3 m^3/m/yr (-3.3 yd^3/ft/yr).

South of the harbor there was a substantial loss of sediment each year (Table 2-8). Before 1972, the sediment eroded at a rate of -16.6 m^3/m/yr (-6.6 yd^3/ft/yr). Although by-passing and nourishments occurred regularly from 1972 to 1998, this stretch of coastline still resulted in a deficit of -7.3 m^3/m/yr (-2.9 yd^3/ft/yr) during that time period. Again it should be noted that these results predict that future loss of sediment will continue to occur south of the harbor if the current by-passing and nourishment practices are continued. This will lead to increasing overtopping events and more severe damage with time.

Seawalls

Method of Defining Seawall Positions

The Oceanside and Carlsbad coastlines are heavily armored with seawalls. Rubble, timber, and concrete structures protect many private properties and public lands along the shoreline. The cross-shore locations and alongshore lengths of the armoring was estimated using three references:

1. Maptech Mapserver (http://mapserver.maptech.com),
2. California Coastal Record Project aerial photographs by Kenneth Adelman (http://www.californiacoastline.org), and
3. AutoCAD files provided by the USACE (Ryan, 2002).

All of the seawalls from the Agua Hedionda discharge jetties to Oceanside Harbor can be seen in the California Coastal Record Project aerial photographs. Figure 2-17 shows an aerial photograph of the shoreline just up-coast of the north Agua Hedionda discharge jetty. A rubble rip-rap seawall protects the parking lot at the south end of the Carlsbad State Beach; and a vertical concrete seawall, which serves as an elevated walkway, spans the length of the Carlsbad State Beach.

The Maptech Mapserver website was used to find the alongshore locations and lengths of the seawalls. Running the cursor over the images on this web site gives the longitudinal coordinates along the coast. Figure 2-18 shows the same area as Figure 2-17 in an over-head view with Maptech Mapserver. The parking lot adjacent to the jetty and the rubble rip-rap seawall between the parking lot and the beach are visible. Using the intersection between the shoreline and the north Agua Hedionda discharge jetty as the initial reference point, the longitudinal coordinates from Maptech were converted into alongshore distances. The alongshore distances were then translated to corresponding

cell locations. Gaps in the seawalls and seawalls less than 50 m (165 ft) were omitted since the cell width resolution is 100 m (330 ft). As a result, the structures appear as continuous seawalls of varying type, cross-shore position, and height.

To determine the cross-shore position of the seawalls, CAD files provided by the USACE, Los Angeles District, were used. These files include a 2001 Eagle Aerial definition of the landward edge of sand. Upon comparison between the Eagle Aerial line and the aerial photographs, it was concluded that the landward edge of sand defines the seaward edge of the seawalls. Therefore, the cross-shore location of each seawall is defined as the distance from the Eagle Aerial 2001 landward edge of sand to the baseline.

To model overtopping events along Oceanside, the crest elevation for each seawall must be known. The crest elevation is the vertical distance from the mean tide level (MTL), which is the reference datum, to the top of the seawall. These elevations were obtained by using a combination of two sources: 1) the GIS study performed along the Oceanside coastline, and 2) a Lidar survey performed for the Oceanside littoral cell. Using these two references gave the elevations at the top of the seawalls with reasonable accuracy. The GIS and the Lidar surveys were taken from the NAVD88 reference datum, which is approximately 0.78 m (2.57 ft) below the MTL datum. Therefore, conversions were made accordingly.

Description of Seawalls Found Within the Project Area

The final results of the seawall analysis revealed that the entire coastline between the Agua Hedionda discharge jetties and the Oceanside Harbor is armored in one form or another (small gaps less than 50 m are neglected). The continuous seawall from the north discharge jetty at Agua Hedionda to the south breakwater at Oceanside Harbor is divided into many sub-seawalls. A sub-seawall is defined as a change in armoring type (vertical

structure or rubble rip-rap), and therefore a change in slope, within the continuous seawall.

The first stretch of the seawall is located in Carlsbad. It is erratic in cross-shore distance and type as it spans across Carlsbad Beach and a number of private properties. The seawall begins as a protective structure for the parking lot just north of the Agua Hedionda discharge jetties mentioned above (Figure 2-17). This first sub-seawall is a rubble rip-rap structure that extends north from the Agua Hedionda jetty. The second sub-seawall is a vertical concrete structure that serves as an elevated walkway and spans along the length of Carlsbad State Beach to Walnut Avenue (Figure 2-17). The third Carlsbad sub-seawall is a rubble rip-rap structure located at the up-coast end of the elevated walkway directly seaward of the Tamarack Beach Resort in Carlsbad.

Immediately north of the third Carlsbad sub-seawall is a rocky cliff with an elevation of approximately 14 m (45 ft) (Figure 2-19). Although no man-made structures exist seaward of this cliff from Pine Avenue to Oak Avenue, the cliff itself acts as a seawall. During significant storm events, the cliff itself may erode and contribute sediment to the littoral system. However, the sandy beach will not erode past the cliff in the same manner as it would if no cliff existed. Therefore, this stretch of coastline is modeled as if it were entirely armored by a seawall.

Moving up-coast from Oak Avenue to the Buena Vista Lagoon, the coast is heavily armored as protection for many private properties (Figure 2-20). Significant variation occurs in the cross-shore position and type of seawalls along this shoreline. Some of the variations in cross-shore position occur within a 100 m (330 ft) span, so the average cross-shore position was used for each cell. Furthermore, several properties located on

this stretch of the Carlsbad coastline do not have seawalls. The buildings on these lots are constructed higher up on the slope that connects Ocean Street to the beach. The buildings themselves or their foundations will prevent erosion to occur landward of them. For this reason, and the fact that many of these unarmored properties are less than 50 m (165 ft) in width and bounded by seawalls on both sides, this shoreline is considered armored at the location of the buildings.

The final Carlsbad sub-seawall is up-coast of the Army Navy Academy and adjacent to Buena Vista Lagoon. This armoring is located along "The Point" and consists of rubble rip-rap (Figure 2-21). Just north of this seawall is a small gap in armoring where Buena Vista Lagoon discharges in to the Pacific Ocean (Figure 2-21). This discharge point cannot be modeled in its actual configuration because its size is too small (approximately 50 m). More accurate results are obtained when the Buena Vista Lagoon discharge cell is modeled as a seawall rather than a gap with no armoring. This assumption is appropriate since Buena Vista Lagoon is maintained at 1.8 m (5.8 ft) above mean sea level (MSL) by the presence of a weir that spans the lagoon mouth (USACE, 1994a).

Continuing upcoast past Buena Vista Lagoon is the Oceanside coastline, where the remaining section of the seawall spans from the lagoon to the Oceanside Harbor. The entire coast of the city of Oceanside is armored and consists of seven sub-seawalls. The first sub-seawall is a long, rubble rip-rap structure that spans the southern coastline of Oceanside (Figure 2-22). This structure extends from Buena Vista Lagoon across St. Malo to Buccaneer Beach (which is adjacent to Loma Alta Creek). A gap exists in the seawall where Cassidy Street intersects the coastline. However, this gap is too small

(approximately 30 m) to be included in the model. The rubble seawall contains a discontinuity point at the Loma Alta Creek discharge point (Figure 2-23). However, the foundation of the South Pacific Street Bridge, which crosses over Loma Alta Creek, provides a landward erosion barrier similar to the cliffs previously mentioned in Carlsbad.

North of Loma Alta Creek, the rubble rip-rap structure continues up-coast to just south of Tyson Street Beach Park. This sub-seawall is divided it into two sections. The first section is a uniform structure that spans from Loma Alta Creek to Wisconsin Avenue across many private properties (Figure 2-24). The second section--comprising the northern portion of this seawall--is very unorganized rubble rip-rap, and was labeled by the USACE (1994b) as emergency revetment placed along The Strand. Figure 2-25 shows a section of this emergency revetment.

The fourth Oceanside sub-seawall is not an actual seawall. The curb that separates Oceanside Beach from The Strand is a landward erosion barrier that is susceptible to overtopping and damage (Figure 2-26). The curb extends up the coast to North Coast Village.

Just south of the San Luis Rey River is the armoring that protects North Coast Village. This sub-seawall is a 150-m (492-ft) vertical timber structure with rubble toe protection that projects farther seaward that the adjacent seawalls to the north and the south (Figure 2-27). This anomaly in the shoreline increases the possibility of overtopping and damage at North Coast Village relative to the adjacent shorelines.

The San Luis Rey River discharge is a discontinuity in the shoreline similar to the Loma Alta Creek discharge point. However, North Pacific Street Bridge, which crosses

over San Luis Rey River, provides a landward erosion barrier (Figure 2-28). Therefore, the foundation to this bridge is the sixth sub-seawall. The curb of North Pacific Street north of the bridge marks the seventh Oceanside sub-seawall. This section is very similar to the curb and street erosion barrier that spans the northern portion of Oceanside beach just south of the North Coast Village. The curb extends from the San Luis Rey River groin to the South Breakwater at Oceanside Small Craft Harbor (Figure 2-29).

Table 2-1. Tide level record at the NOAA/NOS/CO-OPS La Jolla Tide Gage[2].

Tide Levels Given in Feet	La Jolla
Mean Higher High Water (MHHW)	5.33
Mean High Water (MHW)	4.60
Mean Tide Level (MTL)	2.75
Mean Low Water (MWL)	0.90
Mean Lower Low Water (MLLW)	0.00

[2] NOAA/NOS/CO-OPS La Jolla Tide Gage

Table 2-2. Nourishment dates, locations, and volumes (yd^3) within the project area.

Date	Nourishment Location		Volume (yd^3)	Volume (m^3)
	Downcoast End	Upcoast End		
Jun 1942	Inland Fill		1,500,000	1,149,000
May 1945	Inland Fill		219,000	167,000
Nov 1957	9th Street	6th Street	800,000	612,000
Aug 1960	9th Street	6th Street	410,000	313,650
Aug 1961	9th Street	6th Street	481,000	367,965
Jan 1963	North Coast Village	Loma Alta Creek	3,800,000	2,907,000
Aug 1965	9th Street	3rd Street	111,000	84,915
Mar 1966	3rd Street	Ash Street	684,000	523,260
Jul 1967	3rd Street	Tyson Street	178,000	136,170
Apr 1968	San Luis Rey River	Wisconsin Avenue	434,000	332,010
Aug 1969	San Luis Rey River	3rd Street	353,000	270,045
May 1971	3rd Street	Wisconsin Avenue	552,000	422,280
Jun 1973	Tyson Street	Wisconsin Avenue	434,000	332,010
Nov 1974	Ash Street	Whitterby Street	560,000	428,400
Jun 1976	Ash Street	Whitterby Street	550,000	420,750
Nov 1977	Ash Street	Whitterby Street	318,000	243,270
Apr 1981	Hayes Street		863,000	660,195
Feb 1982	Hayes Street		922,000	705,330
Jan 1984	Hayes Street		475,000	363,375
Jan 1986	Hayes Street		450,000	344,250
Jan 1988	Hayes Street		220,000	168,300
Feb 1988	Acacia Avenue	Oak Avenue	118,000	90,335
Jan 1990	Hayes Street		249,000	190,485
Feb 1991	Acacia Avenue	Oak Avenue	25,000	18,933
Feb 1992	Tyson Street		188,000	143,820
Dec 1993	Tyson Street		483,000	369,495
Feb 1994	Acacia Avenue	Oak Avenue	75,000	57,241
Jan 1995	Nearshore Placement (Oceanside Blvd.)		161,000	123,165
Jun 1995	Oceanside Blvd.		40,000	30,600
Feb 1996	Acacia Avenue	Oak Avenue	106,000	108,630
Feb 1996	Nearshore Placement (Oceanside Blvd.)		162,000	123,930
Jan 1997	Nearshore Placement (Oceanside Blvd.)		130,000	99,450
Mar 1997	Oceanside Blvd.		1,000	765
Sep 1997	Oceanside Blvd.		102,000	78,030
Mar 1998	Nearshore Placement (Oceanside Blvd.)		315,000	240,975
Mar 1999	Tyson Street		187,000	143,055
Apr 1999	Acacia Avenue	Oak Avenue	203,000	154,935
Feb 2000	Tyson Street		327,000	250,155
Feb 2001	Tyson Street		80,000	108,630
Feb 2001	Acacia Avenue	Oak Avenue	142,000	61,200

Table 2-2. Continued

Date	Nourishment Location		Volume (yd^3)	Volume (m^3)
	Downcoast End	Upcoast End		
Jul 2001	Vista Way	Wisconsin Avenue	421,000	322,065
Sep 2001	Carlsbad Village Dr	Buena Vista Lagoon	225,000	172,125
Jan 2002	Tyson Street		400,000	306,000
Feb 2003	Tyson Street		438,000	335,070

Table 2-3. Sediment discharge rates by rivers and streams (yd^3/yr).

Discharge Rates yd^3/yr	CCSTWS 88-3 Simons/Li (1988)	Simons/Li (1985)	Inman Jenkins (1983)	Brownlie Taylor (1981)	CCSTWS 84-4 USACE LAD (1984)	CCSTWS 90-1 Moffat/Nichol (1990)	Moffat Nichol (1977)	DNOD (1977)	Brownlie and Taylor (1981)	Simons, Li and Assoc. (1988)
Santa Margarita River	11,430	15,000	24,000	11,000	2,000	20,000	900	15,000	11,300	19,000
San Luis Rey River	6,540	23,000	37,000	18,000	351,000	11,000	20,000	351,000	12,500	11,000
Loma Alta Creek	565	--	--	--	--	1,000	--	--	--	--
Buena Vista Lagoon	0	--	--	--	--	0	--	--	--	--

Table 2-4. Location and sediment contributions used in the DNR simulations for the Santa Margarita River, the San Luis Rey River, and the Loma Alta Creek.

Sediment Source	Sediment Volume (yd^3/yr)	Sediment Volume (m^3/yr)	Alongshore Location
Santa Margarita River	13,000	9,900	2000 m upcoast of the north breakwater
San Luis Rey River	17,000	13,000	2000 m downcoast of the north breakwater
Loma Alta Creek	800	610	5500 m downcoast of the north breakwater

Table 2-5. Shoreline change rates north of Oceanside Harbor.

Time Interval	Shoreline Change (m)	Shoreline Change Rate (m/yr)	Comments
1934 to 1972	-30.0	-0.79	1972 Survey Incomplete
1972 to 1998	+9.4	+0.37	1972 Survey Incomplete
1934 to 1998	-26.2	-0.40	

Table 2-6. Shoreline change rates south of Oceanside Harbor.

Time Interval	Shoreline Change (m)	Shoreline Change Rate (m/yr)
1934 to 1972	-16.4	-0.44
1972 to 1998	-5.5	-0.21
1934 to 1998	-22.0	-0.34

Table 2-7. North fillet volume accumulation rates.

Time Interval	Accumulation (yd^3/yr)	Accumulation (m^3/yr)
1942 to 1972	11,500	8,800
1972 to 1998	26,100	20,000
1942 to 1998	18,300	14,000

Table 2-8. Volume change rates.

Time Interval	South of Harbor		North of Harbor		Comments
	(m^3/yr)	($m^3/m/yr$)	(m^3/yr)	($m^3/m/yr$)	
1934 to 1972	-128,400	-16.6	--	--	1972 Survey Incomplete
1972 to 1998	-61,200	-7.3	--	--	1972 Survey Incomplete
1934 to 1998	-109,300	-12.8	-50,500	-3.5	

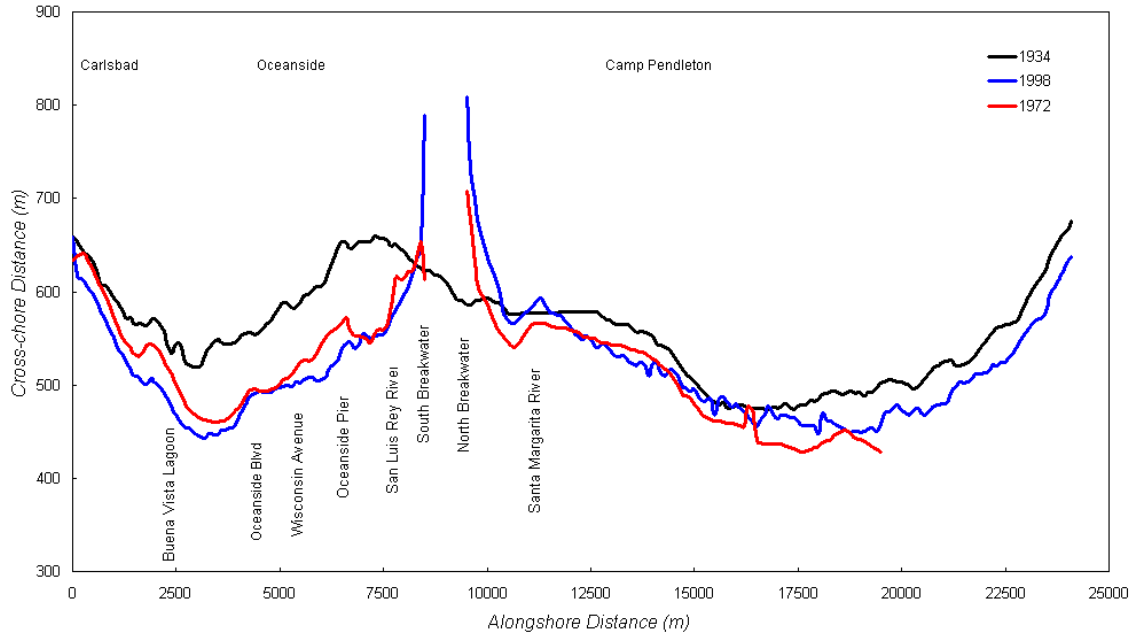

Figure 2-1. Three historical reference shorelines for the Carlsbad, Oceanside, and Camp Pendleton coast.

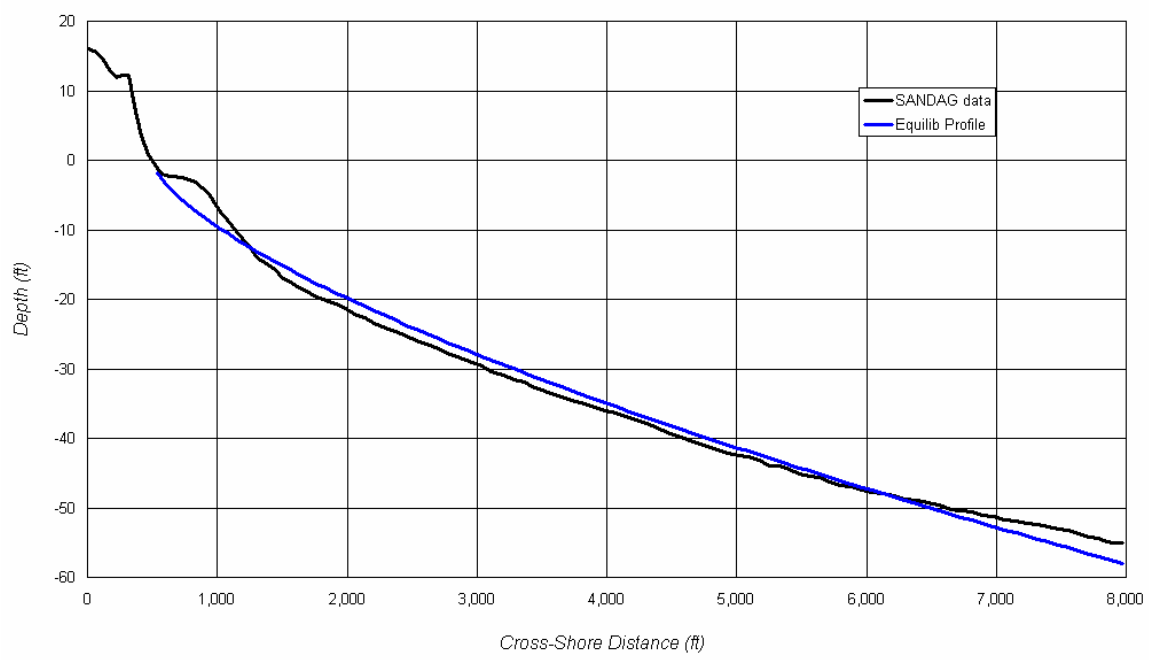

Figure 2-2. Comparison of the equilibrium beach profile used in the DNR model to an actual SANDAG profile of the Oceanside coastline.

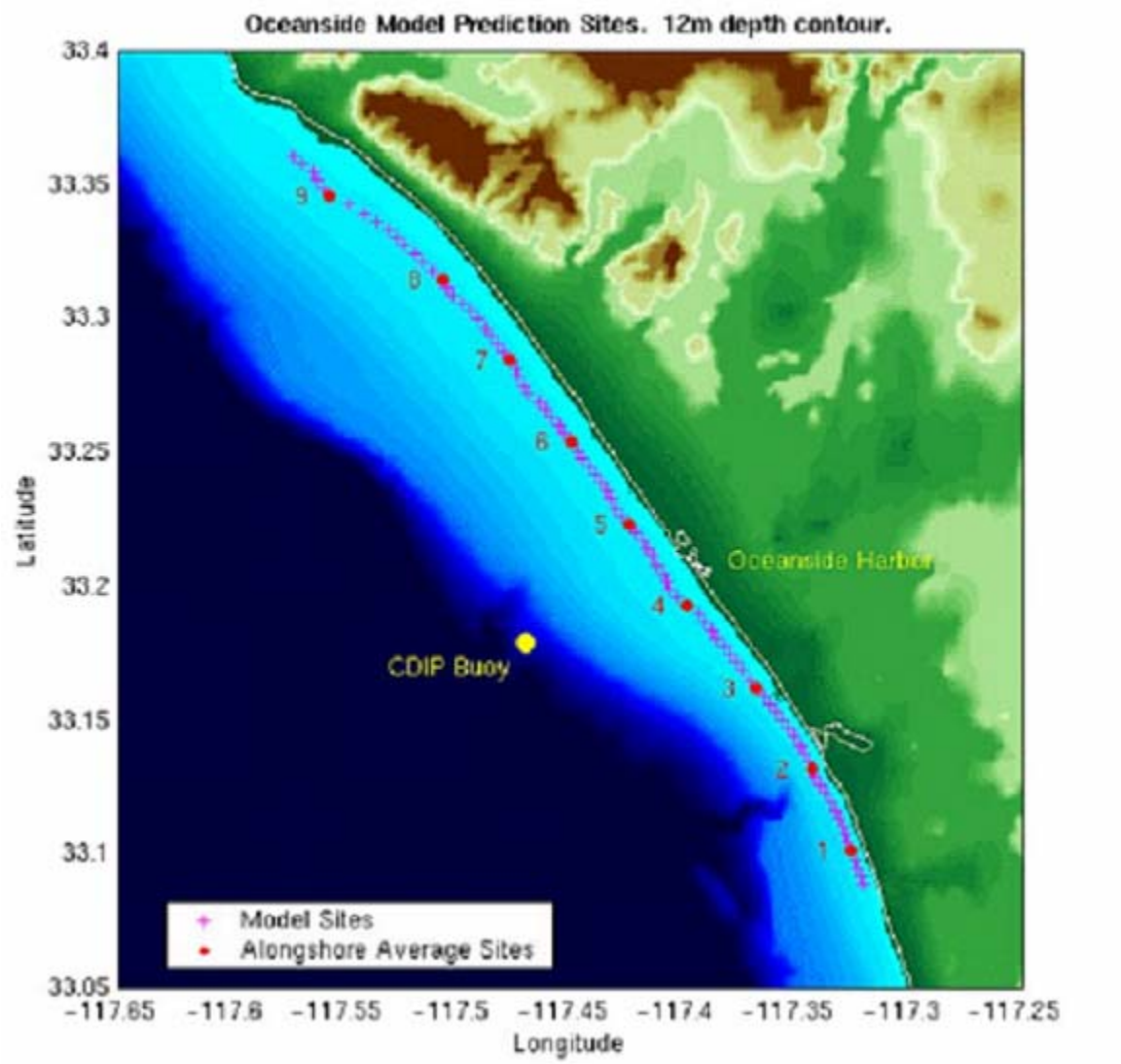

Figure 2-3. The nine wave gages and the 90 computational sites used to create the 50 wave records.

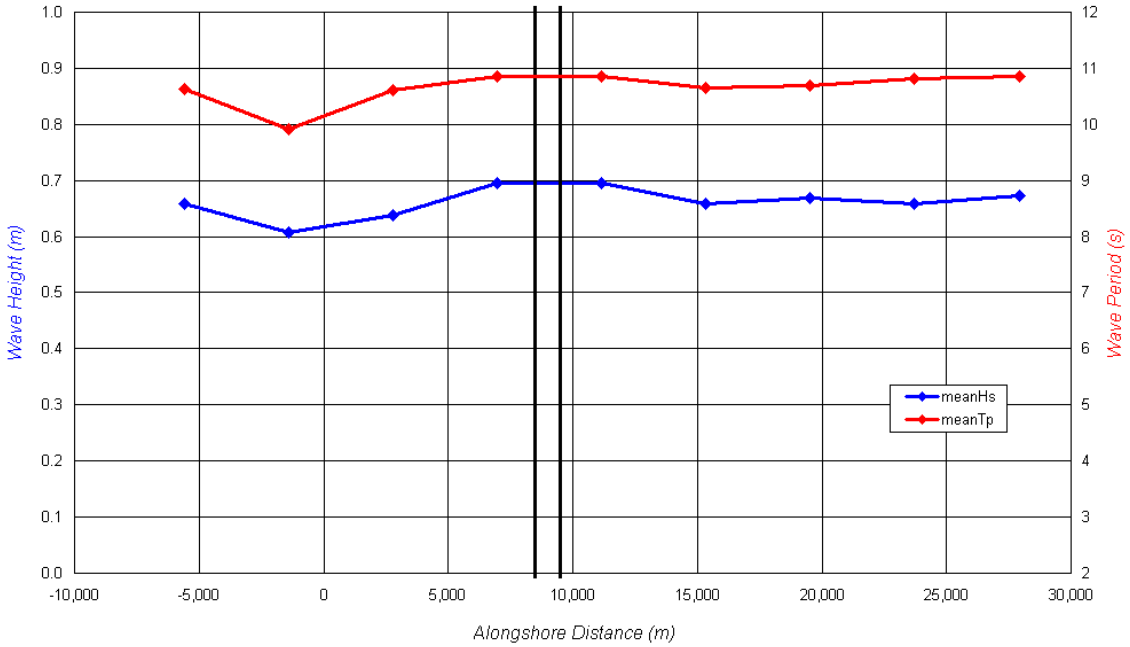

Figure 2-4. Mean wave height and mean period for each of the nine BOR wave gages. The two black lines on the plot show the locations of the north and south breakwaters.

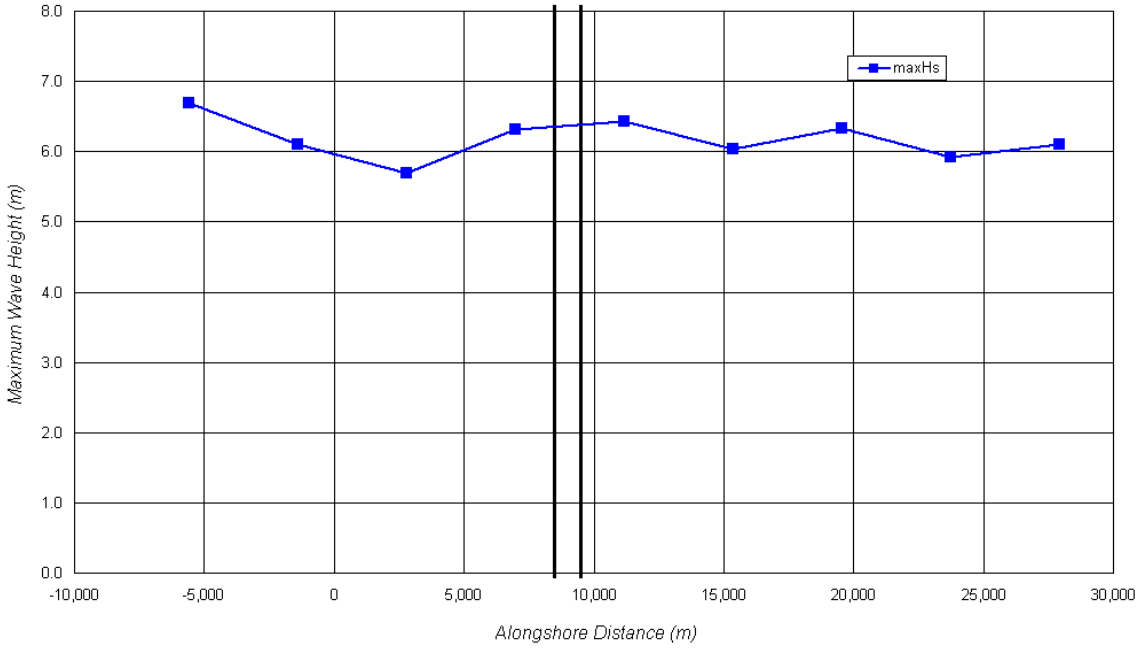

Figure 2-5. Maximum wave height by station for the 50 wave records. The two black lines on the plot show the locations of the north and south breakwaters.

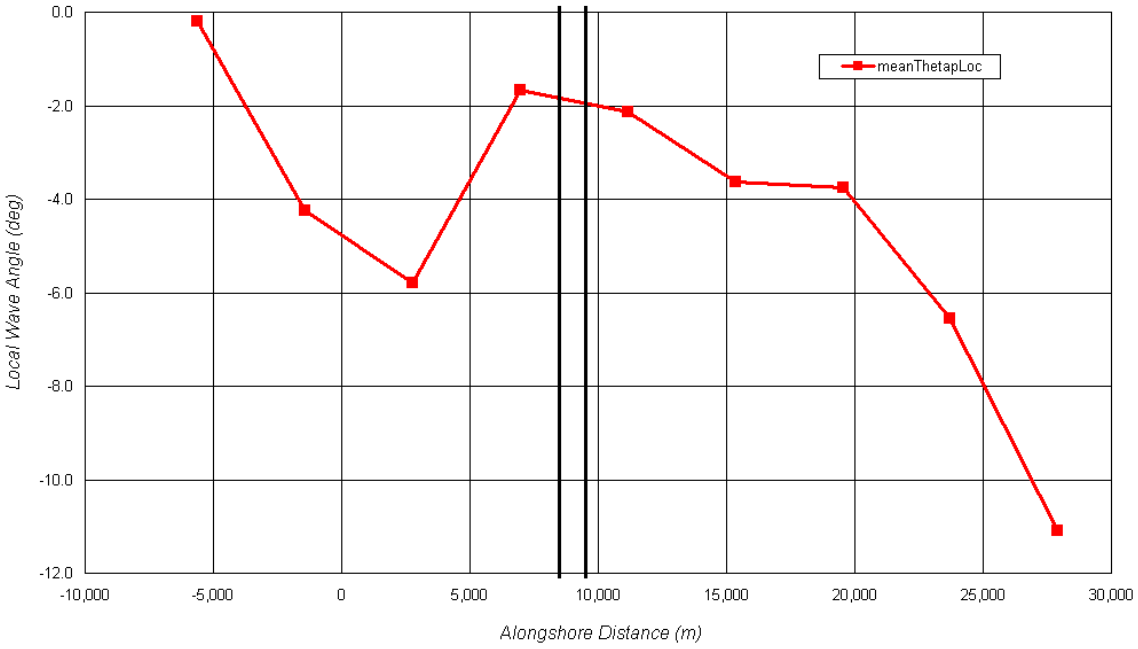

Figure 2-6. Mean local wave angle with respect to the local shoreline orientation for the 50 wave records at the nine wave gages. The two black lines on the plot show the locations of the north and south breakwaters.

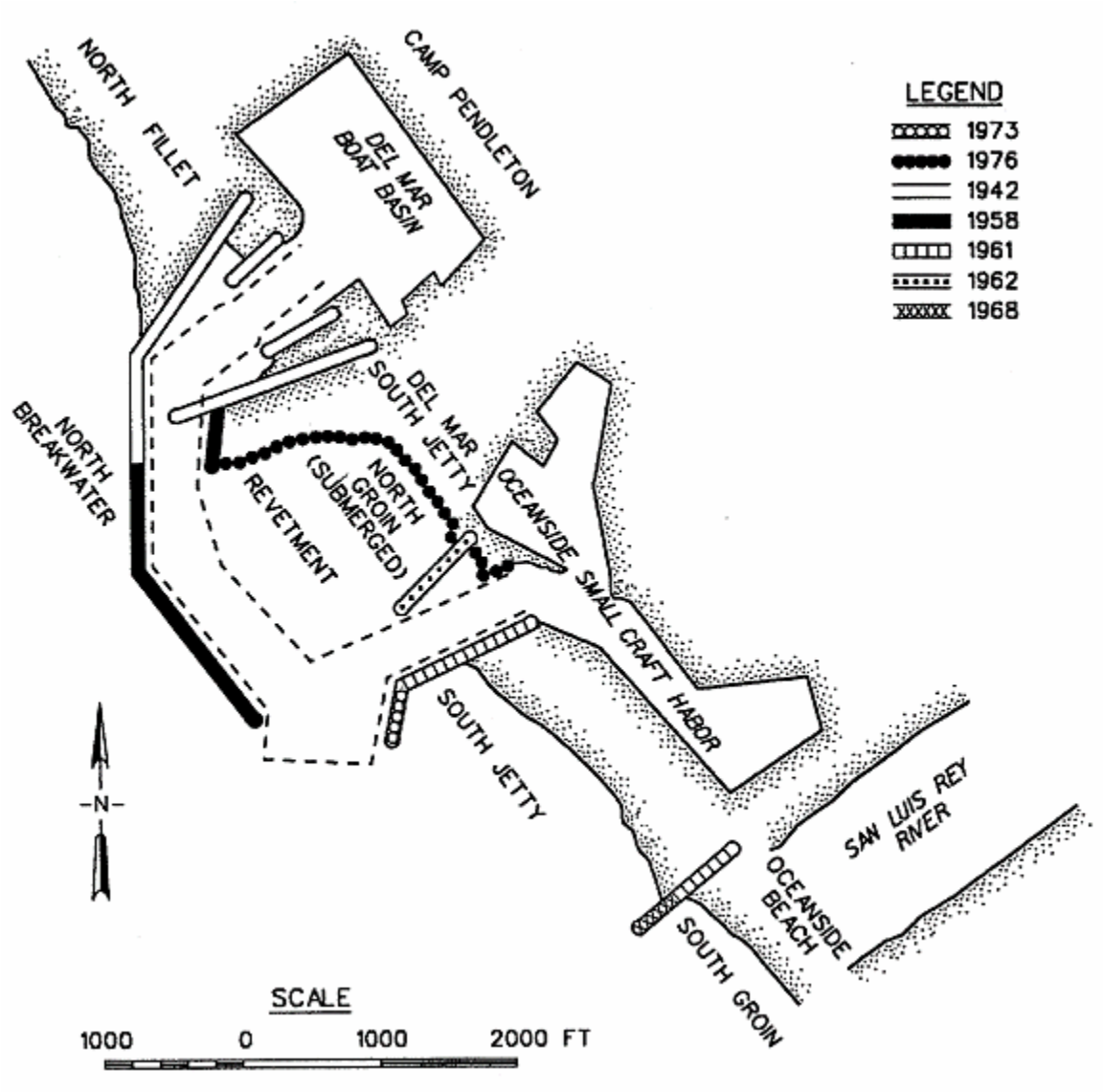

Figure 2-7. Chronological development of Del Mar Boast Basin and Oceanside Small-Craft Harbor. U.S. Army Corps of Engineers (USACE), Los Angeles District (1991b), "State of the Coast Report, San Diego Region: Chapter 7, Application of Beach Change Models", Coast of California Storm and Tidal Wave Study (CCSTWS) Volume 1 – Main Report.

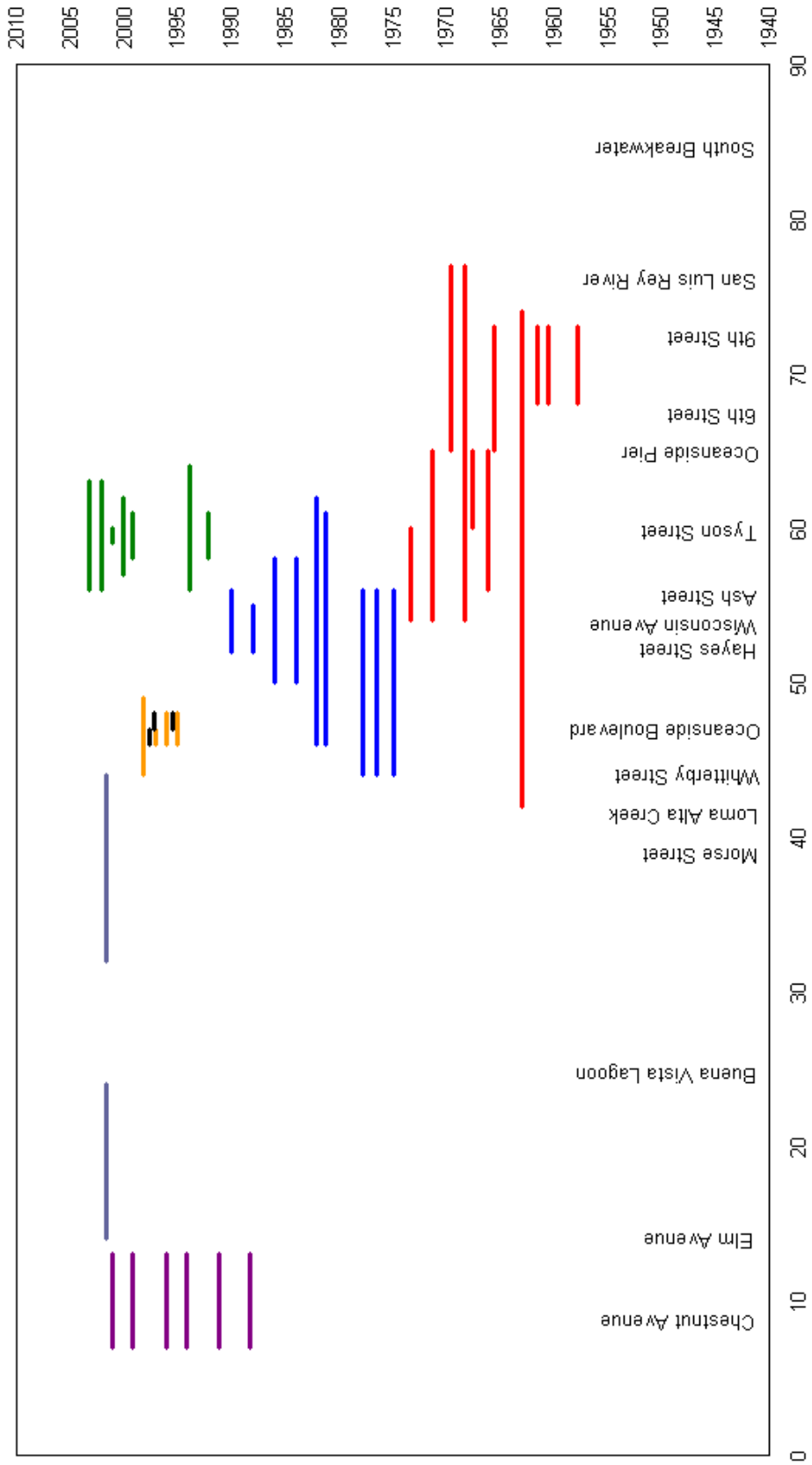

Figure 2-8. Nourishment placements and times for beaches downcoast of Oceanside Harbor.

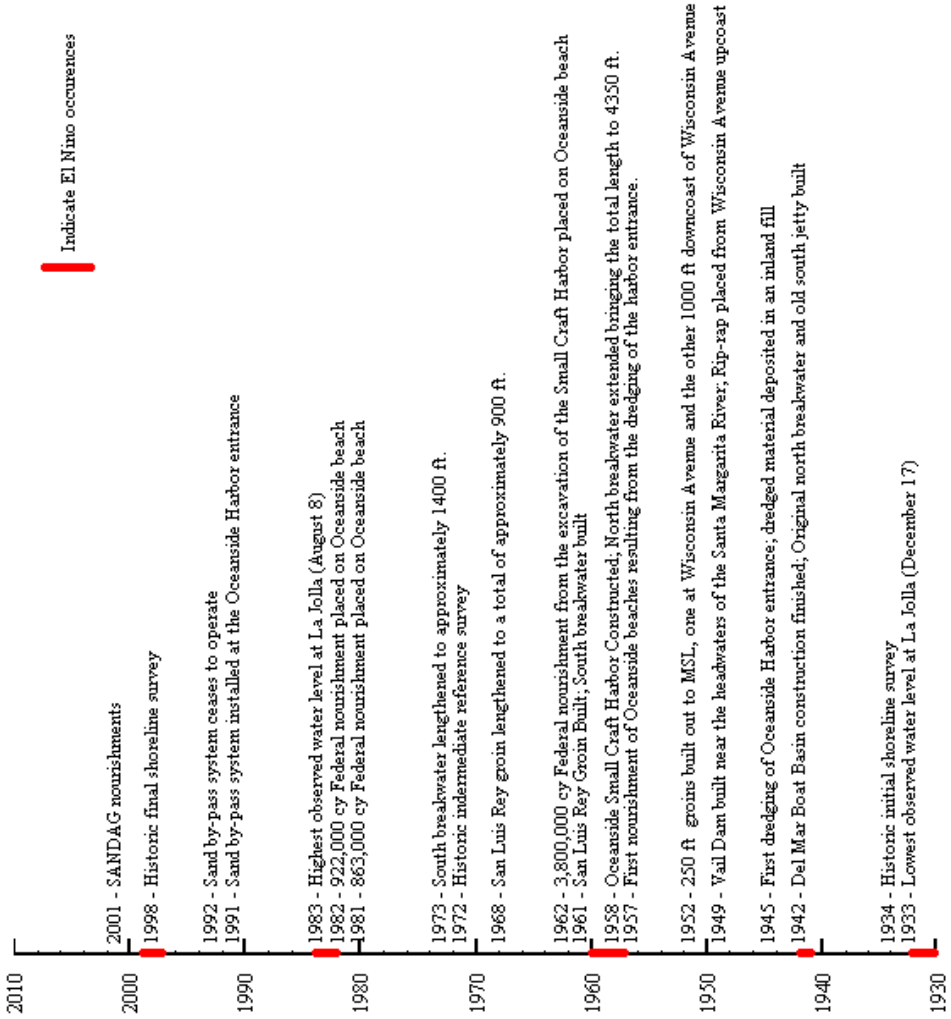

Figure 2-9. Timeline of significant historical events that occurred along the project area coastline.

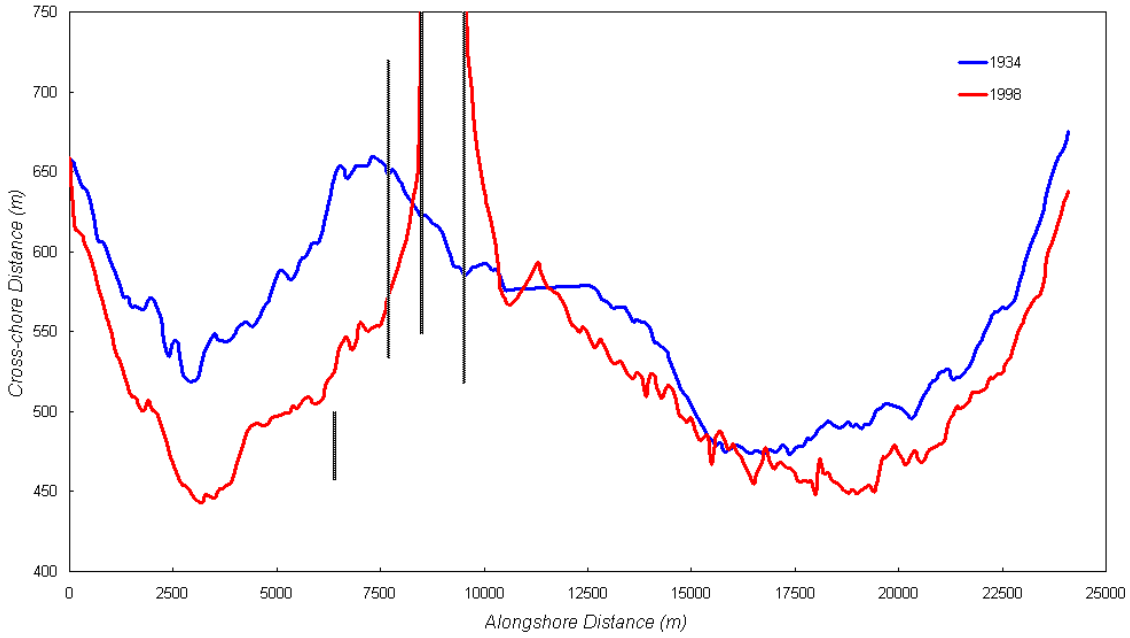

Figure 2-10. Comparison of the actual initial 1934 and final 1998 shorelines.

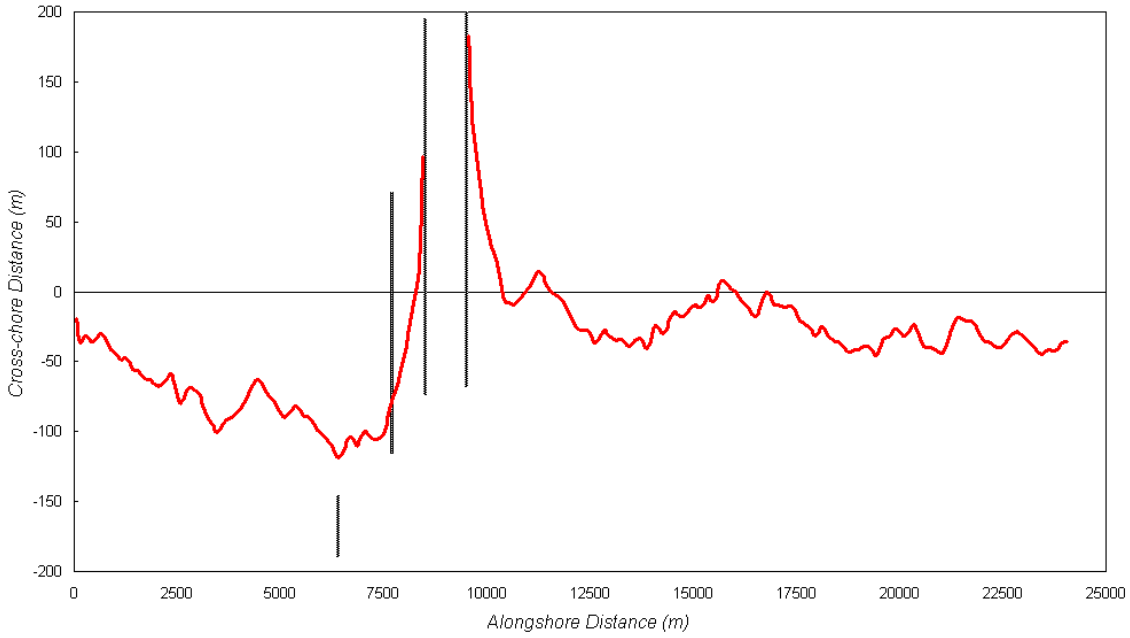

Figure 2-11. Total change in shoreline position from May 1934 to April 1998.

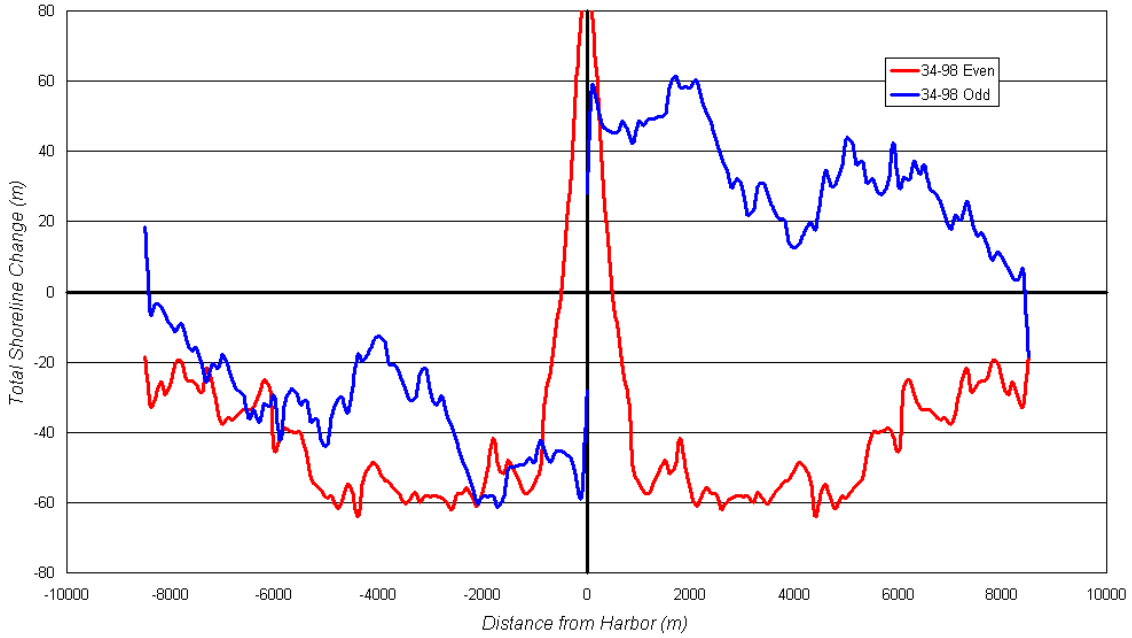

Figure 2-12. Results of the even-odd analysis from 1934 to 1998 for the Oceanside coastline.

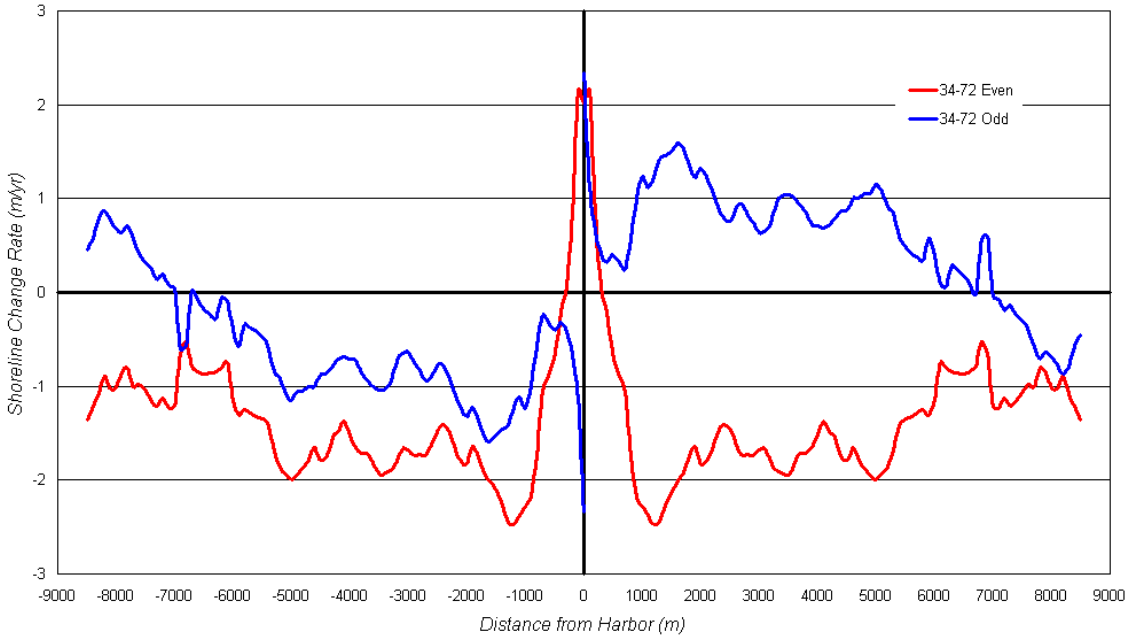

Figure 2-13. Even-odd analysis results and background erosion rates north and south of Oceanside Harbor complex from 1934 to 1972. The background erosion rate is the even function shown in red.

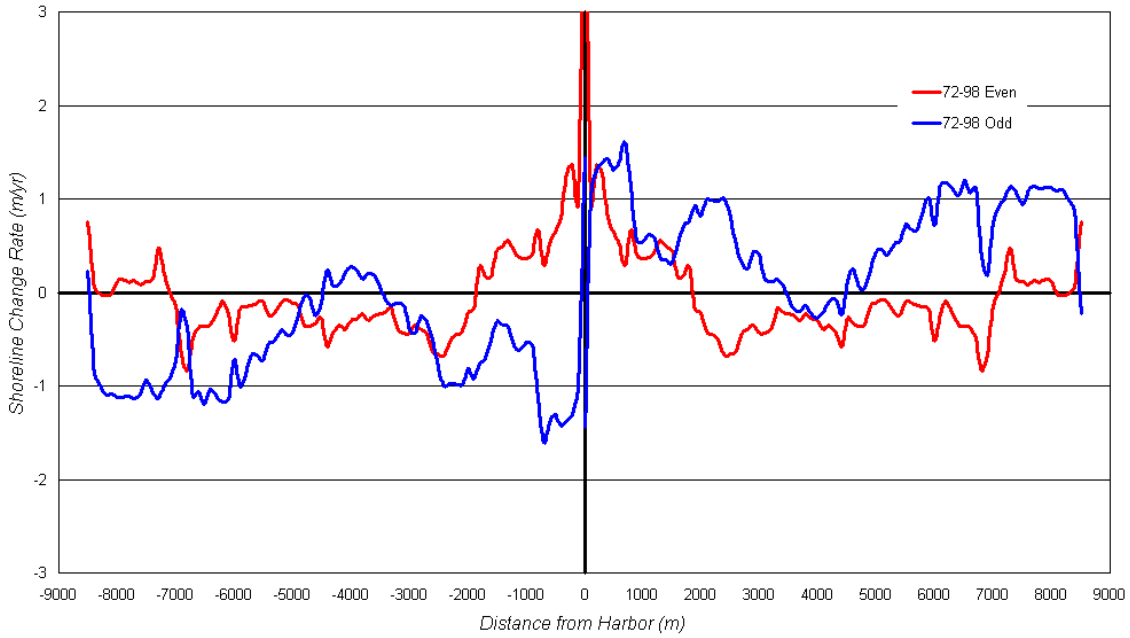

Figure 2-14. Even-odd analysis results and background erosion rates north and south of Oceanside Harbor complex from 1972 to 1998. The background erosion rate is the even function shown in red.

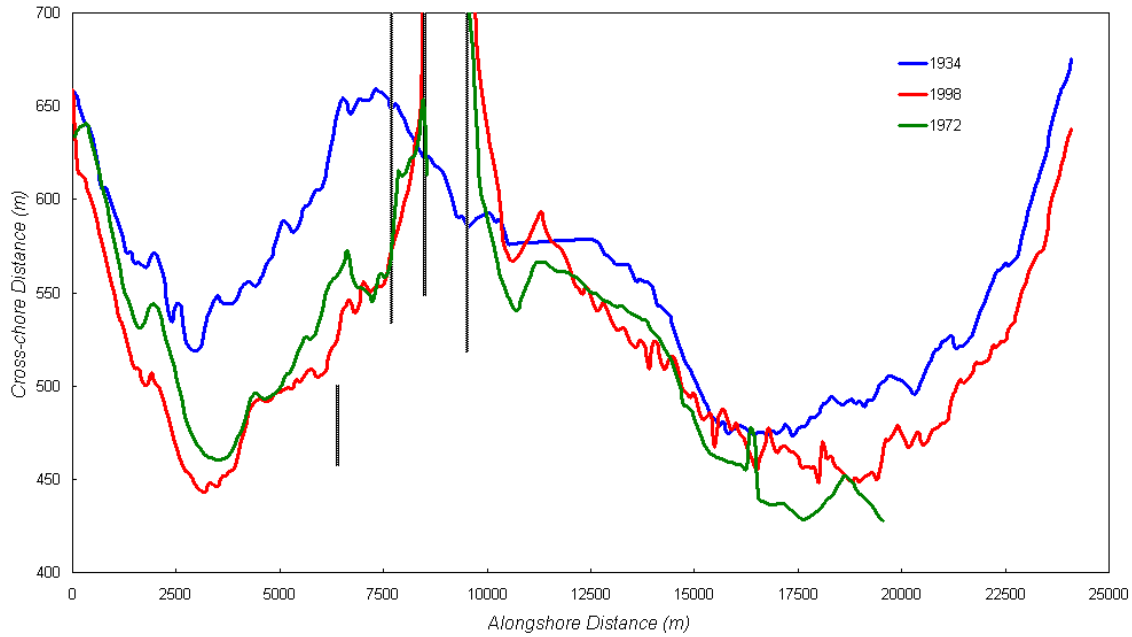

Figure 2-15. MSL shoreline position in 1934, 1972, and 1998.

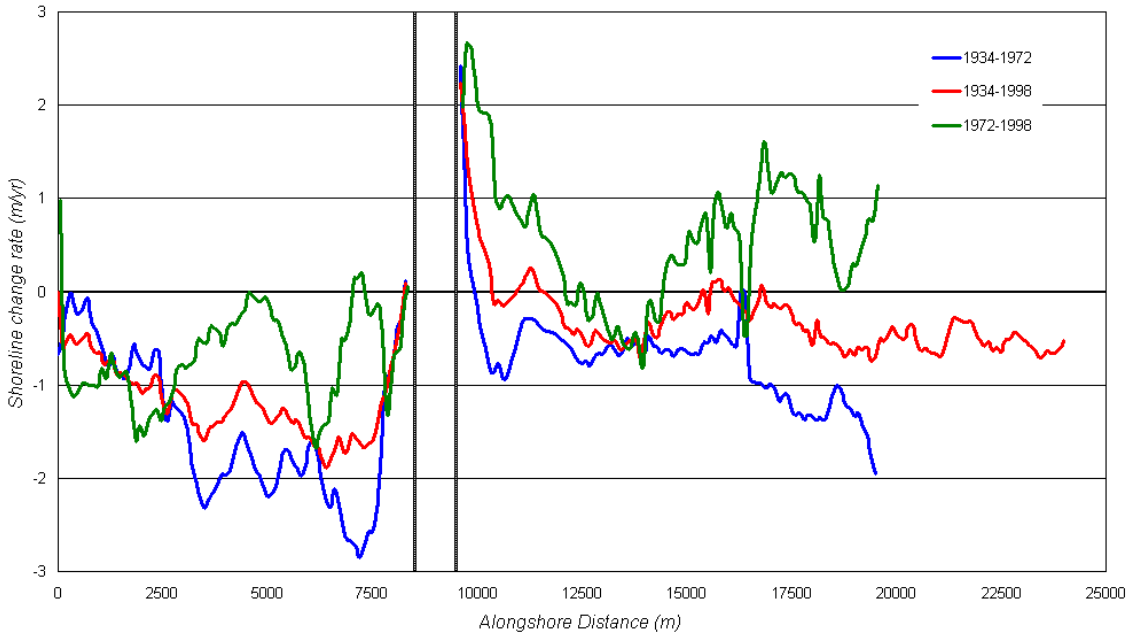

Figure 2-16. Average annual rate of change between the 1934, 1972, and 1998 shorelines.

Figure 2-17. California Coastal Record Project, Image 9032. Parking area at the southern end of Carlsbad State Beach adjacent to the north Agua Hedionda discharge jetty.

Figure 2-18. Maptech Mapserver image of the Agua Hedionda discharge jetties and Carlsbad State Beach.

Figure 2-19. California Coastal Record Project, Image 9017. Rocky cliffs just north of the elevated concrete walkway that spans Carlsbad State Beach.

Figure 2-20. California Coastal Record Project, Image 9011. Erratic portion of seawall along Carlsbad that consists of rubble rip-rap, vertical structures, and home foundations.

Figure 2-21. California Coastal Record Project, Image 9005. Armoring at The Point, Carlsbad, and Buena Vista Lagoon discharge point.

Figure 2-22. California Coastal Record Project, Image 9002. Well-organized rubble seawall that spans from Buena Vista Lagoon to Loma Alta Creek, Oceanside.

Figure 2-23. California Coastal Record Project, Image 8985. South Pacific Street bridge crossing over Loma Alta Creek discharge point, Oceanside.

Figure 2-24. California Coastal Record Project, Image 8971. Well-organized portion of rubble seawall that spans north of Loma Alta Creek to The Strand, Oceanside.

Figure 2-25. California Coastal Record Project's Aerial Photograph, Image 8963. Emergency Revetment along The Strand, Oceanside.

Figure 2-26. California Coastal Record Project's Aerial Photograph, Image 8952. North Pacific Street curb along The Strand that acts as a landward erosion barrier, Oceanside.

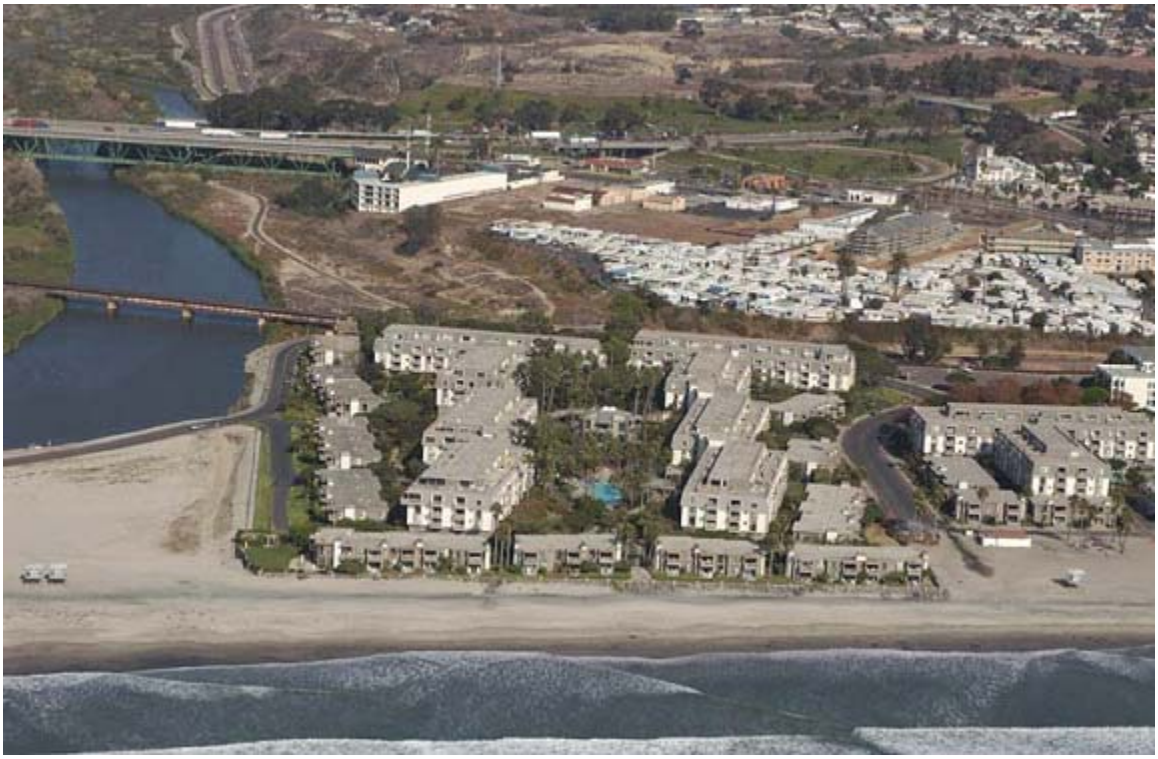

Figure 2-27. California Coastal Record Project, Image 8948. Timber and rubble rip-rap seawall that armors North Coast Village, Oceanside.

Figure 2-28. California Coastal Record Project, Image 8946. North Pacific Street bridge crossing over the San Luis Rey River discharge point, Oceanside.

Figure 2-29. California Coastal Record Project, Image 8944. North Pacific Street curb landward of Oceanside Small Craft Harbor, Oceanside.

CHAPTER 3
DNR MODEL

This chapter briefly explains the theory behind the one-line DNR model. For a more detailed discussion, see Dean and Grant (1989). First a background on one-line models is presented, along with the equations used to calculate longshore sediment transport and shoreline position. This is followed by a discussion on wave set-up, run-up, overtopping, and force estimates as implemented in the DNR model for this project.

Shoreline Position

The DNR model is a one-line model, meaning the model predicts the evolution of one contour (Dean and Grant, 1989). The most common contour to track is the shoreline, which is typically divided into a number of equally spaced cells. A one-line model assumes that the beach profile shape remains constant. Shoreline position change from one time step to the next is a function of the change in volume within a cell between consecutive time steps. The change in volume, in turn, is a function of gradients in longshore sediment transport and additions or subtractions in sediment from sources or sinks in the cell.

The DNR model determines the change in shoreline position using the Brunn rule. Two requirements are necessary to apply the Brunn rule for the new equilibrium profile: 1) The profile shape does not change with respect to the water line, and 2) The sand volume in the profile must be conserved (Dean and Dalrymple, 2002). Once equilibrium occurs, the shoreline position change, Δy, is given by

$$\Delta y = \frac{\Delta V}{h_* + B} \tag{3.1}$$

where ΔV is the volumetric change, h_* is the closure depth, and B is the berm elevation.

Longshore Sediment Transport

Gradients in the sediment flux result in a change in volume. If the longshore sediment transport (LST) entering a cell is greater than the LST exiting the cell, then the cell experiences sediment accretion and the shoreline advances seaward. Conversely, if the LST exiting the cell is greater than the LST entering the cell, then the cell experiences a reduction in sediment volume and the shoreline retreats landward. If erosion or accretion occurs, then the profile simply translates landward or seaward. Since the profile shape is always the same, tracking one point on the profile is sufficient for defining the entire profile.

Figure 3-1 shows various terms that can influence the volume of sediment in a cell. Each cell is a local, small-scale littoral budget. The terms from Figure 3-1 can be summarized in the conservation of mass (volume) equation,

$$\Delta y[\Delta x(h_* + B)] = [(Q_{\text{in}} - Q_{\text{out}}) + Q_{ss}]\Delta t + V_N \tag{3.2}$$

where Δy is the change in shoreline position for time interval Δt, Δx is the alongshore length of the cell, Q_{in} and Q_{out} are the LST at the boundaries of the cells, Q_{ss} is a source/sink, and V_N is the volume associated with nourishment or mining. The terms h_* and B are the closure depth and the berm elevation. Their sum gives the vertical range of the active profile. This equation is written for each cell to get a complete one-line description of the shoreline.

To apply Equation 3.2, the LST must be specified. The DNR model implements a variation of the CERC formula (SPM, 1984),

$$Q = \frac{K}{\rho g (s-1)(1-p)} (EC_g \cos\theta \sin\theta)_b \tag{3.3}$$

where Q is volume transport, ρ is the water density, g is the acceleration due to gravity, s is the specific gravity of the sediment, p is the sediment porosity, and K is a dimensionless empirical transport coefficient. The terms in the parenthesis with the subscript b are evaluated at the breaker line. The term E is the wave energy density, C_g is the group celerity of the waves, and θ is the wave local angle relative to the shoreline.

Using linear wave theory, conservation of energy flux, and Snell's Law for refraction, Equation 3.3 may be written

$$Q = \frac{K}{8(s-1)(1-p)} n\, H^2 \cos\theta \sin\theta\, C_b \tag{3.4}$$

where C_b is the wave celerity evaluated at the breaker line and n is the ratio of the group velocity to the wave celerity. The advantage of Equation 3.4 is that only C_b is evaluated at the breaker line while all other terms may be evaluated at any arbitrary depth outside the breaker line.

The DNR model proceeds by first calculating Q at each cell boundary. The angle θ is the local wave angle and incorporates the influence of the shoreline orientation at the cell. With Q known and all sources/sinks and nourishments specified, Equation 3.2 is solved. The solution technique is an explicit, forward, finite difference scheme. Time steps are made small enough to ensure numerical stability.

Wave Setup

If the water depth as the seawall is greater than zero, then wave setup at the seawall is calculated as

$$\overline{\eta_{sw}} = \frac{3\kappa}{8+3\kappa}\left(h_{BL} - h_{sw}\right) - \frac{\kappa^2}{16}h_{BL} \tag{3.5}$$

In which $\overline{\eta_{sw}}$ is the setup at the seawall, h_{BL} is the still water depth at the breaker line, h_{sw} is the still water depth at the seawall, and κ is a breaker index. This setup equation is valid for depth profiles that increase monotonically with distance offshore. The influence of wave reflection is not included.

Run-up

The run-up is calculated using different formulations for a vertical face and a rubble slope. For a vertical face, the height of the run-up, R_a is taken as the height of a standing wave crest.

$$R_u = H_{sw} + \eta_T + \bar{\eta} \tag{3.6}$$

where H_{sw} is the incident wave height at the seawall. This is added to the tide η_T and wave setup $\bar{\eta}$ to get the total height of the run-up at the seawall. For a rubble slope, the run-up is calculated as (CIRIA/CUR, 1991)

$$R_u = \begin{cases} 0.72\xi H_{sw} & \xi \le 1.5 \\ 0.88\xi^{0.41} H_{sw} & 1.5 < \xi \le 2.84 \\ 1.35 H_{sw} & \xi > 2.84 \end{cases} \tag{3.7}$$

in which ξ is the surf similarity parameter defined as

$$\xi = \frac{m}{\left(2\pi H_{sw} / g T_m^2\right)^{1/2}} \tag{3.8}$$

where m is the slope of the structure face (mV : 1H), g is the acceleration due to gravity, and T_m is the mean wave period. Data for this project are given as peak period, T_p. An approximate conversion is $T_m = 0.83 T_p$ (CIRIA/CUR, 1991).

Overtopping Propagation

Overtopping occurs when the height of the run-up exceeds the crest elevation of the seawall. Overtopping creates the potential for damage to structures from flooding and direct water forces. Cox and Machemehl (1986) present a simple model for propagation of a bore behind the seawall when overtopping occurs. The height of the bore, H, is given as

$$H = \left[\left(\frac{R_u - E_o}{1+\alpha} \right)^{1/2} - \frac{x}{2A} \right]^2 \tag{3.9}$$

where R_u is the run-up height, E_o is the crest elevation of the structure, and x is the distance behind the seawall. The term α is a coefficient with a recommended value of α = 0.1. The term A is defined as

$$A = \alpha(1+\alpha)^{3/2} g^{1/2} T \tag{3.10}$$

where g is the acceleration of gravity and T is the wave period.

The bore height is a maximum at the seawall crest (x = 0) and decreases in height rather quickly as the bore propagates landward of the seawall. The magnitude of the excess run-up determines the distance of the bore propagation (R_u - E_o). In the DNR model, if overtopping occurs, the bore height is calculated at the seawall crest, and then every 5 m (16 ft) behind the seawall until the bore height diminishes to H = 0.

Forces

If a propagating bore impacts a structure, wave forces develop. These forces are estimated as outlined in Ramsden and Raichlen (1990),

$$f_{\max} = \left[\frac{(1+\alpha)^2}{2} + N_F{}^2 \right] \gamma H^2 \tag{3.11}$$

where f_{max} is the per unit width of the structure, γ is the weight density of the water, and N_F is the Froude number. The value of the Froude number is taken to be $N_F = 1.8$, which follows the data given in Ramsden and Raichlen (1990).

Input Parameter Cell Definitions

This section explains the methods used in defining characteristics within a cell of the DNR model. These characteristics include shoreline position, seawall location, longshore sediment transport rate, shore perpendicular structures (breakwaters, jetties, and groins), beach nourishments, and sediment sources/sinks. These definitions are important to define the study area as accurately as possible in the model.

The definitions of shoreline position, cross-shore seawall location, and groin lengths are referenced to the baseline. The baseline is an imaginary line typically located landward of the shoreline with an azimuth similar to that of the shoreline between the boundaries of the study area. The baseline is then segmented into equally spaced intervals that define each individual cell. The baseline origin marks one boundary of the study area and is defined at cell 1. The positive direction along the base coordinate is defined as left to right when facing offshore. Perpendicular lines are then projected from the baseline to define the shoreline position, cross-shore seawall locations, and the seaward tip of shore perpendicular structures.

The study area is sub-divided into cells, which are equally spaced across the domain. The upper boundary is cell I_{max}, which is the last cell in the domain. The upper and lower boundaries are not referenced by the direction of transport; rather they are designated by the location within the domain. For the purposes of this project, the cells are all 100 m (330 ft) in width.

Shoreline positions are defined at the midpoint of each cell. The representative shoreline distance for each cell is found by interpolating the shoreline position at the boundaries for each cell. The number of shoreline position values is equal to the total number of cells from the lower boundary to the upper boundary. Shoreline position is entered in feet from the baseline.

Cross-shore seawall positions are defined in a similar manner as shoreline positions. Representative cross-shore seawall positions are found by interpolating the seawall positions at the boundary of each cell and are defined at the midpoint of those cells. The seawall position value is the same for the entire cell. In the along shore orientation, seawalls represent armoring of the entire cell at the specified cross-shore distance from the baseline. Cross-shore seawall location is entered in feet from the baseline.

Longshore sediment transport (LST) is defined at the boundaries between cells. As a result, there is one more LST value along the reach than there are cells. LST values are positive if the transport is moving from the left to the right of an observer facing offshore. Likewise, transport is negative if it is moving from the observer's right to left. The lower boundary is the location of the first LST value, $Q(1)$, and the upper boundary of the reach is the location of the final LST value, $Q(I_{max}+1)$. LST rate is measured in cubic yards per year.

Groins are defined in both the alongshore and the cross-shore directions. "Groins" is the general term used to describe any shore perpendicular structure capable of blocking the movement of sediment alongshore, and includes breakwaters, jetties, and groins. In the alongshore, groins are defined at the boundaries between cells. The cell whose lower

boundary marks the location of the groin designates the LST. For example, a groin located in cell 100 is placed in the boundary between cells 99 and 100. In the cross-shore direction, groin lengths are given as the distance from the baseline to the seaward tip of the groin. This length is measured in feet.

Beach nourishment input includes the alongshore location, nourishment volume, time of placement, and a fill factor. In the alongshore, nourishment projects are defined with an upper cell and a lower cell. The nourishment volume is then placed uniformly on the coast between the lower and upper cell. Beach nourishment volumes are given in cubic yards. The nourishment is placed at the specified time (in hours). The fill factor is the portion of the nourishment volume that remains in the littoral system.

Sediment sources and sinks are defined as a uniform addition or removal of sediment within the assigned cell. The volume change is an annual rate that remains constant throughout the duration of the model run. Sediment sources and sinks include river contributions, bluff contributions, offshore sediment deflection, sediment removal, and background erosion. Sources/sinks are given in $yd^3/ft/yr$.

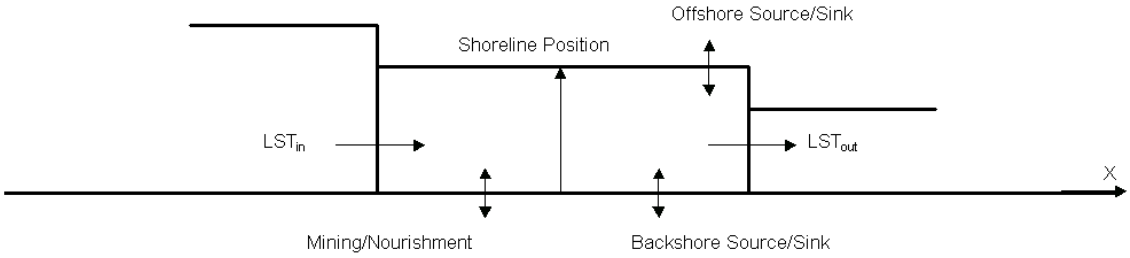

Figure 3-1. Possible changes in sediment amounts within a cell.

CHAPTER 4
SEAWALL MODEL

The DNR model has been modified to include influences from seawalls. If a seawall is in the surf zone, then the surf zone width increases, the longshore sediment transport (LST) is reduced, and the shoreline cannot retreat landward of the seawall cross-shore location. In this chapter, the seawall algorithm is described and examples are presented to show the performance of the seawall routines.

Theory

Profile Definitions

The DNR model is a one-line model that tracks the cross-shore position of the shoreline in response to alongshore gradients in the LST. Along seawalls, the actual shoreline position cannot retreat landward of the seawall location. Therefore, a modification is necessary in the one-line model to determine the shoreline response where the shoreline position becomes fixed. The modification implemented into the DNR model is that for cells with seawalls, the volume of sediment seaward of the seawall is tracked rather than the shoreline position.

The cross-shore profile must be known to determine this volume of sediment. As mentioned in Chapter 2, the beach profile in the DNR model is defined by the Brunn/Dean equilibrium beach profile. The equilibrium profile is based on constant wave energy dissipation per unit volume of surf zone and has been well documented and widely used in coastal engineering. The equilibrium beach profile is given as

$$h = Ay^{2/3} \tag{4.1}$$

where h is the still water depth along the profile, A is the profile coefficient related to the sediment diameter, and y is the cross-shore distance along the profile (Dean and Dalrymple, 2002). The shoreline position corresponds to $y = 0$; and the depth of closure, $h = h_*$, correspond to the width of the active littoral zone, $y = y_*$.

To distinguish between global cross-shore position and local profile position, the subscript "L" is applied to variables that refer to the local coordinate system of the beach profile. The global coordinates begin at the baseline as the origin, and the local coordinates begin with the shoreline position of the equilibrium beach profile as the origin. The global cross-shore distance from the baseline to the shoreline position is defined as $y = y_N$. The shoreline position in reference to the local coordinates of the equilibrium beach profile occurs at $y_L = 0$. Other variables used in the local coordinate system are y_{*L}, which is the cross-shore width of the active littoral, y_{aL}, which defines the cross-shore shoreline displacement when $y_{sw} > y_N$, and y_{swL}, which is the distance from the shoreline position landward of the seawall to the seawall.

A critical location for the profile is when the equilibrium profile shoreline position is defined at the location of the seawall. If the shoreline is seaward of the seawall ($y_N \geq y_{sw}$), then a sub-aerial berm/beach exist seaward of the seawall. If the profile is landward of this critical point ($y_N < y_{sw}$), then no sub-aerial berm/beach exist seaward of the seawall, and there is a finite water depth fronting the seawall.

The volume of sediment calculated at this critical shoreline position is referred to as the critical volume for the profile. If the volume of sand in the profile exceeds the critical volume, then a sub-aerial beach exists seaward of the seawall. If the volume of sediment in the profile is less than the critical volume, then a finite water depth exists at the

seawall. Figure 4-1 shows this critical condition. For an equilibrium profile, the critical volume is

$$V_c = [y_{sw}(h_* + B) + (y_{*L}h_* - 0.6Ay_{*L}^{5/3})]dx \tag{4.2}$$

where V_c is the critical volume, y_{sw} is the cross-shore distance from the baseline to the seawall, y_{*L} is the width of the active littoral zone, h_* is the closure depth, B is the berm elevation, and dx is the cell width.

Figure 4-2 shows the condition where the profile of sand exceeds the critical volume ($y_N > y_{sw}$). For this case, the volume is

$$V = [y_N(h_* + B) + (y_{*L}h_* - 0.6Ay_{*L}^{\frac{5}{3}})]dx \tag{4.3}$$

where y_N is the cross-shore shoreline position seaward of the seawall. This equation is similar to the equation for critical volume. The only difference is that the berm extends seaward of the seawall to the actual shoreline. For this case, the change in shoreline position associated with the volume tracking within the profile is the same as the shoreline position change calculated by profile translation:

$$\Delta y = \frac{\Delta V}{h_* + B} \tag{4.4}$$

Excess volume, V_E, is defined as the actual volume minus the critical volume,

$$V_E = V - V_c \tag{4.5}$$

If $V_E > 0$, then a sub-aerial beach exists seaward of the seawall. If $V_E < 0$, no beach exists and water fronting the seawall. The $V_E < 0$ case is more complex than the $V_E > 0$ case and leads to the modification of tracking the sediment volumes as opposed to simply solving for the shoreline position change with profile translation.

Figure 4-3 shows an example where the seawall is in the surf zone. The submerged profile is still defined as an equilibrium beach profile, but the origin of the profile is displaced landward of the seawall. This landward translation results in an increase in water depth and flattening of the profile at the seawall. The cross-shore position referred to as y_N is actually a fictitious shoreline position, since the actual shoreline cannot retreat onshore beyond the seawall location. However, this fictitious shoreline position is crucial in defining the profile and the volume. The volume of sediment within a cell for the case where the $V_E < 0$ is

$$V = [y_{sw}(h_* + B) + (y_{*L} - y_{aL})(h_* - h_{sw}) - 0.6(h_* y_{*L} - h_{sw} y_{aL})]dx \tag{4.6}$$

where y_{aL} is the distance from the fictitious shoreline position to the cross-shore seawall location.

$$y_{aL} = \left(\frac{h_{sw}}{A}\right)^{3/2} \tag{4.7}$$

Profile Changes

In the preceding section, the volumes of sediment in the profile were determined for the cases with and without a beach fronting the seawall. In this section, the change in shoreline position is determined as a function of the change in sediment volume.

As previously mentioned, in a one-line model, shoreline changes are driven by gradients in the longshore transport. In a cell, if the transport entering the cell exceeds the transport leaving of the cell, then accretion occurs and the shoreline advances seaward. Conversely, if a deficit exists between the boundaries of a cell, then erosion occurs and the shoreline retreats landward. This same principal applies along a seawall, with the exception that if $V_E < 0$, the fictitious shoreline retreats or advances as opposed

to the actual shoreline position, which is fixed at the seawall. This results in a change in water depth fronting the seawall.

Consider the change in sediment volume in a cell to be ΔV. For a one-line model, neglecting sources/sinks and nourishments, this is simply

$$\Delta V = (Q_{in} - Q_{out})\Delta t \tag{4.8}$$

where Q_{in} is the transport going into the cell, Q_{out} is the transport leaving the cell, and Δt is the time interval. ΔV can be positive or negative. If the excess volume is positive, then a beach is fronting the seawall, and there is a one-to-one relationship between volume and shoreline position given by

$$\Delta V = V_n - V_o = (y_n - y_o)(h_* + B)dx \tag{4.9}$$

where the subscript *o*, or old, refers to the initial condition at a time step; and the subscript *n*, or new, refers to final condition (initial time step + Δt). The old shoreline, y_n, is the same as y_N at the new location in global coordinates, and the new shoreline, y_o, is the same as y_N at the old location in global coordinates. Using Equations 4.8 and 4.9 gives an estimate of the new shoreline position.

When the excess volume is negative, there is no dry beach fronting the seawall, and the volume change is still given as

$$\Delta V = V_n - V_o \tag{4.10}$$

except the volumes are defined by Equation 4.6. The volumes V_n and V_o depend on the location of the fictitious shoreline. The location y_o is known, and the value for y_n must be determined that satisfies Equation 4.10.

Consider Figure 4-4, which gives a graphical representation of $-V_E$ and $-\Delta V$ based on the longshore transport gradient where the fictitious shoreline retreats from y_o to y_n.

For convenience, the shoreline position change is expressed in local coordinates. Using Equation 4.4, the volume change is defined as

$$\Delta V = \{0.6A[-(y_{*L} + y_{swL} - y_{aL})^{5/3} + (y_{swL} - y_{aL})^{5/3} + (y_{*L})^{5/3}]\}dx \qquad (3.27)$$

The only unknown variable in Equation 3.27 is y_{aL}, which cannot be solved for explicitly. Therefore, the DNR model iteratively solves for y_{aL} using a numerical technique.

Longshore Transport Modification

A seawall that is in the surf zone modifies LST. On a beach with no seawall the waves break across the surf zone and are completely dissipated at the shoreline. All of the wave power, or momentum, is available for generating longshore currents and sediment transport. With a seawall in the surf zone, the waves break as they propagate across the surf zone, but still have a finite height when they reach the seawall. The wave energy may be dissipated at a rubble seawall or reflected back offshore at a vertical seawall. Either way, the associated wave power does not lead to the development of longshore currents. As a result, the LST on a beach with a seawall in the surf zone is generally less than for the same beach with no seawall. Ruggiero and McDougal (2001) presented an analytical solution for the LST on a plane beach that supports this argument. The response was more complex because partial standing waves developed from reflected waves. It was also found that the reflected wave causes the incident wave to break approximately 10% farther offshore. Never-the-less, the general observation was that the farther out into the surf zone a seawall is located, the greater the reduction in LST.

Figure 4-5 shows the LST as a function of seawall location for four planar beach slopes. The position of the seawall was relative to the location of the breaker line if no

seawall was present. In each case, the LST decreased as the seawall position moved farther offshore. The milder the beach slope, the wider the surf zone became and the influence of the partial standing wave increased.

In Figure 4-5, the seawall reduction factor, R_{sw}, was approximated as

$$R_{sw} = 1 - a\left(\frac{y_{swL}}{B_{sw} y_{blL}}\right) \tag{4.11}$$

where y_{swL} and y_{blL} are the seawall and breaker line locations in local coordinates, B_{sw} is the increase in surf zone width because of reflection from the seawall (B_{sw} = 1.12), and a is the slope of the linear approximation. A value of a = 1.0 was used which yields no LST when the seawall is seaward of the breaker line.

Along-shore Boundary Conditions

The seawall flux boundary conditions are located at the cell boundaries. Every seawall has one more longshore sediment transport value, Q, than y_{sw} values. This extra transport value marks the boundary where LST makes the transition from a cell that does not contain a seawall to a cell that is armored by a seawall. There is an additional transport modification that may occur at the ends of the seawall.

If the seawall is in the surf zone, then the updrift boundary of the seawall can act as a groin and block the LST (Figure 4-6). At this updrift location, the DNR model refers to the groin routine. The end of the seawall can completely block LST until the updrift shoreline advances seaward of the end of the seawall, or the groin can be leaky and allow partial transport before the shoreline reaches the end of the groin.

Seawall/ Nourishment Sensitivity Tests

This section shows the functionality of the seawall routines in the DNR model by examining a variety of hypothetical cases. The base conditions for the tests are:

- Straight initial shoreline located at $y_N = 0$.
- Constant wave of height $H_0 = 0.61$ m (2 ft) and period $T = 12.1$ s.
- Shore-normal wave angle $\alpha_0 = -3°$ (causing transport to move from right to left).
- A study area of 241 cells.
- Duration of simulation = 50 yrs.

The variables are a 150-m (500-ft) breakwater, a beach nourishment at time $t = 10$ yrs (varies in location by case depending on seawall locations), and the presence of one or more seawalls. Table 4-1 gives input parameters for each case. The letters '*a*' and '*b*' in the case titles show whether or not a breakwater exists for that particular simulation: no breakwater for cases that are denoted with an '*a*' and one 150-m (500-ft) breakwater at cell 120 for cases that are denoted with a '*b*.' The cases that do not contain a breakwater do not experience a disruption in the longshore sediment transport, and thus do not result in erosion.

Case 1: One Seawall, No Nourishments

Case 1 incorporates one seawall with a cross-shore location at the initial shoreline position. No nourishment is included for this test. Figure 4-7 gives a graphical representation of the input parameters for Case 1. Case 1a is not presented in Table 4-1, as the results are unimportant. Case 1*a* consists of one seawall and no breakwater or beach nourishments. Consequently, no forcing is present that would cause the shoreline to accrete or erode. The result for Case 1*a* is a straight final shoreline identical to the straight initial shoreline.

Figure 4-8 shows the evolution of the shoreline at the 1-yr, 5-yr, 10-yr, 30-yr, and 50-yr time steps for Case 1*b*, and Figure 4-9 shows the shoreline position at pre-selected cells for every time step. These two figures display the shoreline response when

interacting with a seawall in an area experiencing a gradient in longshore sediment transport attributable to the breakwater. It should be noted that the present version of the DNR model does not include diffraction, so the shoreline response close to shore-perpendicular structures is not simulated accurately.

Figure 4-8 presents an important verification on the behavior at the ends of a seawall. If the shoreline immediately updrift recedes landward past the seawall, the updrift end of the seawall acts as a groin, thus blocking transport. In this simulation, the breakwater acts as the primary sediment trap blocking all transport. Once the shoreline upcoast of the seawall retreats landward of the seawall, the updrift end of the seawall becomes a secondary block in the sediment transport. The shoreline between the breakwater and the seawall then continues to adjust its orientation without any supply in sediment to these cells until the shoreline aligns with the incoming wave angle. This behavior mimics the response of a shoreline between groins. While this is occurring, erosion continues downdrift of cell 100 because of the lack of sediment reaching those cells.

Case 2: No Seawalls, One Nourishment

Case 2 is a simple case with one nourishment and no seawalls. This case is designed to check the functionality of the nourishment routine by isolating it from the seawall routines. Figure 4-10 gives a graphical representation of the input parameters for Case 2.

Figures 4-11 and 4-13 show the evolution of the shoreline for the 1-yr, 5-yr, 10-yr, 30-yr, and 50-yr time steps for Cases 2*a* and 2*b*, respectively. Figures 4-12 and 4-14 show the shoreline position at pre-selected cells for every time step for Cases 2*a* and 2*b*, respectively. These figures show the nourishment spreading effects as time progresses

after the implementation of nourishment projects, both in an area with no disturbance in LST (Case 2*a*) and in an area experiencing reduced LST (Case 2*b*). Figure 4-13 shows that the same volume of sediment is placed for every nourished cell. The cells within the nourishment bounds have a nourished planform that is parallel to the shoreline planform immediately before the nourishment event.

Case 3: One Seawall, One Nourishment

Case 3 combines one seawall and one nourishment. The nourishment spans the updrift half of the seawall, and then extends an equal distance upcoast across the unarmored shoreline. Figure 4-15 gives a graphical representation of the input parameters for Cases 3*a* and 3*b*.

Figure 4-16 shows the shoreline evolution for Case 3*a* for the 1-yr, 5-yr, 10-yr, 30-yr, and 50-yr time steps. The nourishment at the 10-yr time step causes the shoreline to move seaward between cells 100 and 115. As the simulation continues after the 10-yr mark, the nourishment spreads out in the form of a normal distribution in accordance to the one-line Pelnard-Considere model that predicts alongshore diffusion. Since there is no erosion to expose the seawall, the seawall has no influence. Figure 4-17 shows the shoreline position as a function of time at a number of cells along the seawall and beyond the ends of the seawall. The results also show the spreading of the nourishment with no influence from the seawall. Case 3*a* is in agreement with the results of Case 2.

Figure 4-18 shows the shoreline evolution for Case 3*b*, which includes a breakwater at cell 120 that causes erosion in the area of the seawall for the 1-yr, 5-yr, 10-yr, 30-yr, and 50-yr time steps. The results of Figure 4-18 shows the updrift end of the seawall acting as a groin when the shoreline updrift recedes landward of the seawall.

This is in agreement with the results at the seawall updrift end for Case 2*b*. Figure 4-18 also shows an interesting result important in the seawall model verification.

Notice the point in the shoreline position at year 10 that occurs at the upcoast end of the seawall. This point seems to represent an error, or a discontinuity, in the beach nourishment. However, since the shoreline had already retreated back to the armoring before the placement of the nourishment (notice that in the 5-year planform the shoreline position is already landward of the updrift end of the seawall), progressively varying water depth exists seaward of the seawall, increasing from the updrift to the downdrift ends of the seawall. The volume of nourishment assigned to each cell along the seawall first goes toward filling the profile to the critical volume. Once that critical volume is achieved, the shoreline advances seaward in accordance to profile translation. The point in the nourishment project at cell 105 represents the boundary between the end of the seawall, where a water depth existed before the nourishment (from the fictitious retreat of the shoreline landward of the seawall), and the open, unarmored coastline.

Figure 4-19 shows the shoreline position by cell for Case 3*b* and gives a good representation of the seawall effect on shoreline response in a sediment-starved system. Cell 115 (represented by the green line in the figure) is the closest to the breakwater and therefore begins to erode first and more severely than the other cells. Between the 10-yr time step (when the nourishment occurs) and the 15-yr time step, shoreline advance occurs at this cell. This advance is a result of the spreading effect of the nourishment as it reaches cell 115. The consequent shoreline retreat is from the sediment eroding away because of the lack of transport at that location. However, since the sediment becomes essentially trapped between the breakwater and the updrift end of the breakwater, the

erosion rate decreases dramatically toward the end of the simulation as the shoreline aligns itself to the wave angle.

Conversely, cell 80 (represented by the yellow line) is the cell farthest from the breakwater. This cell is the last of the specified cells to start eroding, and its distant location from the nourishment causes only a small advance in the shoreline position as the nourishment spreads out along the coast. The erosion downdrift of the seawall mentioned previously because of the updrift end of the seawall acting as a groin is evident for those cells downcoast of the seawall in Figure 4-19.

Case 4: Two Seawalls, One Nourishment

The main focus of Case 4 is to isolate the shoreline response in gaps between seawalls. To examine the shoreline behavior between seawalls, two seawalls each 1,500 m (4900 ft) long and 1,000 m (3300 ft) apart are examined. Also, a beach nourishment is placed at the 10-yr time step that spans beyond both ends of the updrift seawall. This configuration allows an examination of the shoreline behavior along a seawall fronted by water and at the ends of seawalls. Figure 4-20 gives a graphical representation of the input parameters for Cases 4*a* and 4*b*.

Figure 4-21 shows the shoreline evolution for the 50-yr simulation for Case 2*a*. It is rather uneventful and similar to Figure 4-16. Once again, since no breakwater is included for this case, there is no erosion. Therefore, the nourishment moves the shoreline seaward, and the seawalls have no effect. As time progresses, the beach nourishment spreads out along the coast. This is also shown in Figure 4-22.

Figure 4-23 shows the shoreline response with an updrift breakwater. The shoreline position from the middle of the updrift seawall to the breakwater is similar to that same relative location in Figure 4-18. These results reinforce the conclusions from

Case 3*b*. Continuing downcoast from the midpoint of the updrift seawall, the shoreline position seaward of the seawall continues to increase slowly to the boundary of the nourishment with only a small dip at the downcoast end of the seawall.

As previously mentioned, the sediment volume from the nourishment must first provide a profile with the necessary sediment to reach the critical volume before the shoreline can advance seaward. The shortage of sediment for transport (attributable to the breakwater in this case) results in a progressive removal of sediment from the updrift (adjacent to the sediment sink) to the downdrift direction to satisfy continuity, and in turn, progressively greater depths fronting the seawall in the updrift direction. Consequently, more and more of the nourishment volume must go toward reaching the critical volume along the seawall from the downdrift to the updrift direction of the seawall. The resulting gradual increase in shoreline advance is a result of these processes.

The small dip at the downcoast end of the seawall shows that immediately before the nourishment, the shoreline at that downcoast end of the seawall had already reached the seawall resulting in water depth at that boundary. This means that more sediment volume is necessary to reach the critical volume in those cells, and the resulting shoreline is landward of cells that had less water depth fronting the seawall at the time of the nourishment. This behavior was discussed for the results of Case 3*b*.

The shoreline response downdrift of the second seawall is similar to the results downdrift of the seawall in Case 3*b*. The only other difference between Case 4*b* and Case 3*b* is that now the shoreline must orient itself to the direction of the incoming waves not just between the first seawall and the breakwater, but also between the two seawalls

since the updrift end of the downcoast seawall will also act as a groin once the shoreline recedes landward of the seawall.

Figure 4-24 shows the shoreline position by cell for Case 4*b*. These figures give an accurate description of erosion rates in relation to distance downdrift from the breakwater and proximity to a seawall. Figure 4-24 agrees with previous conclusions for shoreline response from the nourishment spreading out along the coast over time. As the nourishment spreads, temporary shoreline advances are evident in cells affected by this behavior.

Table 4-1. Input parameters for seawall sensitivity test cases.

Case	Groin (yes/no)	Groin (cell)	Nourishment (yes/no)	Nourishment (cells)	Seawalls (yes/no)	1st Seawall (cells)	2nd Seawall (cells)
1*b*	yes	120	no	--	yes	100 to 110	--
2*a*	no	--	yes	90 to 110	no	--	--
2*b*	yes	120	yes	90 to 110	no	--	--
3*a*	no	--	yes	100 to 110	yes	95 to 105	--
3*b*	yes	120	yes	100 to 110	yes	95 to 105	--
4*a*	no	--	yes	85 to 110	yes	65 to 80	90 to 105
4*b*	yes	120	yes	85 to 110	yes	65 to 80	90 to 105

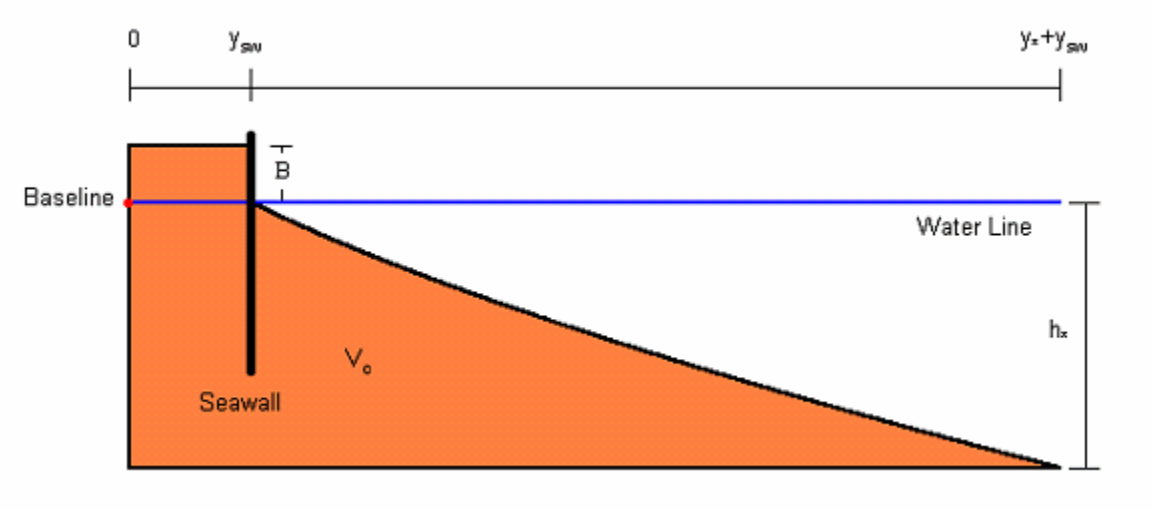

Figure 4-1. Critical volume, V_c, per unit width. The critical volume is the entire area shown in brown.

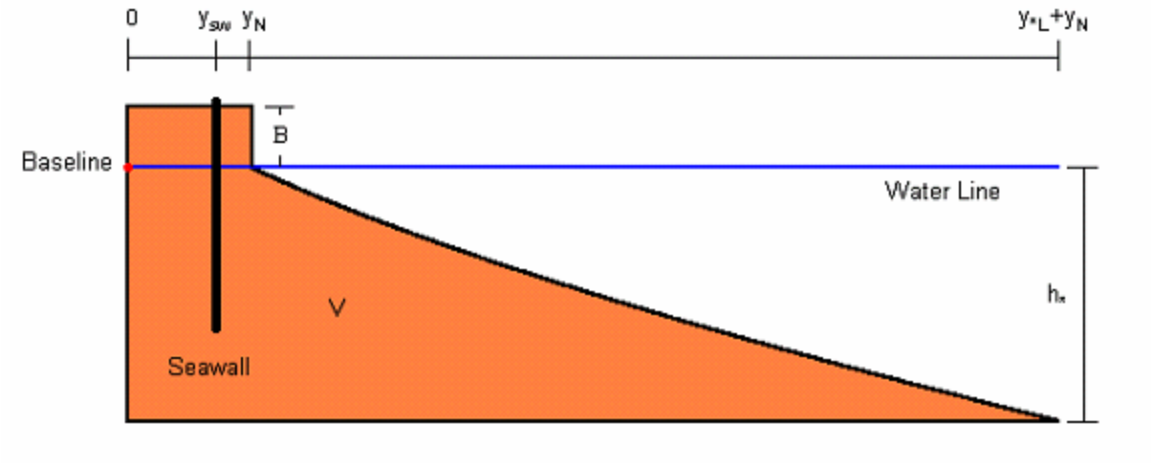

Figure 4-2. Volume per unit width for an aerial beach seaward of the seawall ($y_N \geq y_{sw}$).

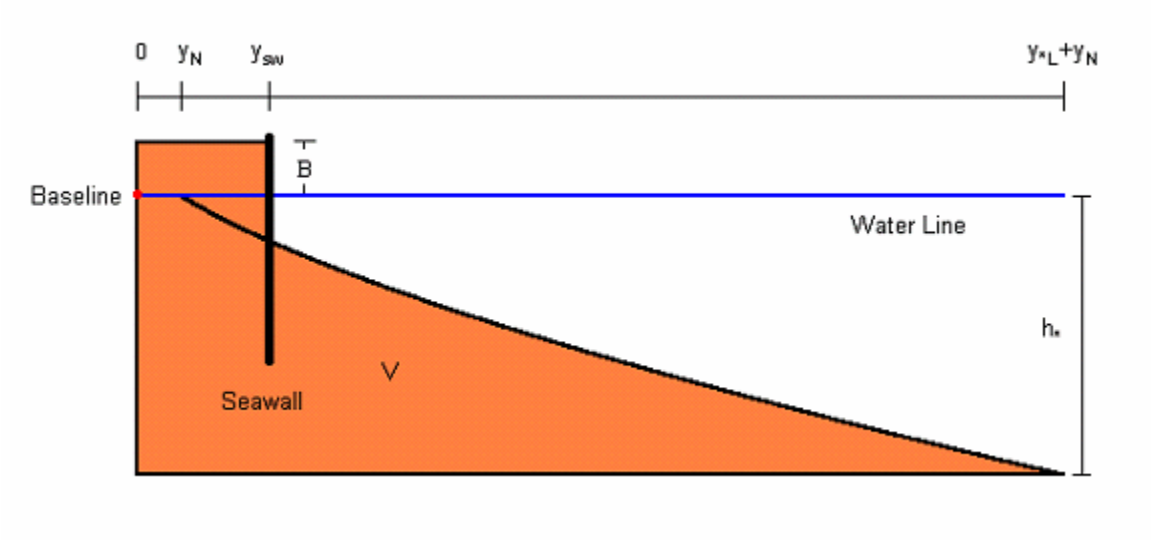

Figure 4-3. Initial volume per unit length for a seawall in the surf zone ($y_N < y_{sw}$).

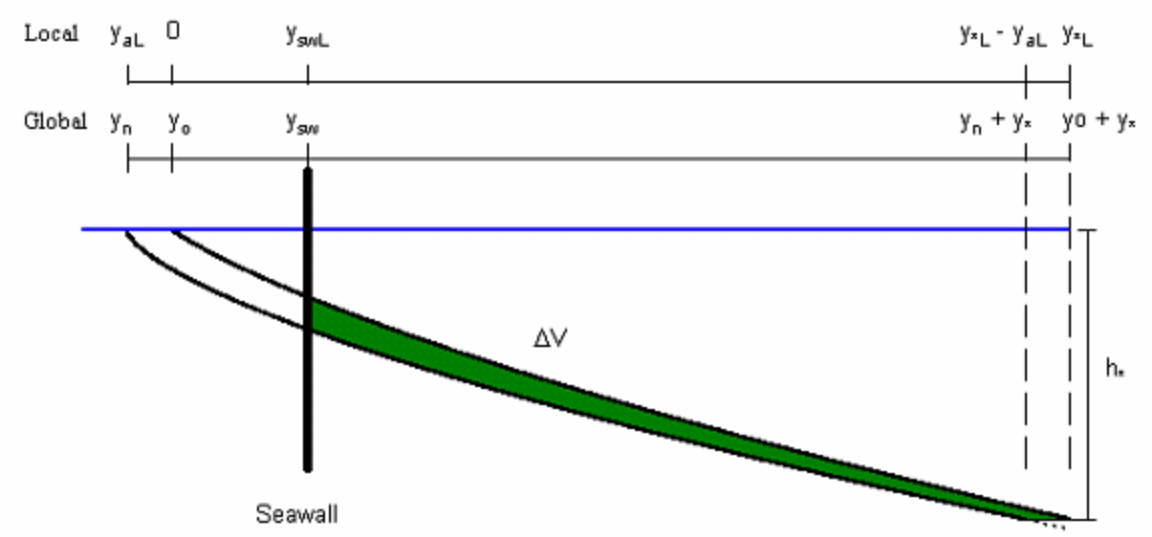

Figure 4-4. Volume change for a fictitious shoreline retreat with locations shown in both global and local coordinates.

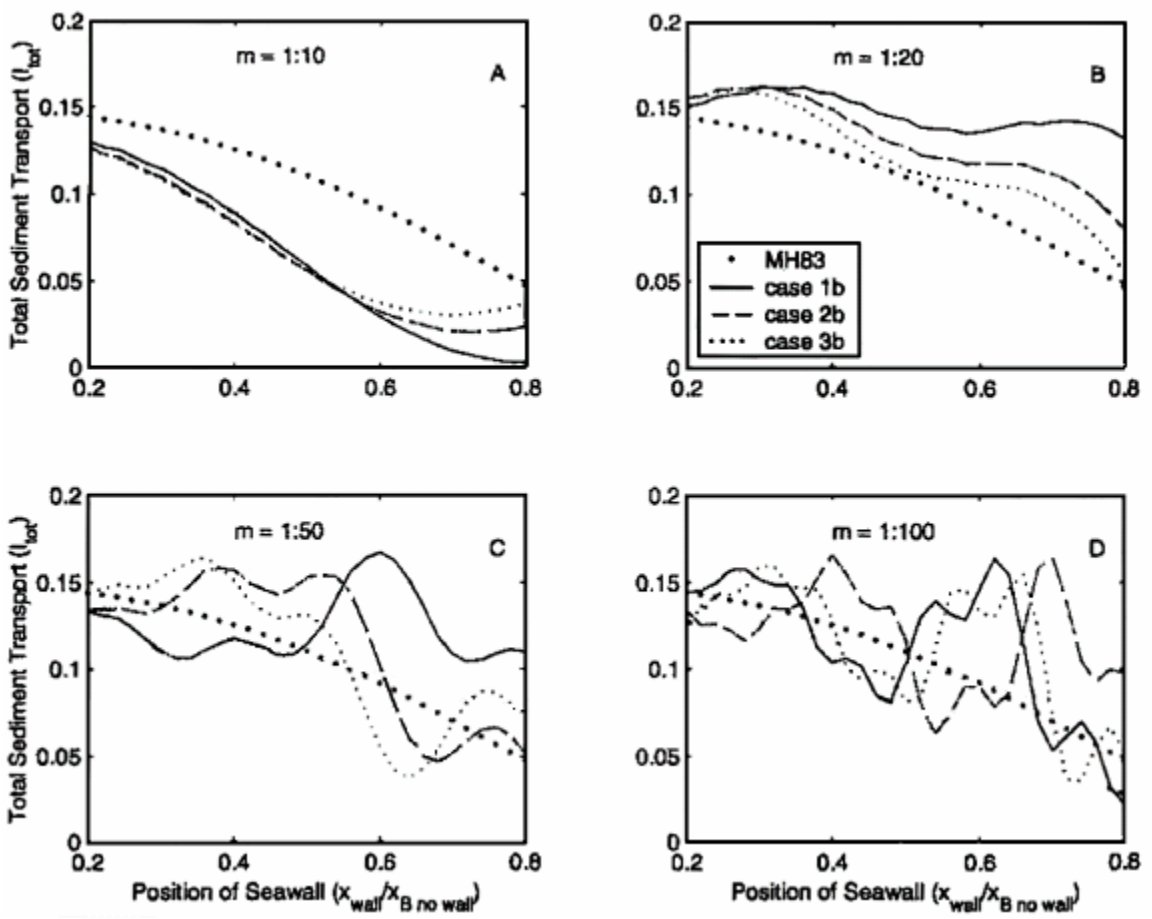

Figure 4-5. Total sediment transport fronting a seawall for four planar beach slopes and several wave conditions shown by different line types. A) Slope, m = 1:10. B) Slope, m = 1:02. C) Slope, m = 1:50. D) Slope, m = 1:100. Ruggerio, P. and W.G. McDougal (2001), "***An Analytic Model for the Prediction of Wave Setup, Longshore Currents and Sediment Transport on Beaches with Seawalls***", Coastal Engineering: An International Journal for Coastal, Harbour and Ocean Engineers, Volume 43, pp. 161-182.

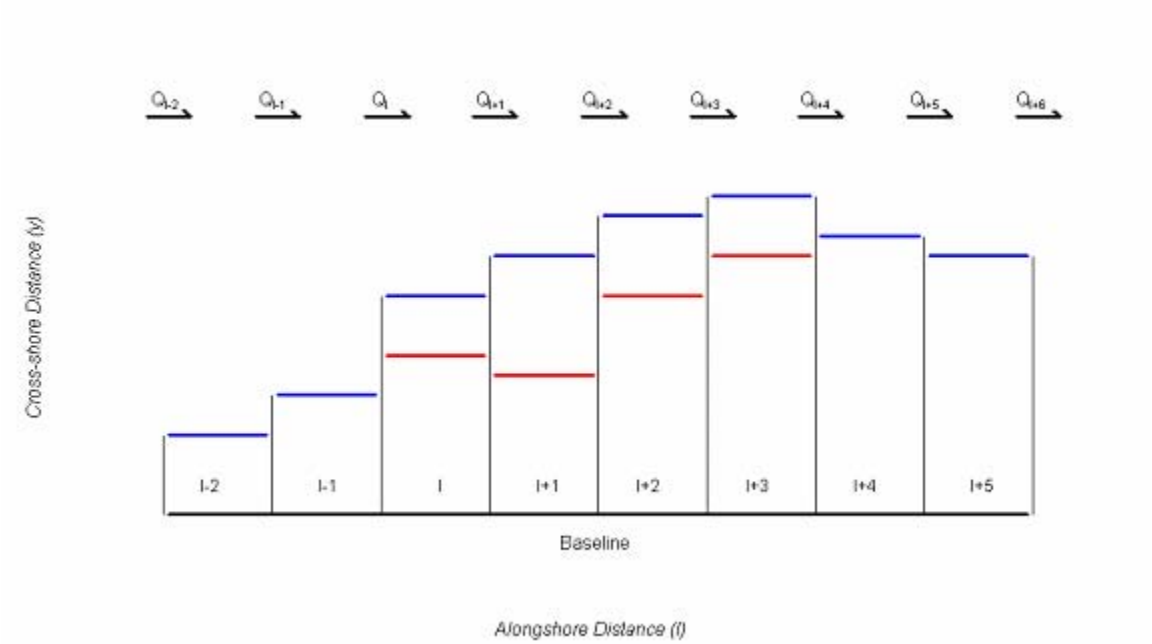

Figure 4-6. Graphical representation of positive transport and $y_{sw}\ (I) < y_N\ (I\text{-}1)$ at the start of the seawall. The shoreline is shown in blue and the seawall is shown in red. This case means the seawall act as a groin and blocks transport ($Q(I) = 0$) as it forms a discontinuity in the shoreline.

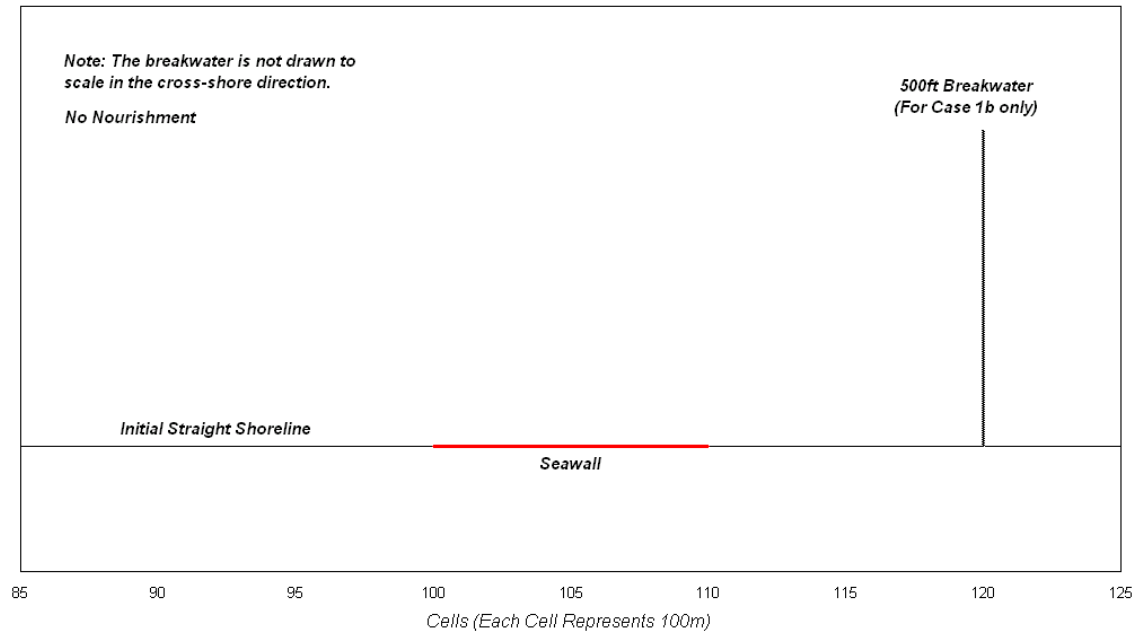

Figure 4-7. Input parameters for Case 1.

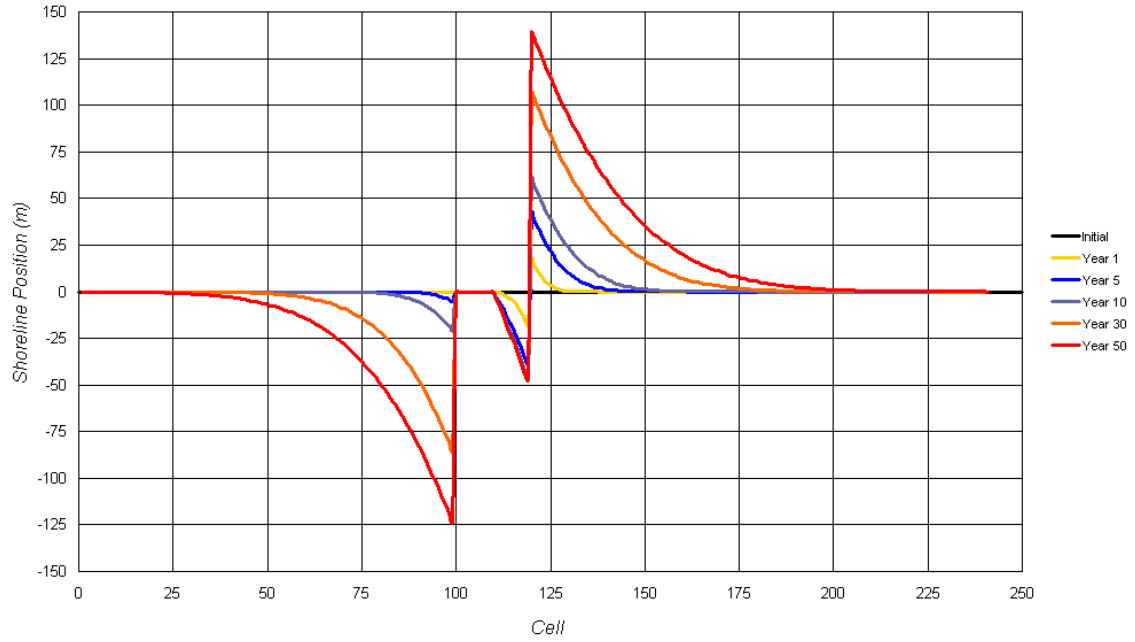

Figure 4-8. Case 1*b*: One seawall, no nourishment. Shoreline evolution.

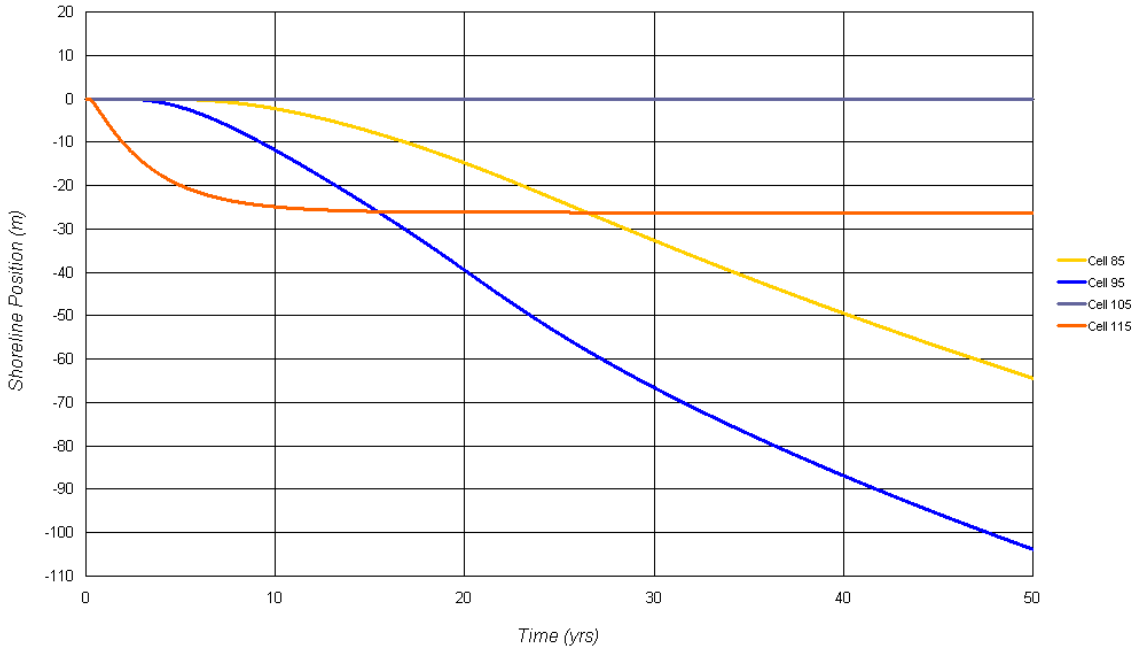

Figure 4-9. Case 1*b*: One seawall, no nourishment. Shoreline position by cell.

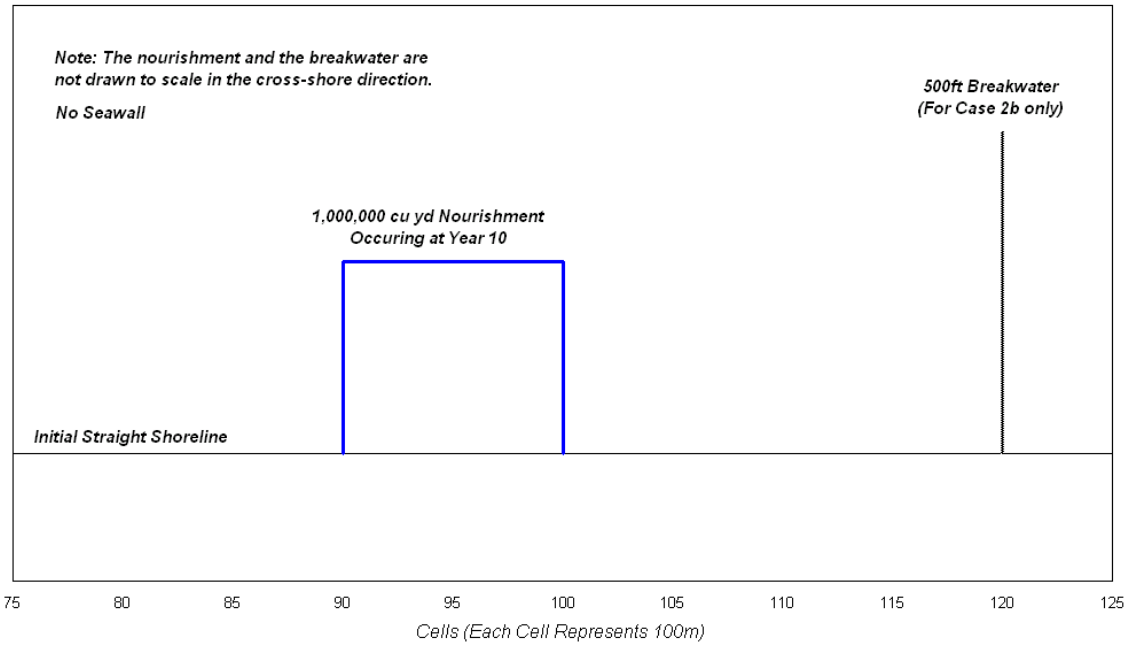

Figure 4-10. Input parameters for Case 2.

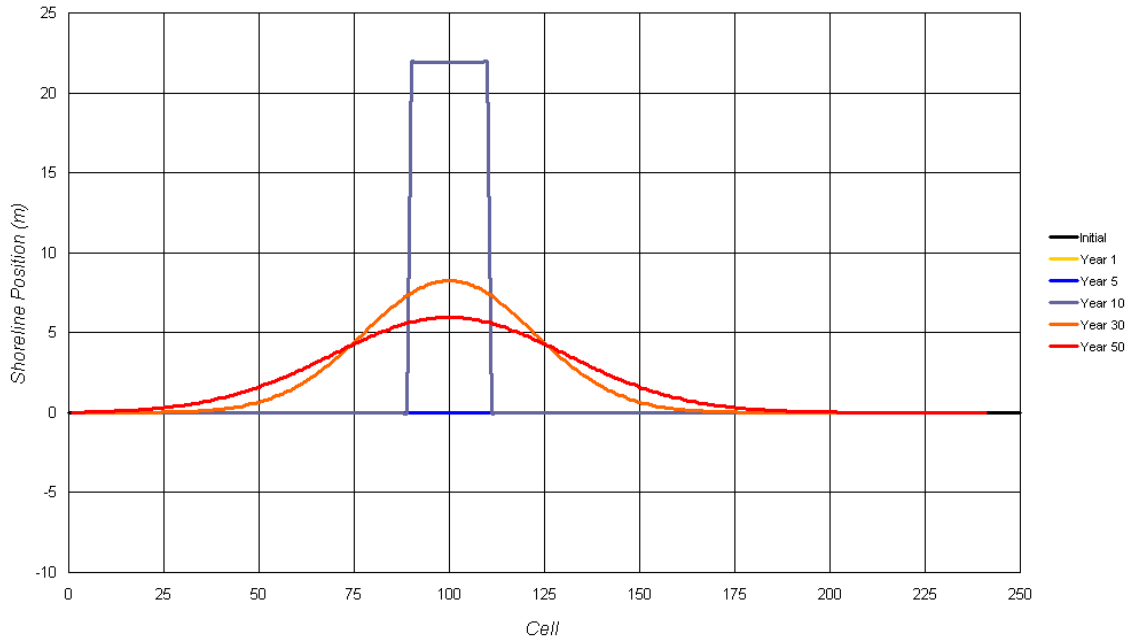

Figure 4-11. Case 2*a*: No seawall, one nourishment, and no breakwater. Shoreline evolution.

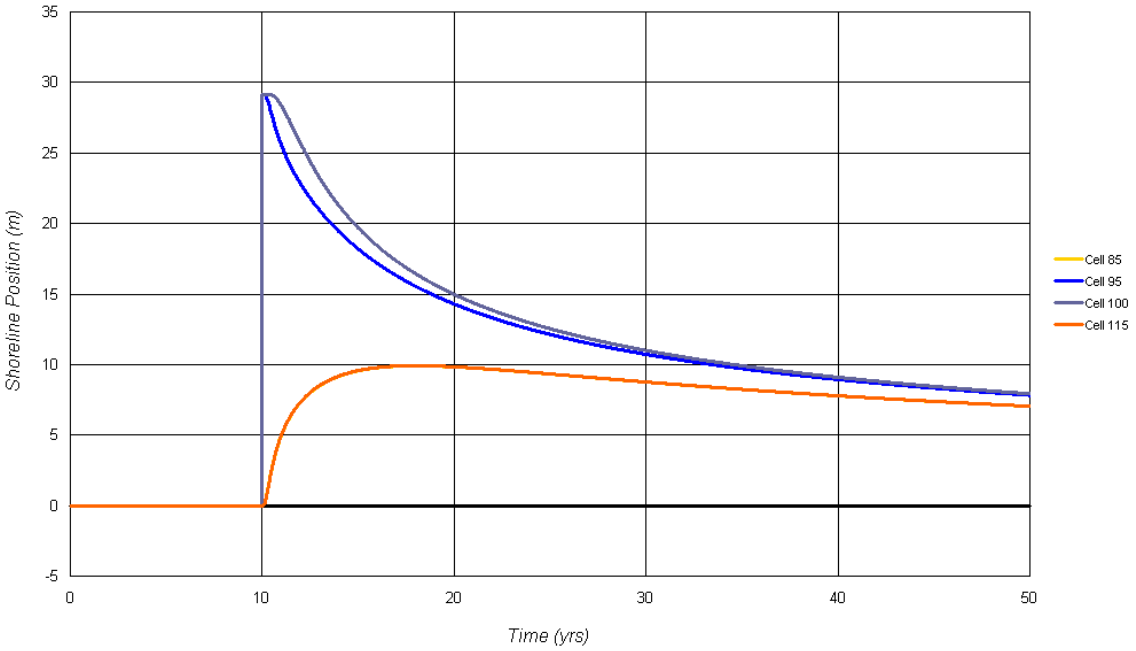

Figure 4-12. Case 2*a*: No seawall, one nourishment, no breakwater. Shoreline position by cell.

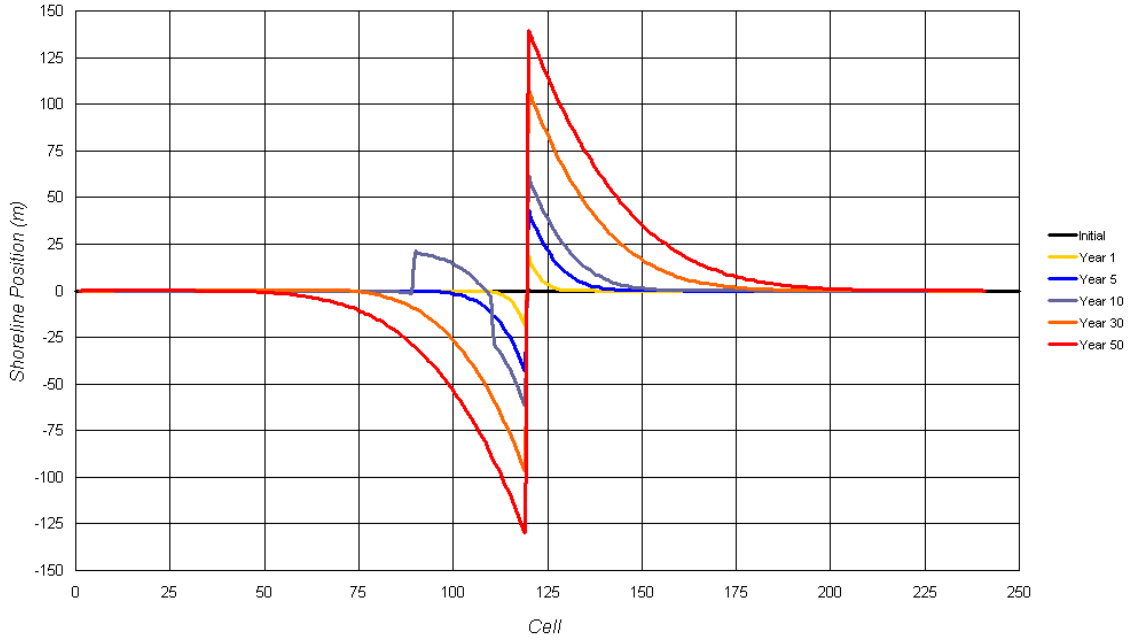

Figure 4-13. Case 2*b*: No seawall, one nourishment, one breakwater. Shoreline evolution.

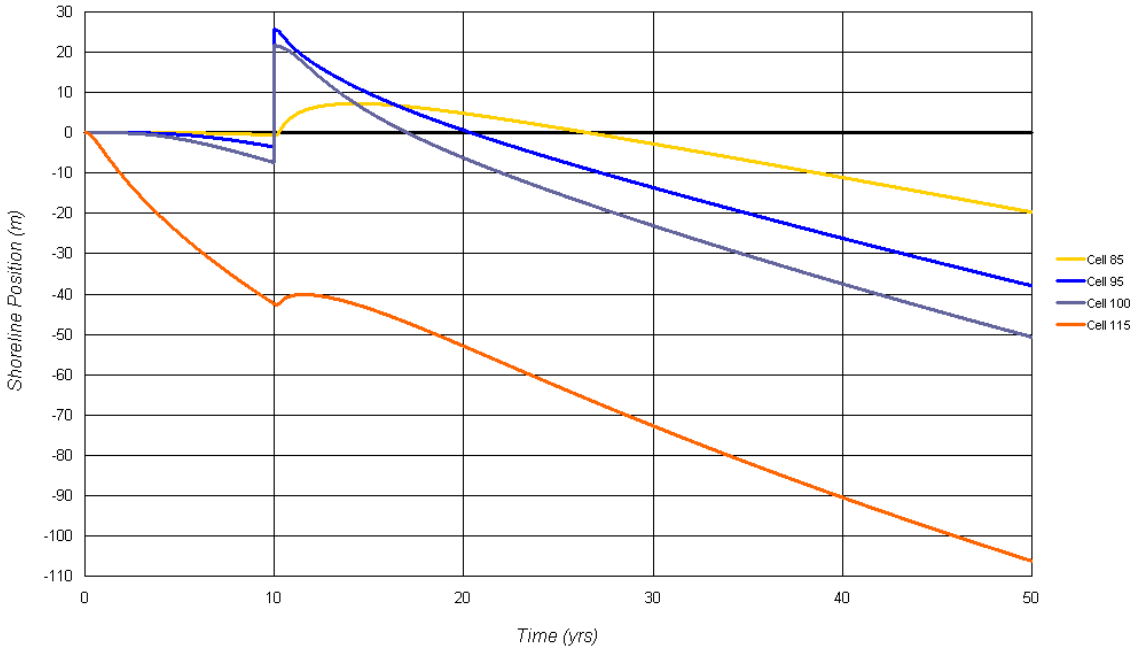

Figure 4-14. Case 2*b*: No seawall, one nourishment, one breakwater. Shoreline position by cell.

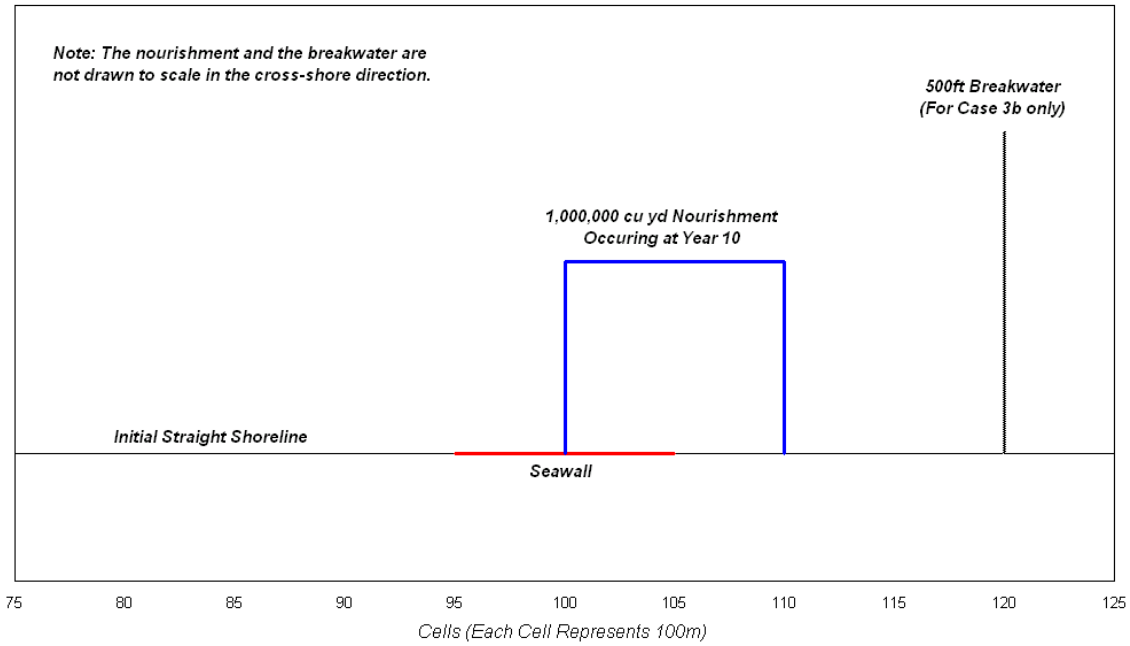

Figure 4-15. Input parameters for Case 3.

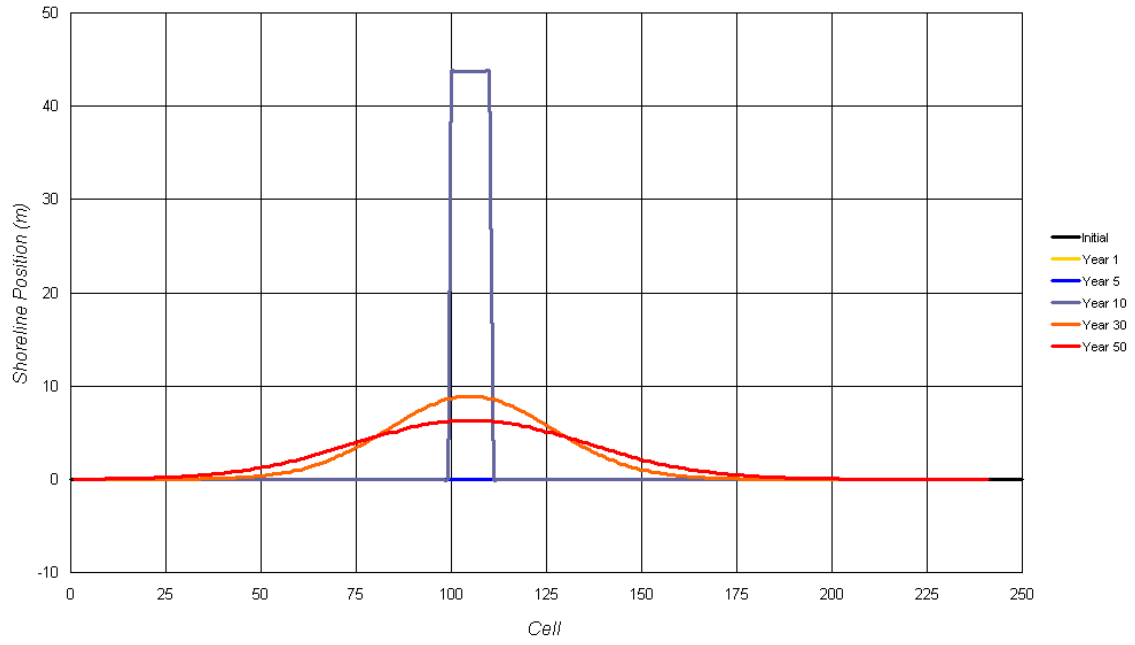

Figure 4-16. Case 3*a*: One seawall, one nourishment, no breakwater. Shoreline evolution.

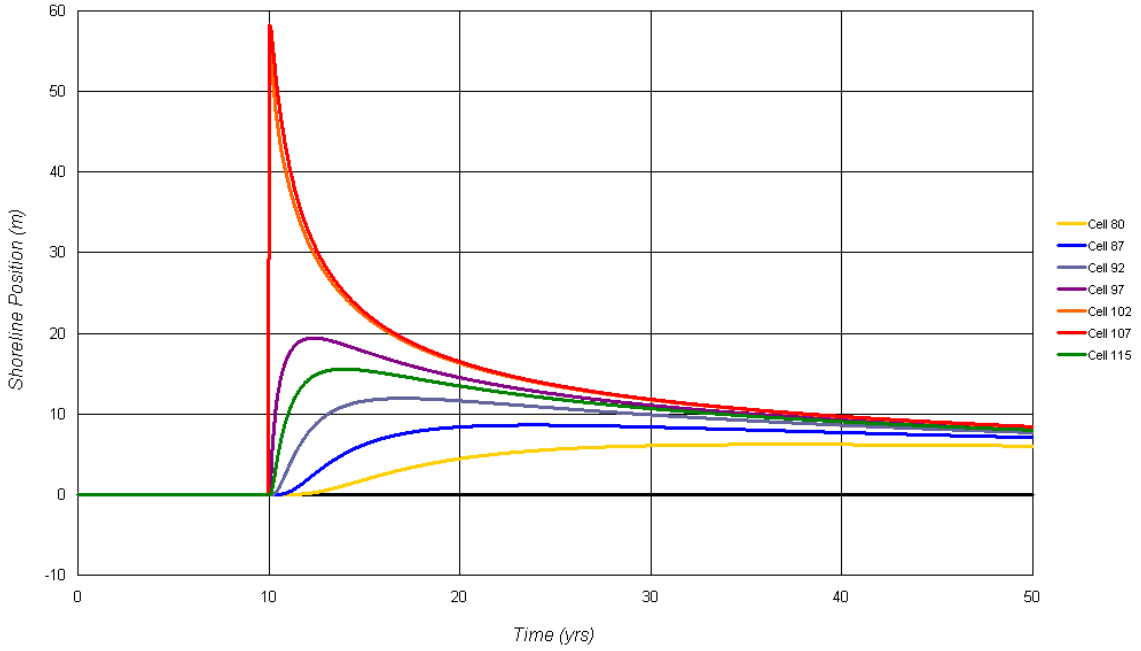

Figure 4-17. Case 3*a*: One seawall, one nourishment, no breakwater. Shoreline position by cell.

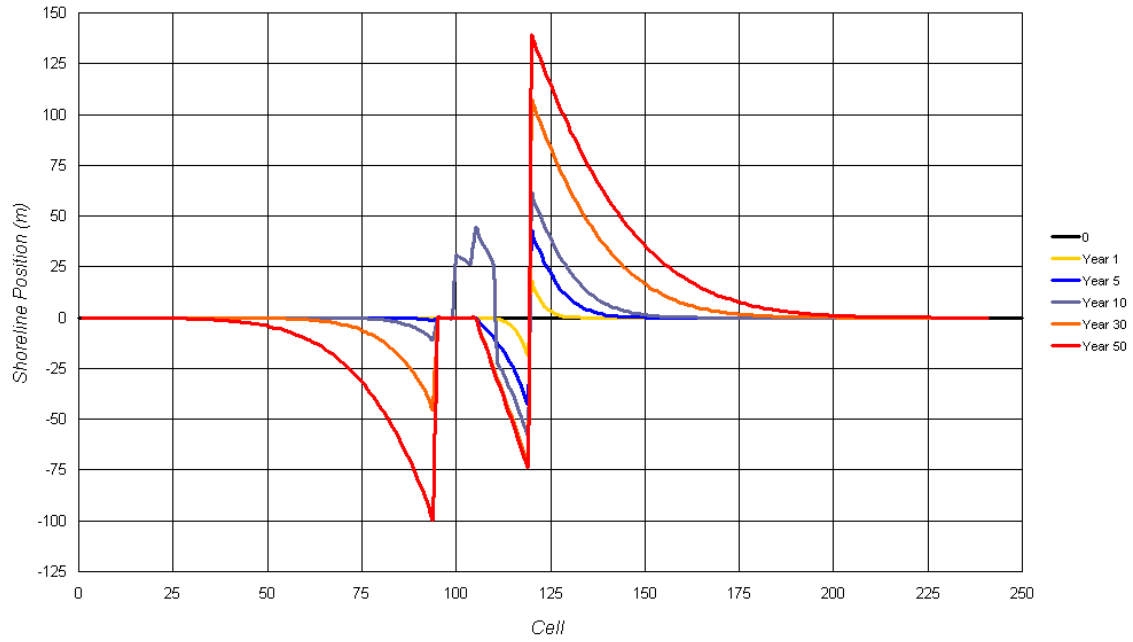

Figure 4-18. Case 3*b*: One seawall, one nourishment, one breakwater. Shoreline evolution.

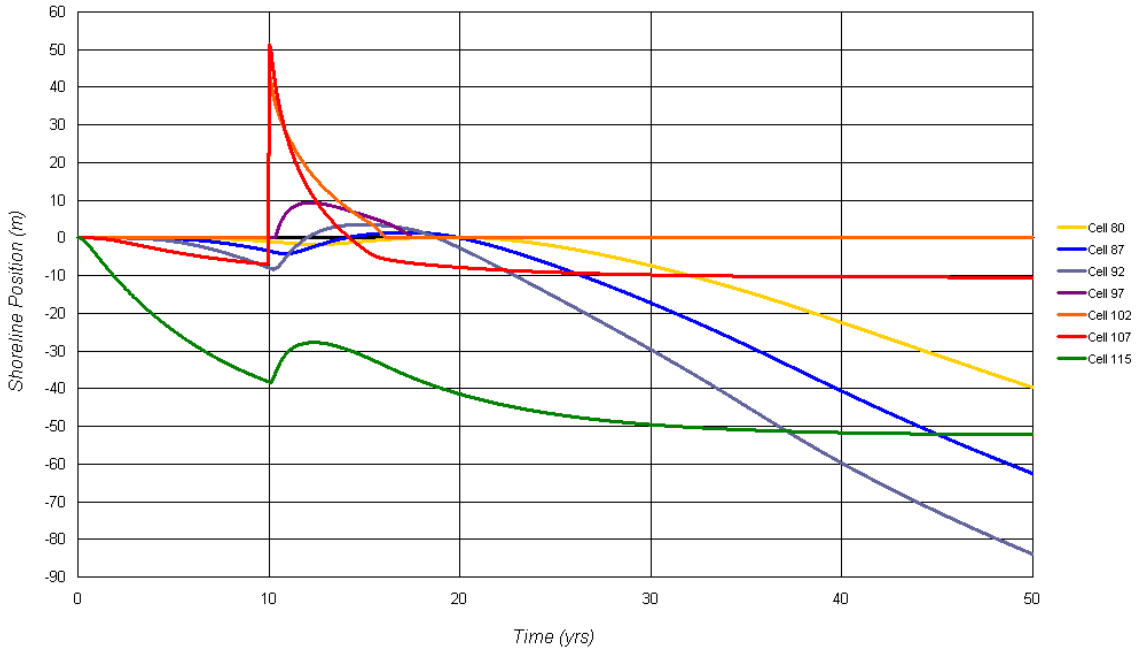

Figure 4-19. Case 3*b*: One seawall, one nourishment, one breakwater. Shoreline position by cell.

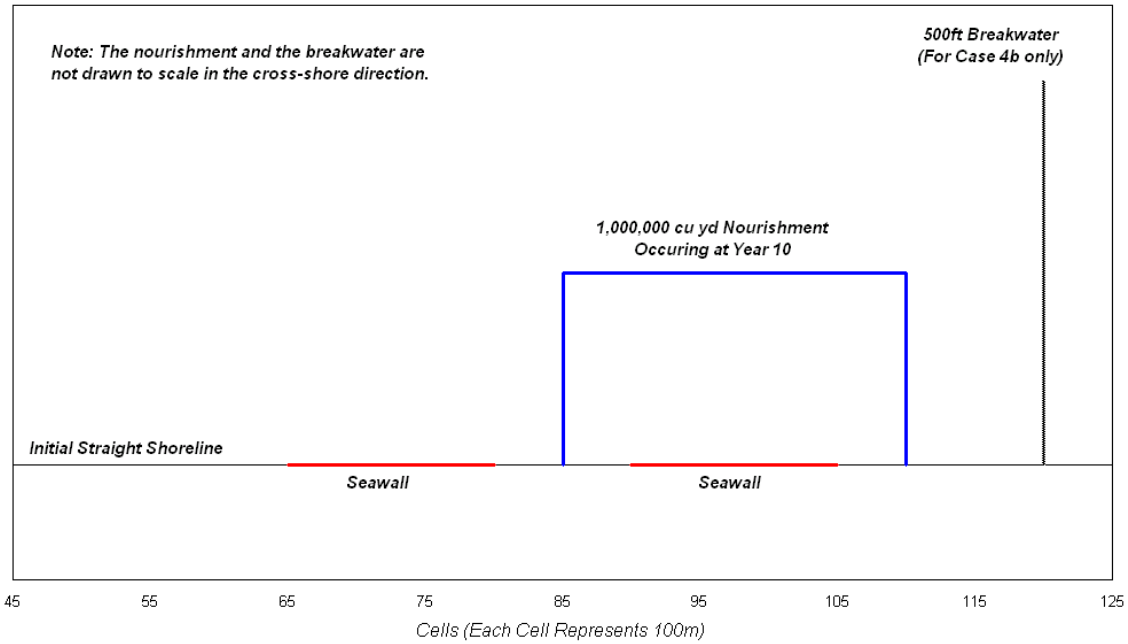

Figure 4-20. Input parameters for Case 4.

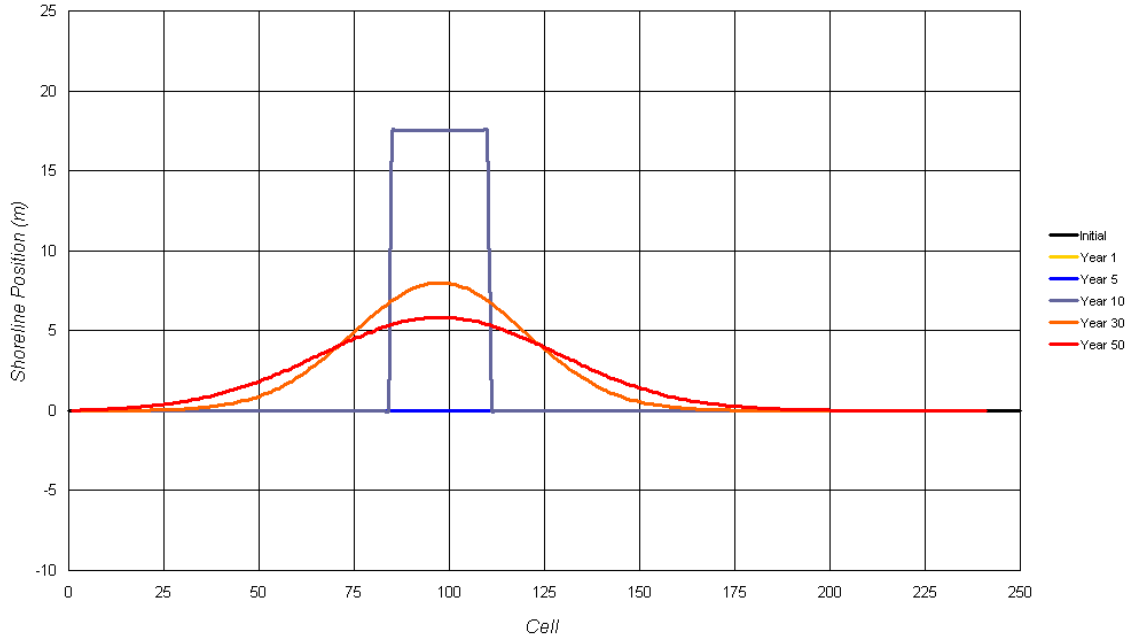

Figure 4-21. Case 4*a*: Two seawalls, one nourishment, no breakwater. Shoreline evolution.

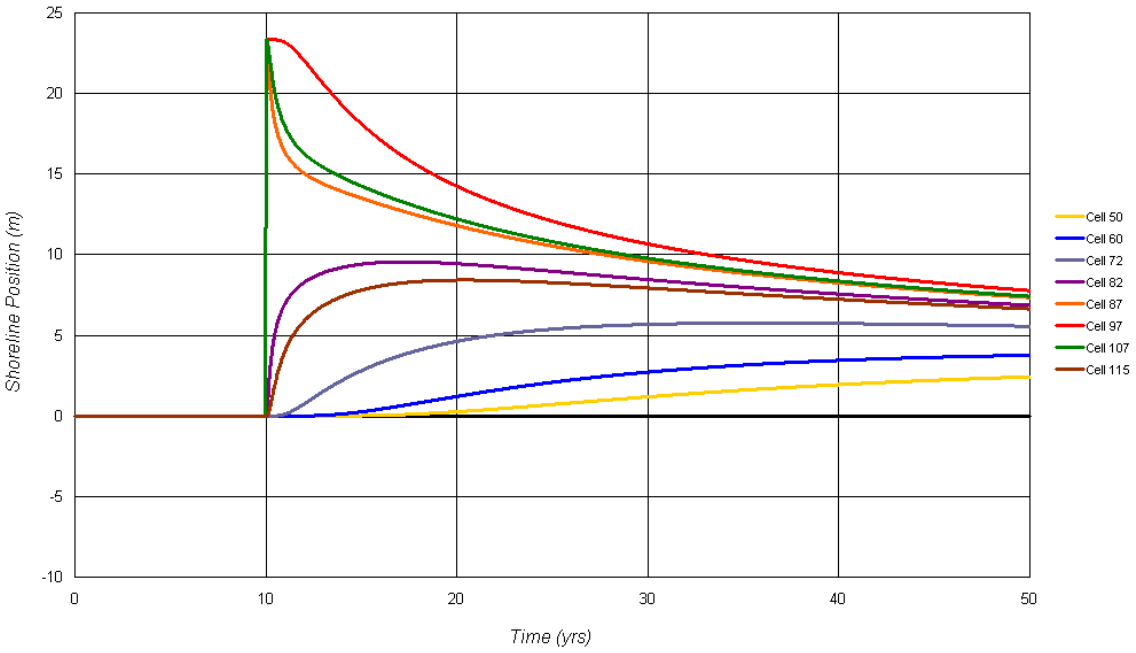

Figure 4-22. Case 4*a*: Two seawalls, one nourishment, no breakwater. Shoreline position by cell.

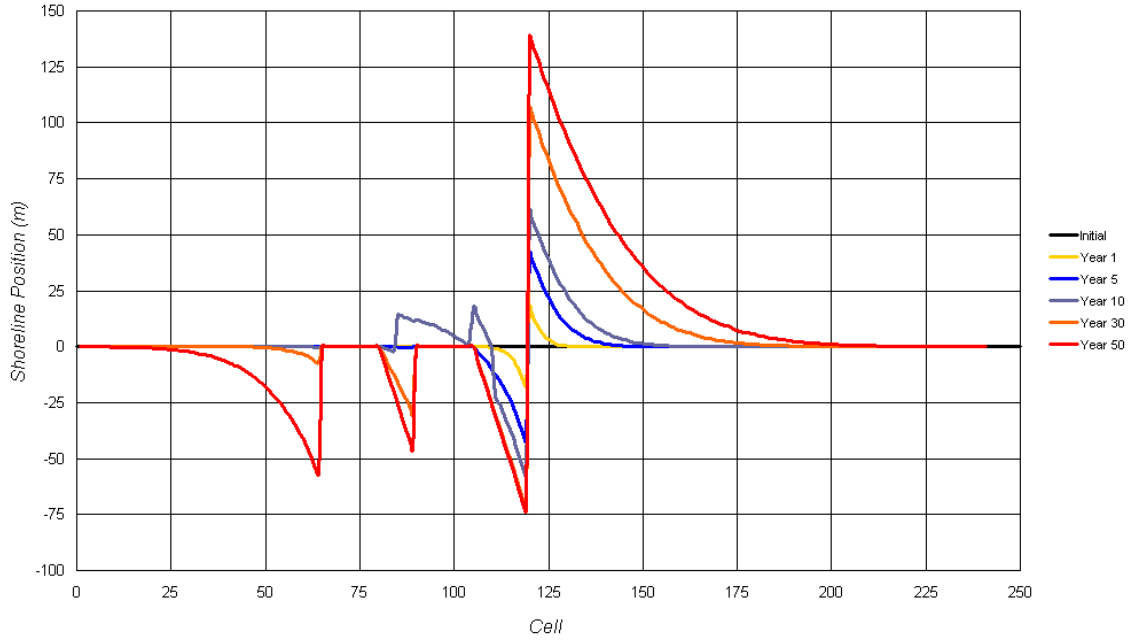

Figure 4-23. Case 4*b*: Two seawalls, one nourishment, one breakwater. Shoreline evolution.

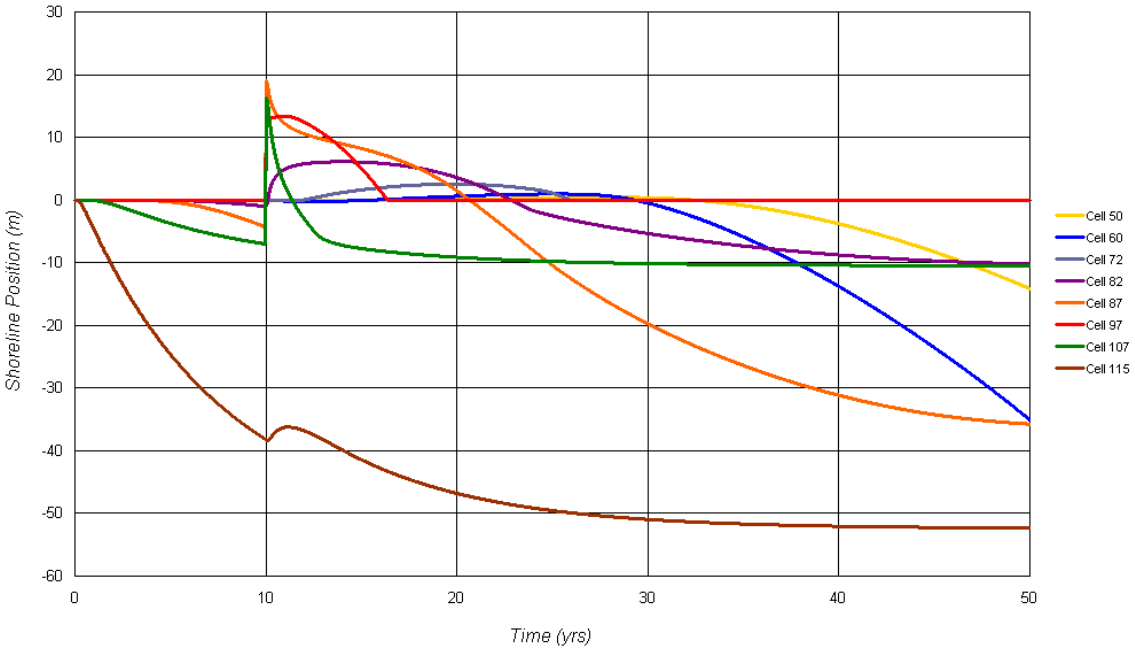

Figure 4-24. Case 4*b*: Two seawalls, one nourishment, one breakwater. Shoreline position by cell.

CHAPTER 5
OCEANSIDE MODEL DATA

This chapter describes the general content of the input/output (I/O) files and the specific values used for the Oceanside simulations. Input files define the groins, initial shoreline, nourishments, seawalls, sources/sinks, waves, and background erosion. The current version of the DNR model requires that input variables be defined in English units. Output files contain the saved variables that define the results of the simulation. The data displayed in the output file are also given in English units.

Input

Main Input File

The main input file must have the name 'InputMain' and must be in the same directory as the DNR executable. This input file provides the full paths and names for all other input files.

Constants

The Constants input file provides information about the sediment and other run parameters that remain unchanged throughout the simulation. These include the longshore sediment transport coefficient ($K = 0.35$), gravitational constant ($g = 9.81$ m^2/s or 32.18 ft^2/s), specific gravity of the sediment (usually defined for sand as 2.65), sediment porosity (usually defined for sand as 0.35), sediment grain size, the profile coefficient for an equilibrium profile, and a breaker index ($\kappa = 0.78$).

Total Depth

The total depth input file provides the closure depth and berm height at each cell. The present version of the DNR model requires these values to be uniform. Some variability exists in published closure depth values for this region of the coast north of San Diego. The United State Army Corps of Engineers (USACE, 1991b) estimated a 9.1-m (30-ft) closure depth in the Oceanside area. Boswell et al. (2004) found the closure depth equal to 7.6 m (25 ft). The 7.6-m (25-ft) closure depth value will be used since this is a more recent result. The berm elevation is 4.3 m (14 ft) (USACE, 1991b).

Groins

Groin lengths are defined as the perpendicular distance from the baseline to the seaward tip of the structure. As discussed in Chapter 2, structures defined in the groins input file include breakwaters, jetties, and groins. The only structures presently affecting littoral transport in the project area are the north and the south breakwaters at Oceanside Harbor, the San Luis Rey River groin, and the rubble base of the Oceanside Municipal Pier.

The lengths of the north and south breakwaters were taken from the USACE shoreline definition AutoCAD files provided by Ryan (2002). The effective lengths of these two structures were defined as the perpendicular distance from the baseline to the point on the structure farthest from the baseline. The lengths for the San Luis Rey River groin and the base of the Oceanside Municipal Harbor were found using the Maptech Mapserver website. First, the distance between the shoreline and the tip of the structures was found by converting the latitude and longitudinal coordinates of these locations to distances. Next, the actual shoreline positions were referenced to the 1998 shoreline to find the total distance from the baseline to the tips of these two structures. The change in

shoreline position from 1934 to 1998 was then incorporated to give the length of the structures referenced to the initial 1934 shoreline position.

The structures may be defined as impermeable or leaky. An impermeable structure blocks all longshore transport until the shoreline position is seaward of the tip of the structure. Leaky, or permeable, groins only block a portion of the transport. This amount is based on the fraction of the breaker zone blocked by the groin. In the groin input file, the location, length, date of installation, and groin type are specified for each groin or breakwater. For the Oceanside simulations, groins are considered leaky and breakwaters are impermeable. Table 5-1 shows the effective lengths these structures used in the model runs. The effective length of the San Luis Rey River groin is approximately 100 m (330 ft) shorter than its actual length because of sand passing through or over the groin.

It should also be noted that at a groin, the shoreline angle is based on the tip of the groin rather than the down drift cell. Normally, the orientation of the cross-shore distance between one cell and its adjacent downdrift cell defines the shoreline angle. However, when a groin is present, the shoreline angle is defined by the orientation between the tip of the groin and the cross-shore position of the adjacent, updrift cell. This results in a local modification of the transport at a groin.

Initial Shoreline

The DNR model can use the actual shoreline or a straight initial shoreline as an initial configuration. Using the actual shoreline requires that the wave heights and directions be accurately known along the shoreline. Furthermore, these wave characteristics are required at a detailed scale in the alongshore direction to avoid

interpolation errors. Small inaccuracies in the wave estimates can lead to large errors and dominate the results in the long-term simulations.

It has been observed that on most open coastlines, the alongshore wave conditions with respect to the local shoreline orientation tend to be uniform. If the local waves are uniform, then referencing to the local shoreline is equivalent to taking a straight initial shoreline and spatially constant wave conditions. The change in shoreline position over time is computed using this straight shoreline as the initial shoreline. The changes are then added to the actual initial shoreline position to give the actual predicted shoreline position.

This approach is less sensitive to small inaccuracies in wave conditions and is the approach recommended by Dean (2001) for shoreline modeling. This is the technique employed for the Oceanside simulations. However, the conditions at Oceanside are somewhat atypical. Carlsbad Canyon results in an alongshore variation in local wave conditions. This influence is included in the DNR model and discussed later in the waves section.

The actual initial shoreline for the historical runs is the May 1934 survey, which is shown in Figure 5-1. For the forecast runs, the initial shoreline is the April 1998 Lidar survey. The variation of the wave angles resulting from the Carlsbad Canyon at the southern end of the study area necessitates a modification of the wave direction in this area. This adjustment was developed for the 1934 to 1998 calibration runs using the 1934 shoreline as the initial condition. Since the model was calibrated for the 1934 initial shoreline, the 1998 shoreline was defined with respect to the 1934 shoreline for the forecast runs. This preserves the calibration coordinate system. The forecast runs do not

begin with a straight initial shoreline. Instead, they begin with the position of the 1998 shoreline relative to the 1934 shoreline.

The initial shoreline input file is also used to specify the computational cell length (must be constant), the number of cells, and the orientation of the local beach alignment with respect to north. For the present version of the model, all characteristics must be defined in English units.

Nourishment

The DNR model can address multiple nourishments at arbitrary times and locations. For each nourishment, the total volume of fill, the cells in which the fill is placed, and the date of the placement must be specified. It is assumed that the total volume of each individual nourishment is evenly divided among the cells. Cases with longshore variations in the fill volume may be addressed through multiple fills placed at the same time.

The nourishments input file defines the alongshore extent of the nourishment (first and last cell), volume (yd^3), placement time (hr), and fill factor. The fill factor is the relationship between the total volume of sediment in the beach nourishment and the volume of sediment that remains as part of the littoral system. The smaller the fill factor, the more sediment is lost from the littoral system. If all the sediment remains in the littoral system, the fill factor is equal to 1.0. Conversely, if all the sediment from the nourishment is lost from the littoral system, the fill factor is equal to 0.0.

A comparison between native and the fill sediments revealed that the median sediment size used as nourishment is smaller than the native sediment size located at Oceanside Beach (USACE, 1984). Because of this difference in sediment size, a fill factor with a value less than one is expected. Beach monitoring by Coastal Frontiers

Corporation (2004) resulted in a fill factor approximation of 0.8. For this project, a fill factor of 0.7 provides the best shoreline predictions. A detailed explanation of the historical nourishment locations and volumes was presented in Chapter 2.

For the nourishment input in the forecast simulations, the recent practices are assumed to continue in the future. The average dredged volume from the harbor from 1992 to 2003 had been 184,600 m^3/yr (241,500 yd^3/yr). This is the volume used for the future nourishments. Figure 2-8 shows the historical nourishment patterns, which reveals three major placement areas shown by the red, blue, and green lines. Future nourishments placements are assumed to alternate repeatedly between these three areas for the duration of the simulations.

At the southern end of the project area, several nourishments occurred that were associated with back-passing at Agua Hedionda Lagoon. In the forecast simulations, the back-passing rates are 38,000 m^3/yr (50,000 yd^3/yr). These nourishments are placed in the area denoted by the purple lines in Figure 2-8 along the Carlsbad shoreline.

Seawalls

The DNR model can accommodate multiple seawalls along the reach. At each cell with a seawall, the cross-shore location, height, and slope of the wall are given. Since the cells are 100 m wide, the seawalls are fit into cells by rounding their lengths accordingly either up or down. Furthermore, small spaces, or gaps in armoring, and very short seawalls (less than 50 m) are omitted. If the slope is set to 99, the model assumes a vertical wall. The water depth/berm elevation at the seawall is also specified. Berm elevation is given as a negative number and water depth as a positive number. Elevations in the DNR model for the Oceanside simulations are referenced to MSL.

The seawall height, or crest elevation, is the vertical distance from MSL to the top of the seawall. These elevations are obtained from two sources: 1) The GIS Study performed at Oceanside and 2) The Lidar Survey performed for the Oceanside littoral cell. These two references enable estimates of the elevations at the top of the seawalls with reasonable accuracy. This is important for the calculation of overtopping events. The GIS and the Lidar Surveys are taken from the NAVD88 reference, which is approximately 0.78 m (2.57 ft) below the MSL reference datum. Therefore, conversions are made accordingly. This topic was discussed in Chapter 2.

The cross-shore distance used for the seawall data input is a function of the initial shoreline position. If the actual initial shoreline is used, then the actual distance from the baseline to the seawall defines the seawall cross-shore position. If a straight initial shoreline is used, the cross-shore seawall distance is relative to the distance from the shoreline being referenced. In the Oceanside simulations, the initial shoreline is straight and referenced to the 1934 shoreline. Therefore, cross-shore seawall locations, y_{sw}, are the distances from the actual seawall locations, y_{swa}, to the 1934 shoreline positions, y_{1934} ($y_{sw} = y_{swa} - y_{1934}$). Table 5-2 shows the seawall parameters for the project area. For details on the specifications of the seawalls along the Carlsbad and Oceanside coastlines, refer to Chapter 2.

Sources/Sinks

Sources and sinks are gains or losses of sediment from the littoral system to or from external sources. Sources or sinks may be specified for any cell. A source may be used to account for sediment influx from a river or sand introduced to a down drift beach by bar by-passing. A sink may be used when there is shoreline retreat and the eroded sediment is finer than the native material. A portion of this finer sediment will be

removed from the littoral system. A sink may also be used at an up drift breakwater to account for by-passing sediment or loss to the offshore.

Sources and sinks are specified as volume per unit length per year. This definition is convenient for shoreline recession. For point processes, such as the sediment added by rivers, the total volume of sediment added in one year must be divided by the cell length to get the per unit length value for the cell. Input parameters for river sediment contributions for the project area are described in Chapter 2. Another important source/sink consideration is in the by-passing boundary condition at Oceanside Harbor.

The DNR model does not include inlet processes as the sediment passes the entrance to the harbor. By-passing may be included as a source/sink by removing the source nourishment sediment from one or more specified cells. At Oceanside Harbor, a source/sink is placed updrift of the north breakwater and also downdrift of the south breakwater.

The strength of the sources/sinks is estimated from a sediment budget at the breakwaters. In Figure 5-2, Q is the longshore sediment transport (LST) rate, $\underline{Q_d}$ is the dredging rate (the main source for downdrift nourishments), Q_f is the accumulation rate in the fillet north of the breakwater, and Q_o is the rate sediment is lost to the offshore. The amount of sediment lost to the offshore is a function of the LST rate ($Q_o = cQ$), where c is a constant.

Table 5-3 is an example of the sources/sinks for an annual longshore transport rate of 153,000 m^3/yr (200,000 yd^3/yr). The rate of accumulation in the north fillet was discussed in Chapter 2. The sediment from the north breakwater may be transported into the harbor, develop a shoal at the harbor entrance, by-pass the harbor, or be jetted by

currents into deeper water. In Table 5-3, it is assumed that the volume of sediment in the harbor is in equilibrium and the offshore loss coefficient is $c = 0.05$. The dredged volume of sediment removed from the harbor must have been supplied from either the north or south side of the harbor. The available sediment from the north side has been estimated, so the remainder must be provided south of the harbor. This is the source/sink strength for the south breakwater. The volume change rates for the areas marked 1 and 2 in Figure 5-2 are as follows:

$$\frac{dV_1}{dt} = Q - (Q - Q_f - Q_o) - Q_o = Q_f \tag{5.1}$$

$$\frac{dV_2}{dt} = -Q + (Q - Q_f - Q_o) - Q_d = -Q_f - Q_o - Q_d = -Q_f - cQ - Q_d \tag{5.2}$$

In the cell north of the harbor, the volume change rate is not a function of the LST rate. This is a result of the fillet accumulation rate being given as a constant based on limited field observations. At the cell south of the harbor, the updrift fillet accumulation rate is constant and the annual dredging rate is also constant, so the rate of volume change is weakly dependent on the LST through the term $Q_o = cQ$. A consequence of these harbor boundary conditions is that the shoreline response is insensitive to the magnitude of the LST. In a one-line model, shoreline changes are driven by gradients in longshore processes.

Waves

The waves are the most complex input file. The waves define the time step, run duration, and to a great extent, the mode in which the DNR model executes. The DNR model can be run in three modes, which are specified by the type of wave data: 1) Waves that are constant in space and time, 2) Waves that are constant in space and variable in

time, and 3) Waves that are variable in space and time. The complexity and computational effort increases with each of these cases. In each case, the specified wave data are the height (either significant or RMS), period, direction, and water depth.

For the case of waves that are constant in space and time, just a single, constant wave condition is provided. Some variation may be added to this constant wave to account for seasonal variations in direction by adding an annual sinusoidal change in the dominant wave direction. For waves that are uniform in space and variable in time, a single time series of waves is provided. This constant in space, variable in time condition is the wave case used for the Oceanside project. For waves that are variable in space and time, wave time series are provided at several wave stations along the reach. The waves at these stations are linearly interpolated to provide wave conditions at each computation cell at each time step. Waves that are variable in space and time significantly increase the run time for the model.

The wave input is also used to define the time step, run duration, and the length of the wave time series. If the run duration exceeds the length of the wave time series, the time series is repeated from the beginning. This process will repeat up to a maximum of five times. In the present version of the DNR model, the time step must be one hour.

The wave hindcast series, provided by O'Reilly are given at nine wave stations along the study area at the -12-m (-40-ft) contour. These are shown with respect to the April 1998 shoreline in Figure 5-3. The wave records from O'Reilly provide hourly estimates of significant wave height, H_s, peak wave period, T_p, peak wave direction, θ_p, radiation stress, S_{xy}, and water depth change from El Nino events. Radiation stress is determined by summing the radiation stresses at each wave frequency and direction in the

spectrum to get a total integrated value. This is important because it quantitatively determines the direction and magnitude of the LST. The LST equation in the DNR model uses H_s and T_p to compute the transport rather than directly using S_{xy}. The peak wave direction is slightly different than the direction of the integrated radiation stress. The local wave angle, θ_{eff}, which corresponds to the radiation stress direction, is determined by equating the integrated radiation stress with the computed radiation stress using H_s and T_p. This is done for every hour of wave data in the 50-year records. Figure 5-4 shows a comparison of θ_p and θ_{eff}. The average difference between the two is rather small (1.3º), and this definition of wave direction is consistent with the LST formulation in the DNR model.

The Carlsbad Canyon causes the offshore profile to become steeper. This is seen in Figure 2-3 where the -12-m (-40-ft) depth contour becomes closer to the shoreline from Oceanside Harbor to Agua Hedionda. This longshore variation in depth can also be seen in Figure 5-5, where the depth contours are given in 5-fathom intervals. The depth contours not being parallel to the shoreline introduces two difficulties: 1) The DNR model is a one-line model and assumes that the profile is the same at all alongshore locations, and 2) The wave angles referenced to the -12-m (-40-ft) contour are not the same as those referenced to the shoreline.

Figure 5-6 shows the shore normal directions used in the 90 O'Reilly wave computation locations and the shore normal directions determined from the 1934, 1972, and 1998 surveys. The orientation for the waves is based on NOS hydrographic surveys conducted in the 1970's and early 1980's (O'Reilly, 2004). North of the harbor, an offset exists of approximately 2º. South of the harbor, the difference is more significant and

varied. To partially account for this difference, the waves are transformed to the 1934 shoreline orientation since the 1934 shoreline is the initial shoreline condition used in the model simulations. The transformation applies a three-step procedure: 1) Refract the O'Reilly waves back out to deep water, 2) Convert to the 1934 shoreline orientation, and 3) Refract the waves back into the -12-m (-40-ft) contour. Results for this transformation are shown in Figure 5-7. North of the harbor, local wave angles are very similar. South of the harbor, there is a nearly constant 2º difference.

Figure 5-8 shows the local wave angle with respect to the 1934 shoreline for all O'Reilly wave calculation locations in the study area for one wave case (not the average of all 50 simulations). The head of Carlsbad Canyon comes close to the shoreline approximately 1,200 m (3,900 ft) south of Agua Hedionda Lagoon, which is outside of the project area. However, this anomaly affects processes occurring within the model bounds. The canyon causes the distance from the shoreline to the -9-m (-30-ft) contour to decrease almost linearly from Carlsbad Canyon to Oceanside Harbor. At the Oceanside pier, the -9-m (-30-ft) contour is approximately 750 m (2,500 ft) offshore, and at Agua Hedionda the -9-m (-30-ft) contour is approximately 600 m (2,000 ft) offshore. The result is that the -9-m (-30-ft) contour has an angle of 1.3º with respect to the shoreline. This causes a mean variation in wave direction south of the harbor.

The variation in mean direction is estimated by the piecewise linear approximations shown in Figure 5-8. North of the harbor, a great deal of variability exists. The blue line north of the harbor is the mean for all computational sites. The pink line is the location and local wave angle for Station 6. The wave time series at Station 6 is used in the project simulations, so the local wave angle variation south of the harbor is expressed

with respect to the wave directions north of the harbor. The variable wave direction at the southern end of the study area is explicitly included within the DNR model. This relationship between the highly variable wave directions north of the harbor and the wave directions south of the harbor is discussed in Chapter 6.

North of the harbor, waves are taken to be uniform in space and variable in time for the model simulations. A great deal of variability exists in the wave direction north of the harbor, so a single shoreline orientation was selected which gave the appropriate LST (153,000 m^3/yr or 200,000 yd^3/yr) at a location north of the harbor that was outside the influence of human intervention near the northern part of the project area. LST rates were discussed in Chapter 2.

Background Erosion

As mentioned earlier, the background erosion input file creates a gradient in the longshore sediment transport to simulate a specified shoreline retreat. This method of defining background erosion was not used in the Oceanside simulations.

Output

The output file specifies which variables are to be saved (including shoreline positions, areas, volumes, and transport rates). The time interval and/or locations at which these values are saved are specified in this file. The DNR model automatically saves a shoreline position output file, a run summary file, and an error message file. For the Oceanside project, an overtopping and bore propagation file was also saved.

Table 5-1. Cross-shore location and effective lengths of breakwaters and groins along the Oceanside coastline.

Structure	Cross-shore Location (Cell)	Effective Length from Baseline (ft)	Effective Length from Baseline (m)
Oceanside Pier	65	-482	-147
San Luis Rey Groin	78	-95	-29
South Breakwater	86	636	194
North Breakwater	96	1860	567

Table 5-2. Seawall input parameters for the Oceanside and Carlsbad shorelines.

Cell	y from 1934 Straight Initial Shoreline (ft)	MTL Seawall Elevation (ft)	Seawall Slope	Depth at Toe (ft)	MTL Backshore Elevation (ft)	SW Description
1	-211.62	10.23	0.5	-14.0	10.23	Rubble
2	-196.44	20.83	0.5	-14.0	33.13	Rubble
3	-184.74	20.83	99.0	-14.0	35.43	Vertical seawall walkway
4	-193.23	20.83	99.0	-14.0	40.73	Vertical seawall walkway
5	-188.40	20.83	99.0	-14.0	46.33	Vertical seawall walkway
6	-184.44	20.83	99.0	-14.0	46.93	Vertical seawall walkway
7	-177.09	20.83	99.0	-14.0	46.33	Vertical seawall walkway
8	-174.96	20.83	99.0	-14.0	45.63	Vertical seawall walkway
9	-186.17	20.83	99.0	-14.0	45.93	Vertical seawall walkway
10	-174.94	20.83	99.0	-14.0	48.23	Vertical seawall walkway
11	-169.17	20.83	99.0	-14.0	48.63	Vertical seawall walkway
12	-185.92	20.83	99.0	-14.0	47.93	Vertical seawall walkway
13	-186.02	43.33	0.5	-14.0	43.33	Rubble
14	-199.81	25.93	99.0	-14.0	25.93	High cliff
15	-223.55	25.93	99.0	-14.0	25.93	High cliff
16	-222.20	17.93	99.0	-14.0	17.93	Home foundations
17	-233.64	17.93	0.5	-14.0	17.93	Rubble
18	-242.74	16.93	99.0	-14.0	16.93	Private vertical seawall
19	-249.28	12.53	0.5	-14.0	32.73	Rubble
20	-256.23	24.53	99.0	-14.0	25.13	Private vertical seawall
21	-258.53	16.93	99.0	-14.0	18.73	Home foundations
22	-252.39	18.73	0.5	-14.0	38.43	Rubble
23	-221.04	15.83	99.0	-14.0	18.43	Private vertical seawall
24	-220.67	16.43	0.5	-14.0	37.23	Rubble
25	-254.15	9.43	0.5	-14.0	9.43	Bridge over Buena Vista Lagoon
26	-277.77	10.43	0.5	-14.0	10.43	Rubble
27	-266.25	11.43	0.5	-14.0	12.43	Rubble
28	-246.98	11.43	0.5	-14.0	11.43	Rubble
29	-248.77	11.43	0.5	-14.0	12.43	Rubble
30	-255.60	13.43	0.5	-14.0	15.43	Rubble
31	-267.22	12.43	0.5	-14.0	13.43	Rubble
32	-290.70	12.43	0.5	-14.0	14.43	Rubble
33	-316.78	14.43	0.5	-14.0	16.43	Rubble
34	-334.52	15.43	0.5	-14.0	16.43	Rubble
35	-366.82	13.43	0.5	-14.0	15.43	Rubble
36	-373.41	11.43	0.5	-14.0	13.43	Rubble
37	-351.67	13.43	0.5	-14.0	14.43	Rubble

Table 5-2. Continued

Cell	y from 1934 Straight Initial Shoreline (ft)	MTL Seawall Elevation (ft)	Seawall Slope	Depth at Toe (ft)	MTL Backshore Elevation (ft)	SW Description
38	-335.60	11.43	0.5	-14.0	13.43	Rubble
39	-321.33	15.43	0.5	-14.0	15.43	Rubble
40	-320.28	12.80	0.5	-14.0	12.43	Rubble
41	-324.31	12.00	0.5	-14.0	11.43	Rubble
42	-440.84	10.60	99.0	-14.0	11.43	Bridge over Loma Alta Creek
43	-299.51	12.90	0.5	-14.0	12.43	Rubble
44	-284.15	15.50	0.5	-14.0	17.43	Rubble
45	-282.10	15.80	0.5	-14.0	17.43	Rubble
46	-286.87	14.80	0.5	-14.0	16.43	Rubble
47	-296.83	15.80	0.5	-14.0	13.43	Rubble
48	-334.37	12.80	0.5	-14.0	17.43	Rubble
49	-373.33	15.50	0.5	-14.0	17.43	Rubble
50	-396.43	13.43	0.5	-14.0	14.43	Rubble
51	-413.39	11.43	0.5	-14.0	11.43	Rubble
52	-428.55	11.43	0.5	-14.0	13.43	Rubble
53	-405.33	13.43	0.5	-14.0	13.43	Rubble
54	-366.06	11.43	0.5	-14.0	11.43	Rubble
55	-369.01	11.20	0.5	-14.0	11.43	Rubble
56	-389.85	11.20	0.5	-14.0	9.43	Rubble
57	-406.51	11.20	0.5	-14.0	9.43	Rubble
58	-420.75	11.20	0.5	-14.0	9.43	Rubble
59	-430.30	11.20	0.5	-14.0	9.43	Rubble
60	-434.78	11.20	0.5	-14.0	9.43	Rubble
61	-455.35	11.20	99.0	-14.0	10.43	Curb
62	-482.27	11.20	99.0	-14.0	10.43	Curb
63	-506.80	11.20	99.0	-14.0	10.43	Curb
64	-525.75	11.20	99.0	-14.0	9.43	Curb
65	-537.58	11.20	99.0	-14.0	9.43	Curb
66	-544.38	11.70	99.0	-14.0	9.43	Curb
67	-552.60	11.70	99.0	-14.0	9.43	Curb
68	-569.35	11.70	99.0	-14.0	10.43	Curb
69	-569.69	11.70	99.0	-14.0	10.43	Curb
70	-560.51	11.70	99.0	-14.0	9.43	Curb
71	-574.73	11.70	99.0	-14.0	9.43	Curb
72	-592.60	11.70	99.0	-14.0	9.43	Curb
73	-596.29	11.70	99.0	-14.0	9.43	Curb
74	-524.60	11.70	99.0	-14.0	9.43	Curb

Table 5-2. Continued

Cell	y from 1934 Straight Initial Shoreline (ft)	MTL Seawall Elevation (ft)	Seawall Slope	Depth at Toe (ft)	MTL Backshore Elevation (ft)	SW Description
75	-447.94	14.80	99.0	-14.0	11.43	Timber vertical SW
76	-666.33	14.80	99.0	-14.0	11.43	Timber vertical SW
77	-781.12	9.43	99.0	-14.0	9.43	Bridge
78	-602.95	13.30	99.0	-14.0	9.43	Curb
79	-540.18	13.30	99.0	-14.0	9.43	Curb
80	-506.21	14.30	99.0	-14.0	9.43	Curb
81	-488.18	13.30	99.0	-14.0	9.43	Curb
82	-492.07	14.20	99.0	-14.0	9.43	Curb
83	-435.57	13.80	99.0	-14.0	9.43	Curb
84	-283.44	13.80	99.0	-14.0	9.43	Curb
85	-164.43	13.80	99.0	-14.0	9.43	Curb

Table 5-3. Source/sinks at the north and south breakwaters.

Longshore Transport (yd^3/yr)	North Fillet (yd^3/yr)	North BW Source/Sink (yd^3/yr)	Dredging (yd^3/yr)	Offshore Losses (yd^3/yr)	South BW Source/Sink (yd^3/yr)
200,000	40,000	-160,000	241,500	10,000	-91,500

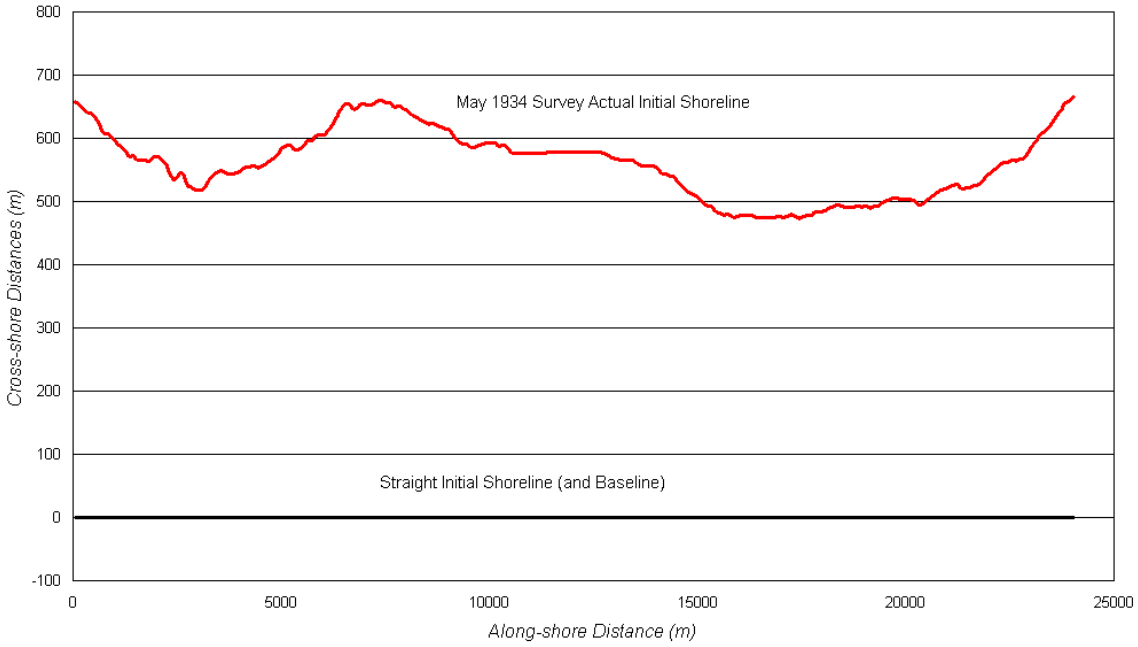

Figure 5-1. May 1934 shoreline and straight initial shoreline.

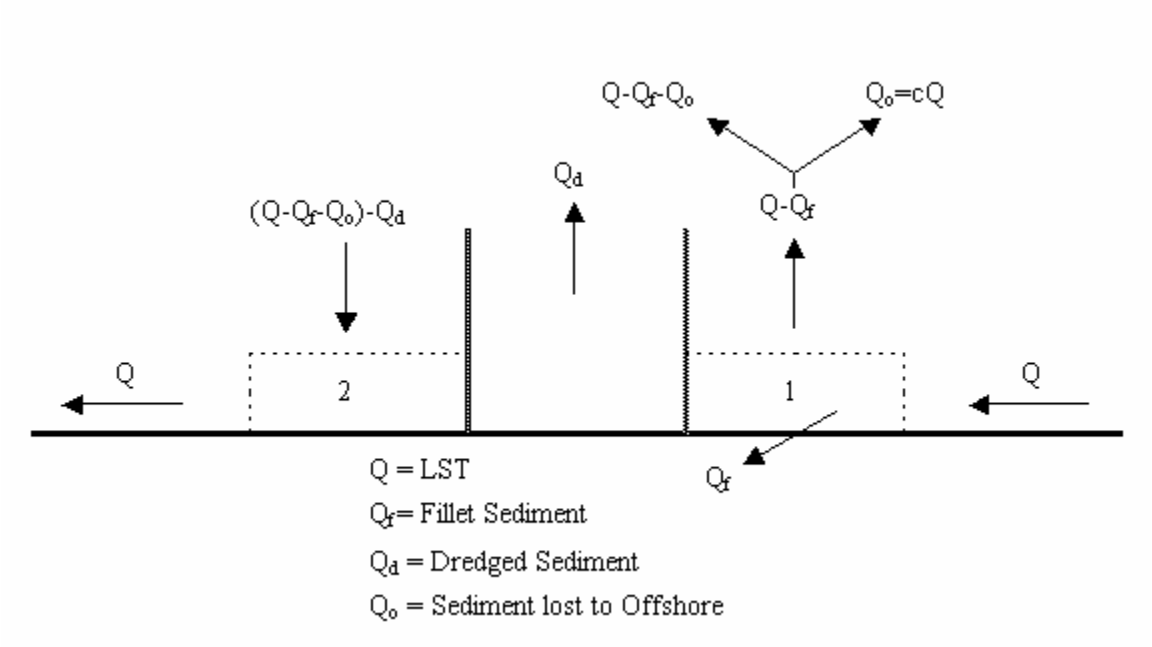

Figure 5-2. Sediment budget north and south of Oceanside Harbor.

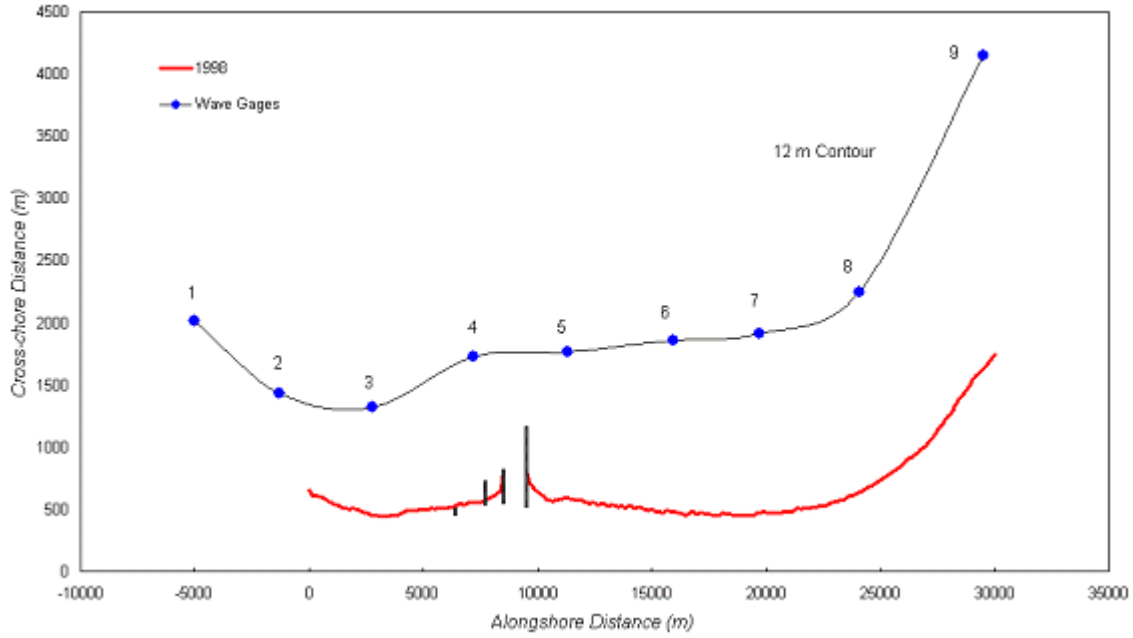

Figure 5-3. O'Reilly hindcast wave gage locations and approximate -12-m contour.

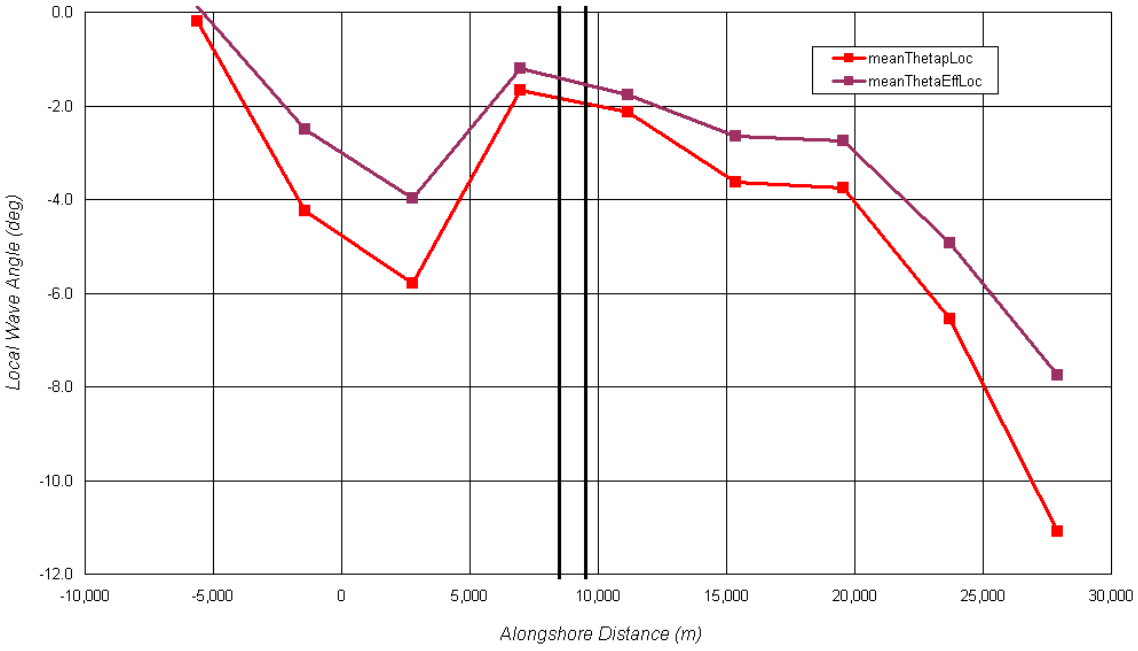

Figure 5-4. Mean peak wave angle and mean effective wave angle from the 50 wave records for each of the nine wave station.

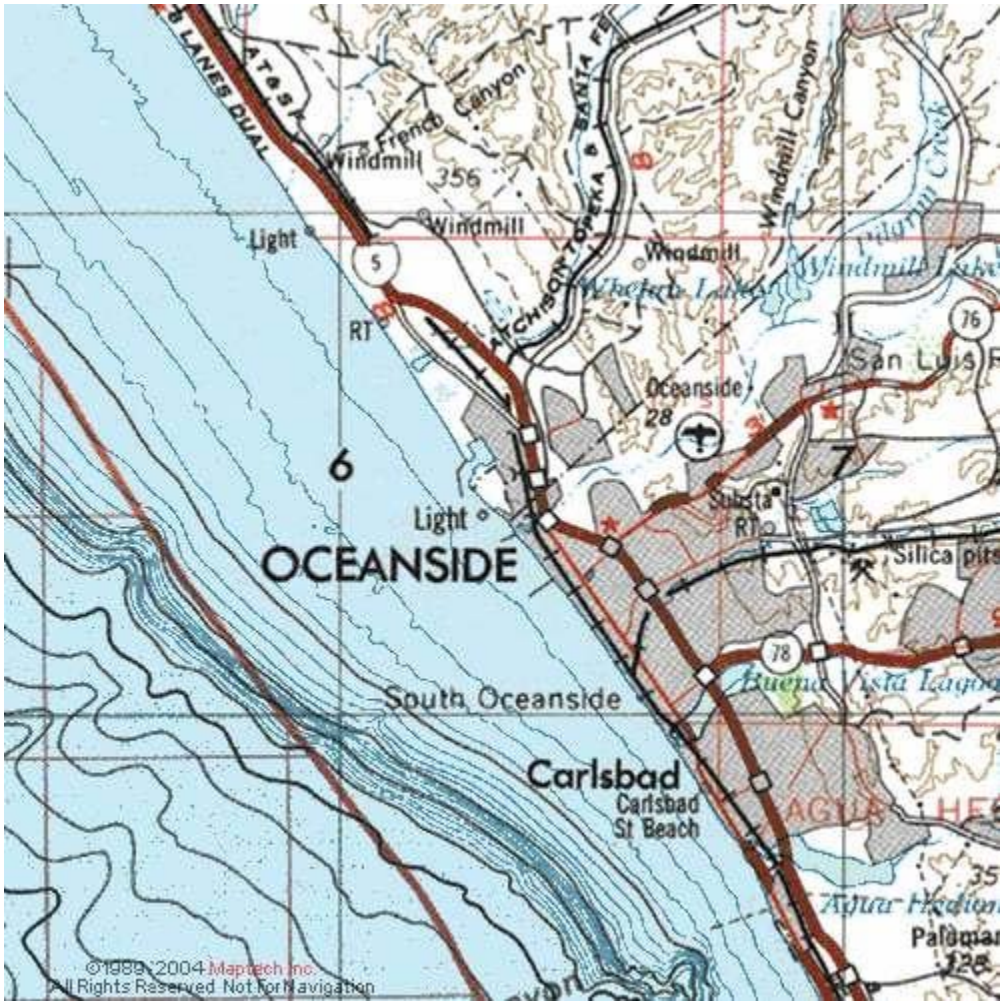

Figure 5-5. Depth contours along the study area shown in 5-fathom intervals.

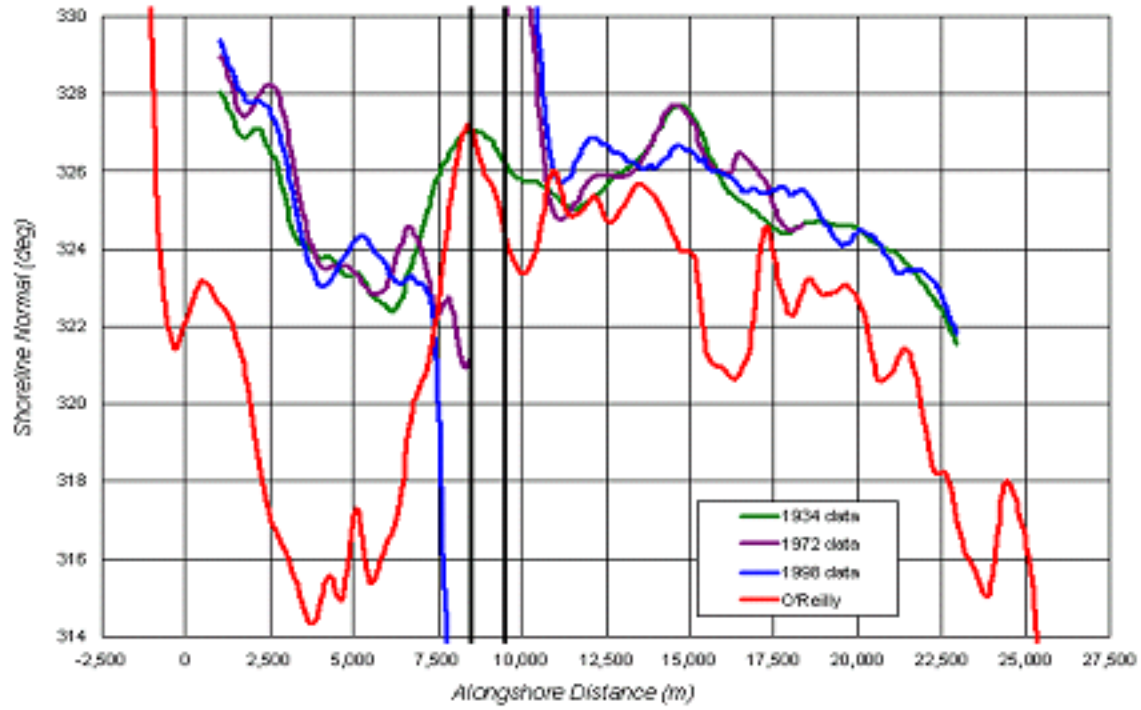

Figure 5-6. The shore normal direction used in the O'Reilly wave computations and the shore normal directions determined from the 1934, 1972, and 1998 surveys.

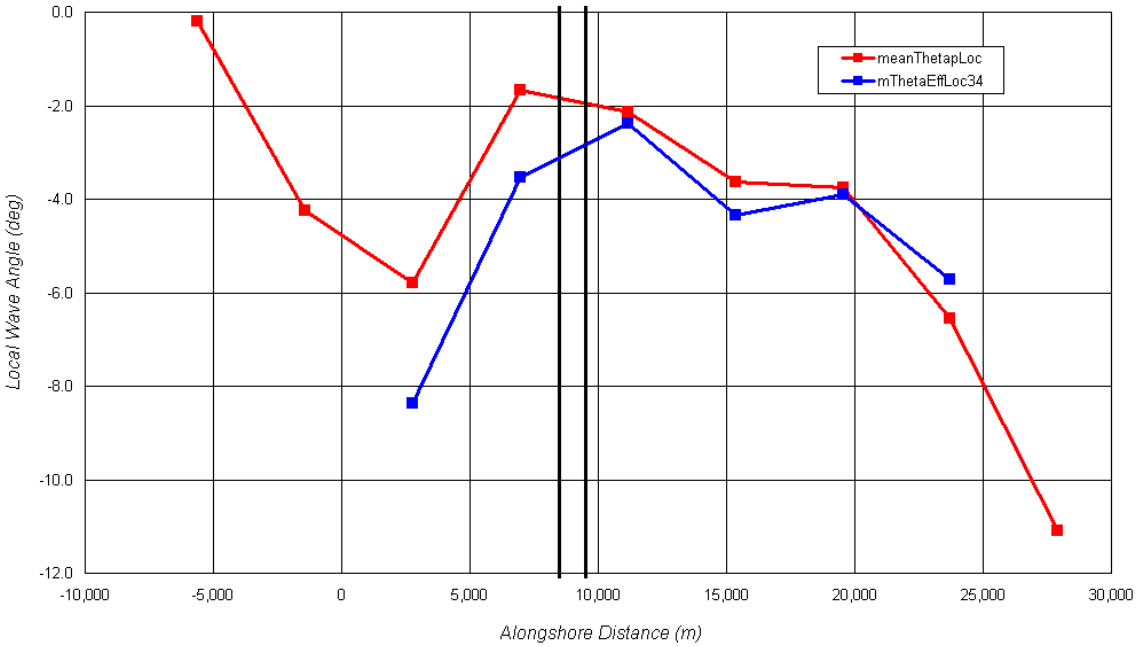

Figure 5-7. Mean peak wave angle and mean effective wave angle results from the wave transformation to the 1934 shoreline orientation.

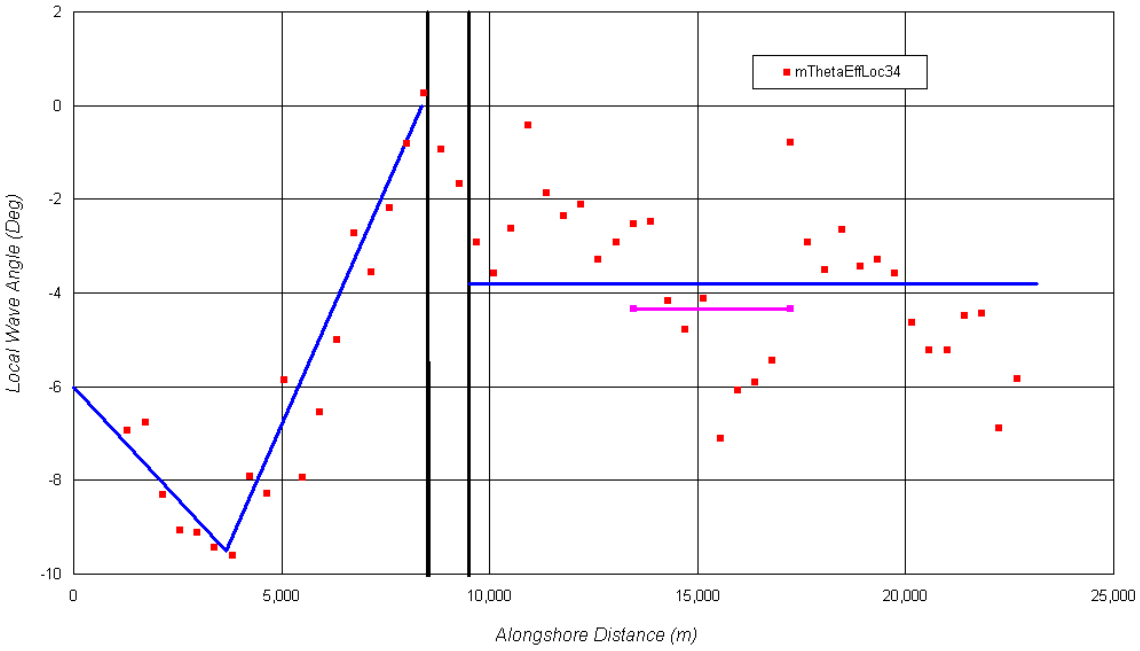

Figure 5-8. The local wave angle with respect to the 1934 shoreline for all the O'Reilly wave calculation locations within the study area. This data is representative of only one of the wave records with values similar to the mean of the 50 wave records.

CHAPTER 6
RESULTS

This chapter presents preliminary results for the Oceanside shoreline simulations. Sensitivity analyses results are presented for the alongshore wave variation, the nourishment fill factor, and the offshore loss coefficient. Calibration results are evaluated by comparing calculated shorelines with the 1972 and 1998 measured shorelines. After calibration, the model was run to estimate the historical responses from 1934 to 1998 with and without the harbor. Forecast runs were made for the period from 1998 to 2058 with and without the harbor that included damage estimates.

Sensitivity Analysis

A number of DNR runs are conducted to determine the sensitivity to input parameters. The calibration simulations begin with the measured 1934 shoreline, and end in 1998. The RMS errors between the predicted and measured shorelines in 1972 and 1998 are computed. Results lead to the refinement of several input parameters, and the process is repeated until the RMS error is minimized. Seawall locations, initial and final shorelines, and nourishment volumes and placement locations are available from previous studies, so these parameters are not adjusted. Although guidance for other input variables, such as the nourishment fill factor, offshore loss of sediment at the north breakwater, and local wave angle can be taken from other published studies, the actual processes that define these characteristics are not as well known. Therefore, calibration is necessary for these parameters to achieve satisfactory results.

Alongshore Wave Variation

The alongshore variation in wave direction follows from the discussion in Chapter 5. Figure 5-8 shows a V-shaped variation in local wave angle south of the harbor. The local wave angle at Agua Hedionda, which is the southern end of the "V", is estimated to be -6º. The wave input for the entire coast is referenced to Station 6, which is north of the harbor and has an average local wave angle of -4º. However, the local wave angles for the entire reach north of the harbor show significant variations. Using Station 6 as the reference presents an obstacle since it may or may not be a good representation of local wave angle north of the harbor. Furthermore, the local wave angle adjustments south of the harbor are dependent on the constant value chosen for the coastline north of the harbor.

The variation in local wave angles north of the harbor does not greatly influence the shoreline planform evolution north of the harbor. However, since the shoreline south of the harbor is dependent on the local wave angle of Station 6, adjustments are necessary to achieve reasonable results. Figure 6-1 shows the RMS error between the predicted and the measured shorelines south of the harbor in 1972, 1998, and for both combined based on the V-shape wave angle variation south of the harbor as a function of the local wave angle at Agua Hedionda Lagoon. The reference local angle at Agua Hedionda is changed from -3º to +3º. The optimum local wave angle at Agua Hedionda in terms of minimizing the RMS error for all 50 wave runs is +1º. This result suggests that the local wave angle at Agua Hedionda is equal to +5º the local wave angle at Station 6, which is -4º.

Fill Factor

The fill factor is the portion of nourishment that remains in the littoral system. Coastal Frontiers (2004) determined a fill factor of $FF = 0.8$ from field surveys

conducted at Oceanside Beach. Figure 6-2 shows the RMS errors for the shoreline south of the harbor for different fill factors. Results are given for three longshore sediment transport (LST) rates and for a range of offshore loss coefficients. The offshore loss coefficient was discussed in Chapter 5. A fill factor of $FF = 0.7$ gives the best agreement with the shoreline data.

Offshore Loss Coefficient

Inman and Jenkins (1983) assumed that 20% of the longshore transport on the north side of the harbor was either trapped or lost offshore. In the present analysis, the trapping by the north breakwater and the offshore losses are separated. The trapping in the north fillet is taken as 30,600 m^3/yr (40,000 yd^3/yr). The loss to the offshore is considered to be a portion of the longshore transport. It is expected that the greater the LST, the greater the amount of sediment that is deflected to the offshore. Results from Inman and Jenkins (1983) showed that offshore loss is approximately 4% of the net transport for a net transport of 194,200 m^3/yr (254,000 yd^3/yr) and a fillet-trapping rate of 30,600 m^3/yr (40,000 yd^3/yr).

Figure 6-3 shows the RMS error as a function of LST rates for various offshore loss coefficients. At all LST rates, the lowest RMS error occurs for zero offshore loss. At a LST of 152,900 m^3/yr (200,000 yd^3/yr), the RMS error difference between $c = 0.00$ and $c = 0.05$ is approximately 0.6 m (2 ft), which is not a significant difference. Since it is recognized that offshore losses do occur, an offshore loss coefficient of $c = 0.05$ is used for the Oceanside simulations.

Calibrated Shoreline Planform Results

A range of LST rates exist, which in combination with reasonable choices for other input information, yields similarly accurate estimates for the predicted shorelines. The

shoreline response is rather insensitive over long periods of time to the magnitude of the LST since shoreline changes are primarily attributable to gradients in the LST rather than the magnitude of the transport. Using constant values for the accumulation rate of the north fillet, the by-passing of the harbor, and the harbor dredging combine to reduce the sensitivity of the shoreline response with respect to the magnitude of the LST. Therefore, published values for LST are used as guidance. As discussed in Chapter 2, reported LST rates range from approximately 76,000 to 191,000 m^3/yr (100,000 to 250,000 yd^3/yr) with a typical value of 153,000 m^3/yr (200,000 yd^3/yr). A LST of 153,000 m^3/yr (200,000 yd^3/yr) is used in the DNR model runs.

Historical Runs

Historical runs are from 1934 to 1998. Figure 6-4 shows the shoreline positions in 1972 and in 1998. The figure gives the RMS errors north and south of the harbor and the combination of the 1972 and 1998 RMS errors. Comparison of the measured and calculated shorelines shows good results north of the harbor. The RMS error for 1972 is 13.1 m (43.0 ft) and the RMS error for 1998 is 18.3 m (60.0 ft). The combined RMS error for the shoreline north of the harbor is 15.9 m (52.2 ft). South of the harbor, the agreement is reasonable between the measured and the calculated shorelines. The RMS errors for 1972, 1998, and the combination of the two dates are 22.0 m, 20.6 m, and 21.3 m (72.1 ft, 67.6 ft, and 69.9 ft), respectively. A substantial amount of the error occurs between the San Luis Rey river groin and the south breakwater. The DNR model does not include wave modifications associated with breakwaters, so less accurate result near breakwaters are expected.

Figure 6-5 shows the annual shoreline recession rates for the periods 1934 to 1972, 1972 to 1998, and 1934 to 1998. The 1934 to 1972 and 1934 to 1998 measured and

predicted shoreline change rates are in good agreement both north and south of the harbor. The main differences occur near the breakwaters where the DNR model does not include breakwater effects. The measured changes for 1972 to 1998 show significant alongshore variation not seen for the other time intervals. The DNR model approximates the trends in the result, but does not capture all of the variation.

Figure 6-6 shows the shoreline positions as a function of time. Figure 6-6 (A) is the actual shoreline position, and Figure 6-6 (B) is the change in position from an initial straight shoreline. Both plots show recession of the shoreline north of the harbor. Closer to the north breakwater, the shorelines do not show development of a fillet. Since little shoreline change occurs, the fillet growth must approximately balance with the shoreline recession, offshore losses, and by-passing. South of the harbor, the dominant response is major shoreline retreat from 1942 to the mid-1950s. In 1957, by-passing and nourishments began and the shoreline immediately shows a decrease in erosion rate.

Figure 6-7 shows the historical shoreline response without breakwaters. The planform approaches an equilibrium shape that is somewhat similar to the 1934 pre-harbor shoreline. The delta shape in the shoreline is located at the south breakwater rather than near the San Luis Rey groin. The waves were developed and calibrated for conditions with the harbor present. If the harbor had not been present, the V-shape in the local wave angle may have terminated near the San Luis Rey groin rather than the south breakwater. The resulting shoreline evolution for this case is shown in Figure 6-8. The final shoreline result is quite similar to the 1934 planform.

Forecast Results

The initial shoreline in the forecast runs is the measured 1998 shoreline. However, the 1998 shoreline position is referenced to the 1934 shoreline, which is the coordinate

system used for the wave calibrations. The run duration is 60 years to estimate the damage costs for 50 years from 2008 to 2058. Input for the forecast runs is very similar to input for the historical runs. It is assumed that the processes that occurred in the recent past will continue to occur into the future. Historic dredging and nourishments are assumed to continue at the same magnitudes and time intervals.

Figure 6-9 shows the predicted 2058 shoreline position. The 1998 shoreline is shown for reference. The fillet to the north of the harbor continues to grow. The volume of sediment in the fillet corresponds to 60 years of accumulation at a rate of 30,600 m^3/yr (40,000 yd^3/yr). South of the harbor, significant shoreline recession exists between Buena Vista Lagoon and the Oceanside Pier. The shoreline retreats back to the seawall and significant overtopping events occur. Figure 6-9 shows that if the natural processes such as the LST rate and human influences such as by-passing and nourishment continue to occur in the future as they have in the recent past, erosion will continue and the shoreline will retreat back to the seawall. This will result in a dramatic increase in the number of overtopping events and damage potential. Figure 6-10 shows the shoreline planform evolution in 10-yr intervals. Minor shoreline changes occur north of the harbor. However, the shoreline south of the harbor retreats back to the seawall.

To estimate the influence of the breakwaters, simulations without breakwaters are done for two cases: 1) Assuming the breakwaters were removed in 1998 and the 1998 shoreline was taken as the initial shoreline, and 2) Assuming the breakwaters were never constructed and the 1934 shoreline was taken as the initial shoreline. Figure 6-11 shows the shoreline position in 2058 if the breakwaters were removed in 1998. For reference, the measured 1934 and 1998 shorelines are also shown. The 2058 shoreline

configuration is somewhat similar to the 1934 shoreline. The evolution of the shoreline for this case is shown in Figure 6-12. Figures 6-13 and 6-14 show the same results if the breakwaters never existed.

Damage Comparisons

The economic analyses for damage costs are based on the largest overtopping event that occurs each month. It is possible that many months will not have any overtopping events. The DNR model actually determines the overtopping events every hour. These are then sorted to select the largest event each month.

The number of overtopping events is determined for the forecast simulations with and without the breakwaters in place. The without-breakwaters simulations are done for two cases: 1) Assuming the breakwaters are removed in 1998 using the 1998 shoreline as the initial shoreline and 2) Assuming the breakwaters were never constructed with the 1934 shoreline as the initial shoreline. With breakwaters, 39,272 hourly overtopping events and 4,168 monthly events occur. For the same simulation conditions with the breakwaters removed in 1998, 11,345 hourly events and 1,789 monthly events occur. For the case where breakwaters were never installed, 1,298 hourly events and 305 monthly events occur. For the case with breakwaters there are approximately 30 times as many hourly events and 14 times as many monthly events compared to the case where breakwaters were never installed. This is a significant difference and indicates the potential magnitude of the harbor on future shoreline stability and the need for increased nourishment.

Figure 6-15 shows the number of monthly overtopping events for each cell with and without breakwaters. These results are for wave case 38, which has a net longshore transport rate approximately equal to the rate for all 50 wave cases. Many more

overtopping events occur with the breakwaters, and they occur from cells 30 to 60. For the case where no breakwaters were installed, the damage was distributed from cells 40 to 47.

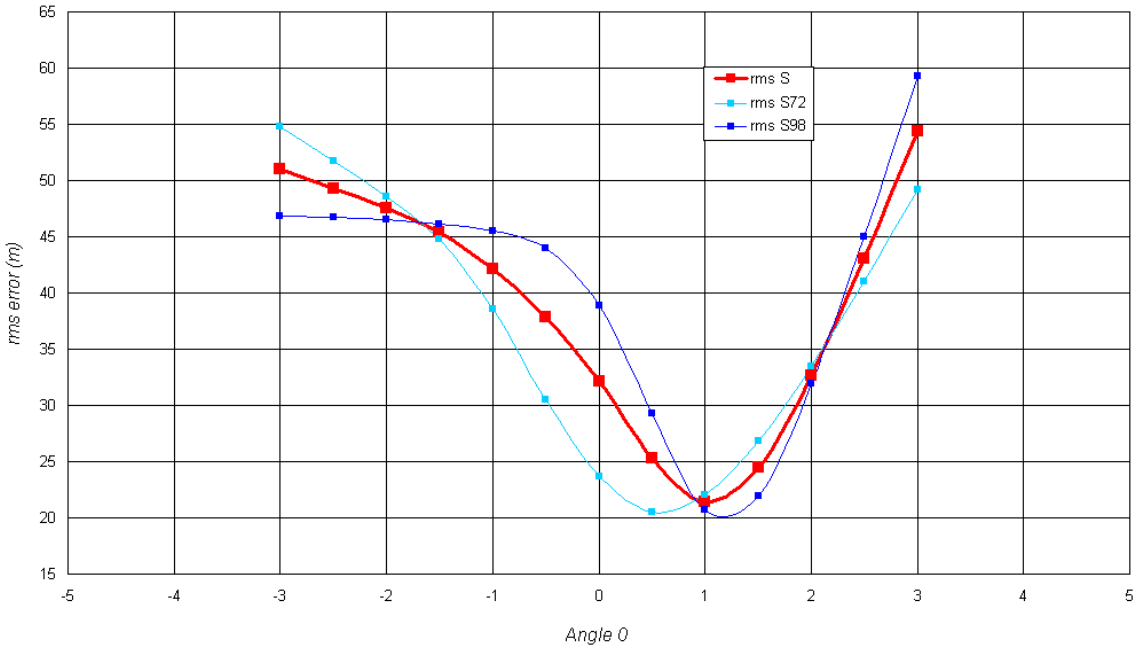

Figure 6-1. RMS error between the predicted and the measured shorelines south of the harbor in 1972, 1998, and for both combined based on the V-shaped wave angle variation as a function of the local wave angle at Agua Hedionda Lagoon.

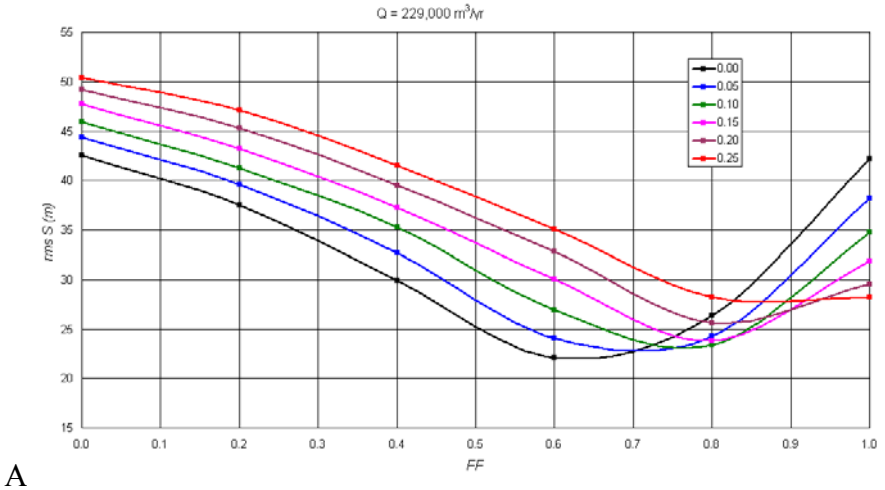

A

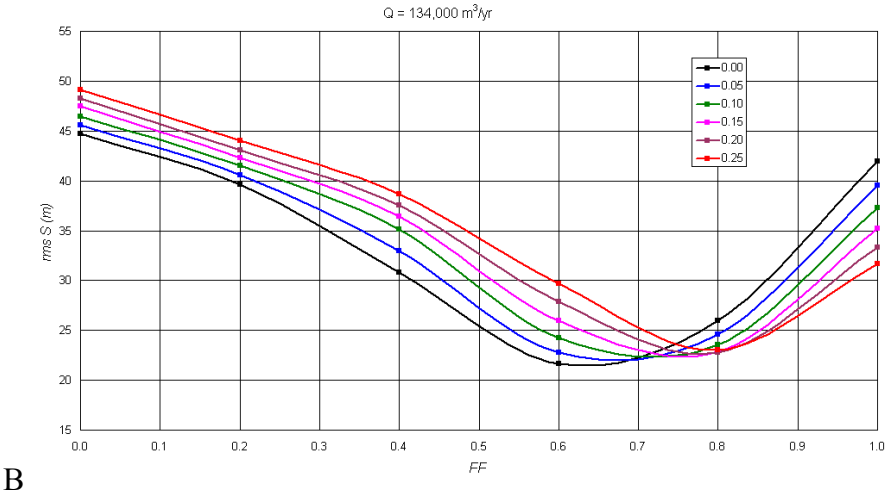

B

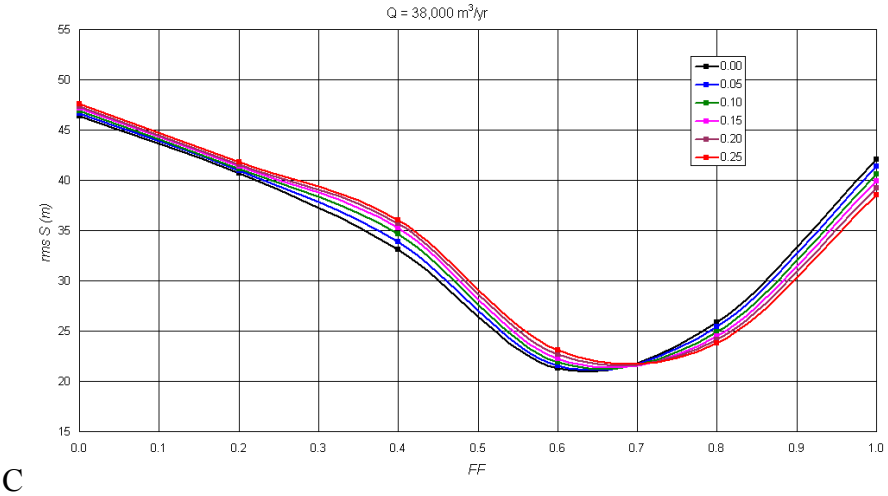

C

Figure 6-2. RMS errors for different fill factors and different values of offshore loss coefficients, c. A) Transport, $Q = 229{,}000$ m^3/yr. B) Transport, $Q = 134{,}000$ m^3/yr. C) Transport $Q = 38{,}000$ m^3/yr.

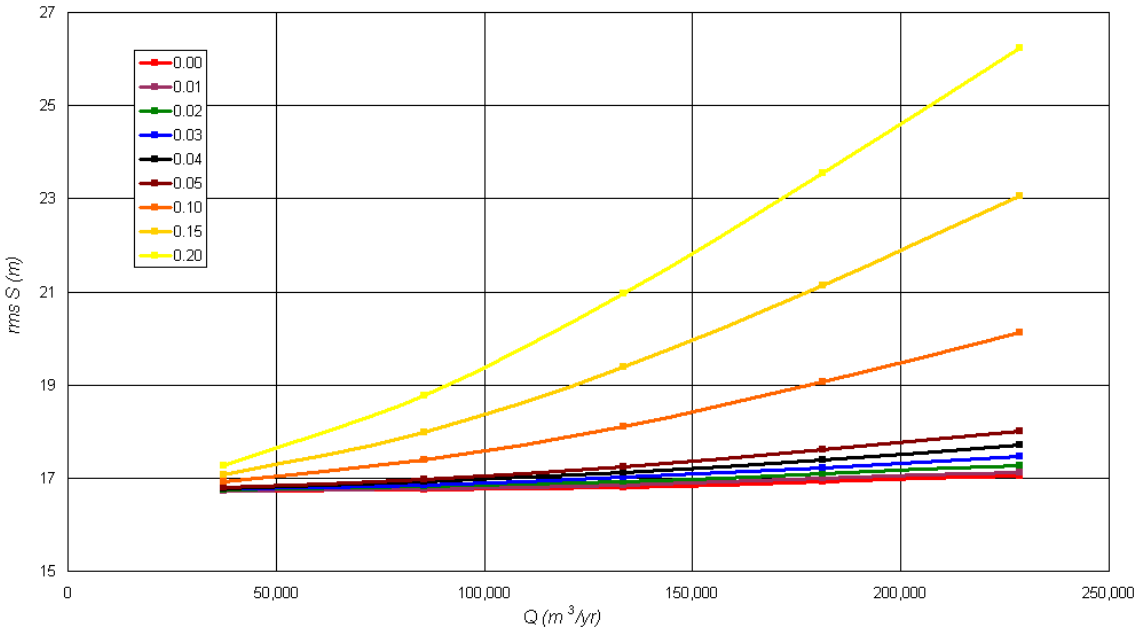

Figure 6-3. The RMS error as a function of LST rates for various offshore loss coefficients.

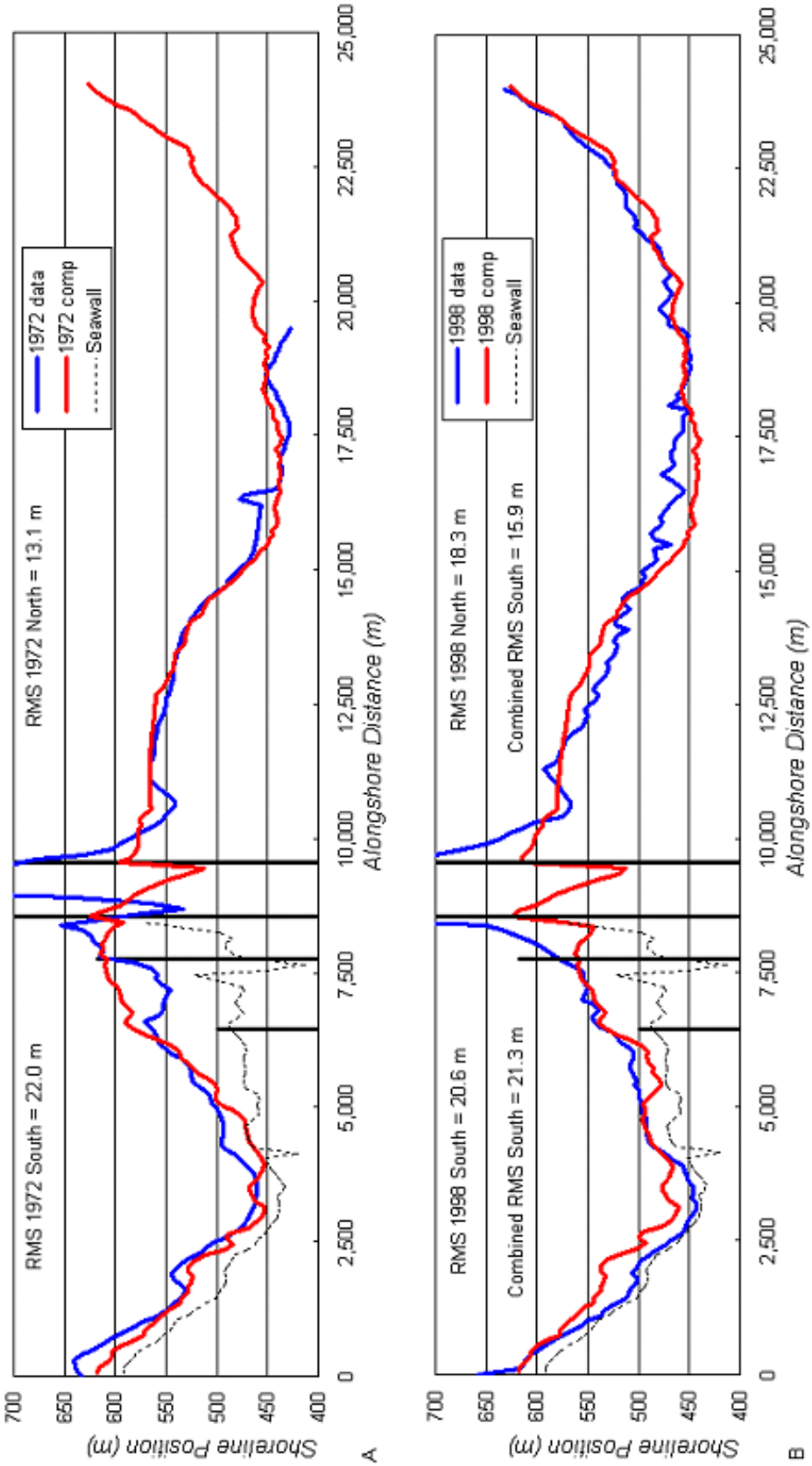

Figure 6-4. Shoreline planform results referenced to the actual 1934 initial shoreline. A) 1972. B) 1998.

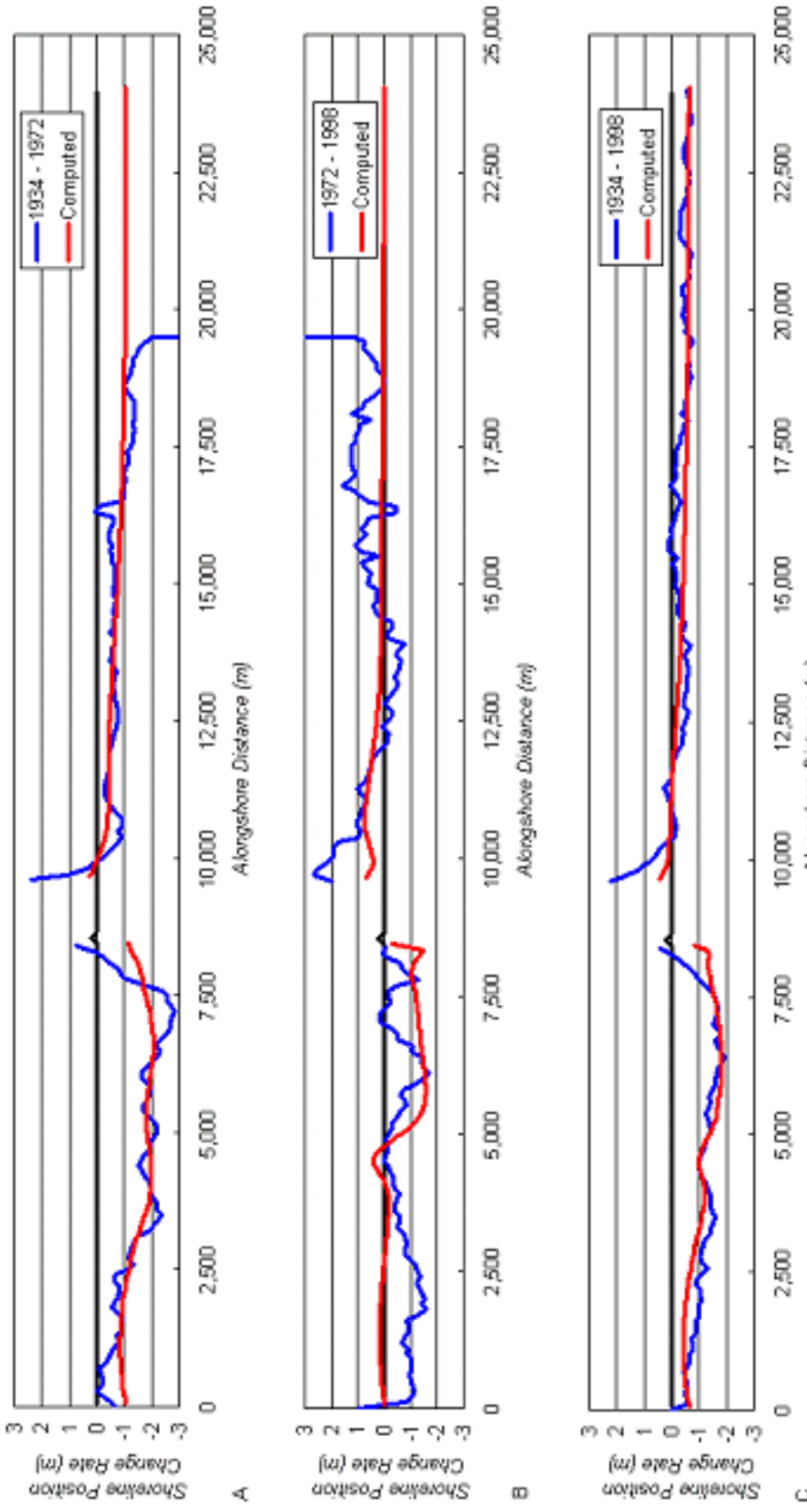

Figure 6-5. Annual shoreline change rates. A) 1934 to 1972. B) 1972 to 1998. C) 1934 to 1998.

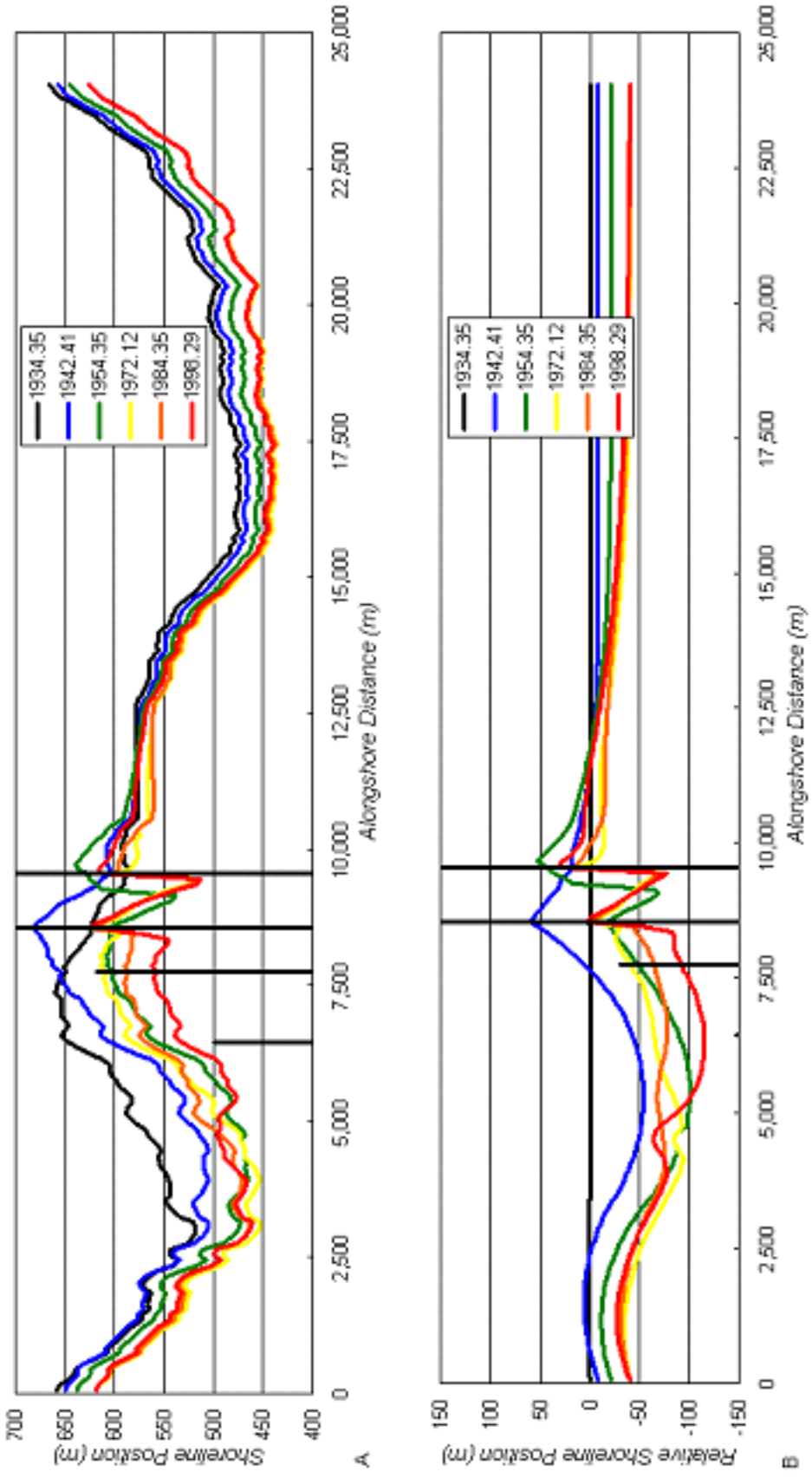

Figure 6-6. Historical shoreline evolution. A) Referenced to actual shoreline positions. B) Change from a straight initial shoreline.

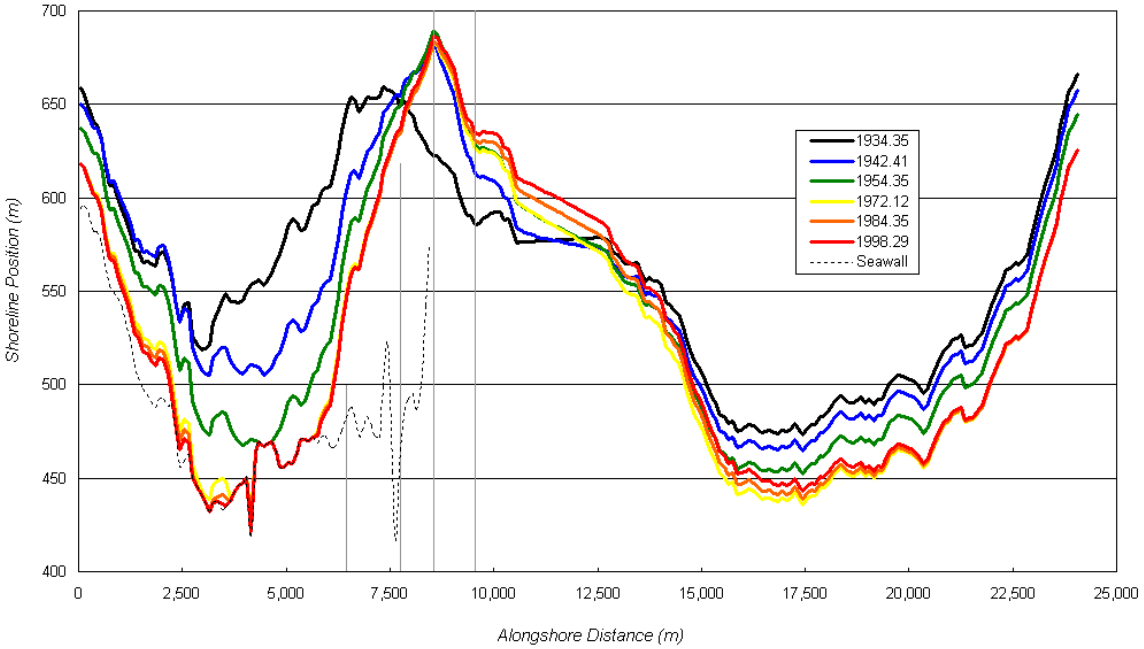

Figure 6-7. Historical shoreline planform evolution without breakwaters for waves developed with the harbor presence.

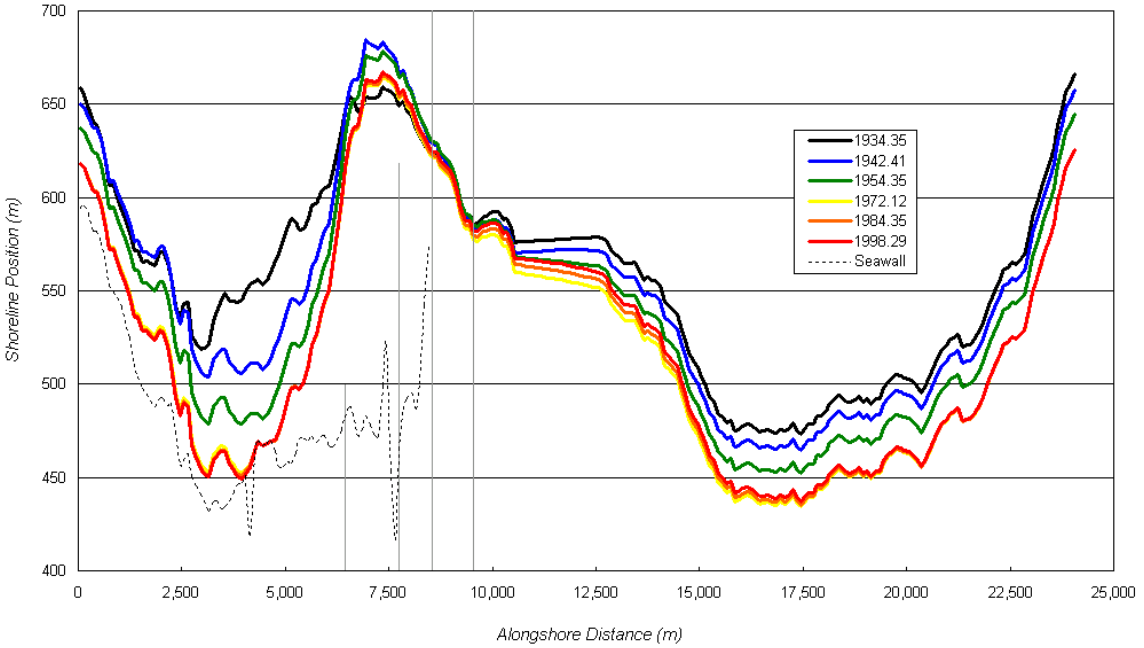

Figure 6-8. Historical shoreline planform evolution without breakwaters for wave angles adjusted to remove harbor effects.

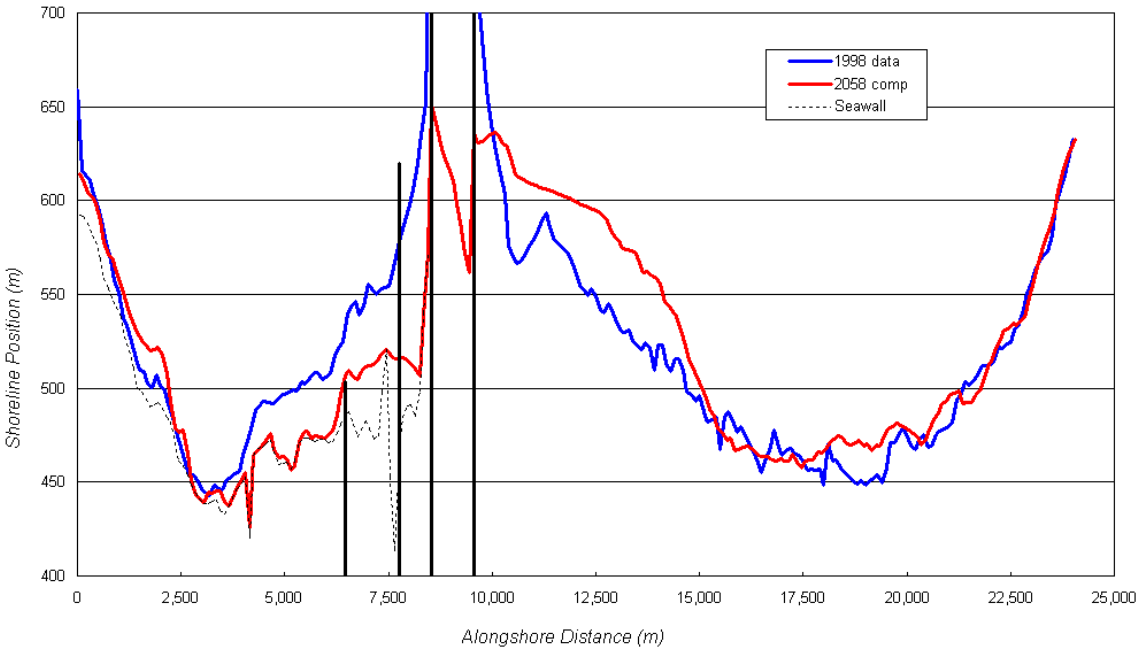

Figure 6-9. Forecast final shoreline position with breakwaters.

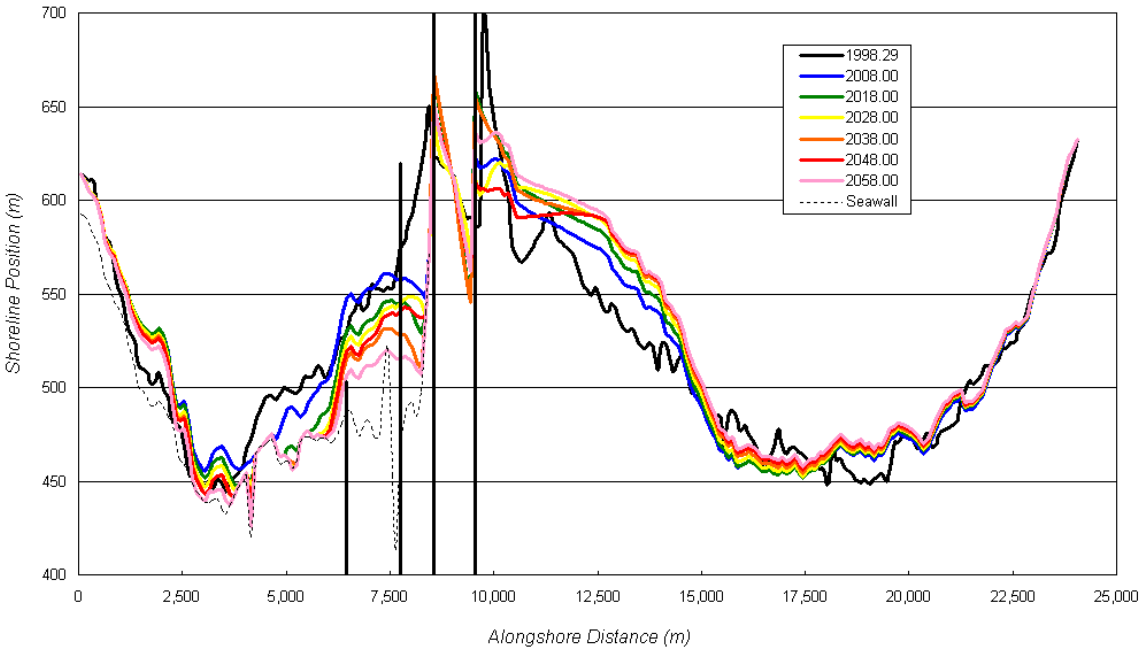

Figure 6-10. Forecast shoreline evolution with breakwaters.

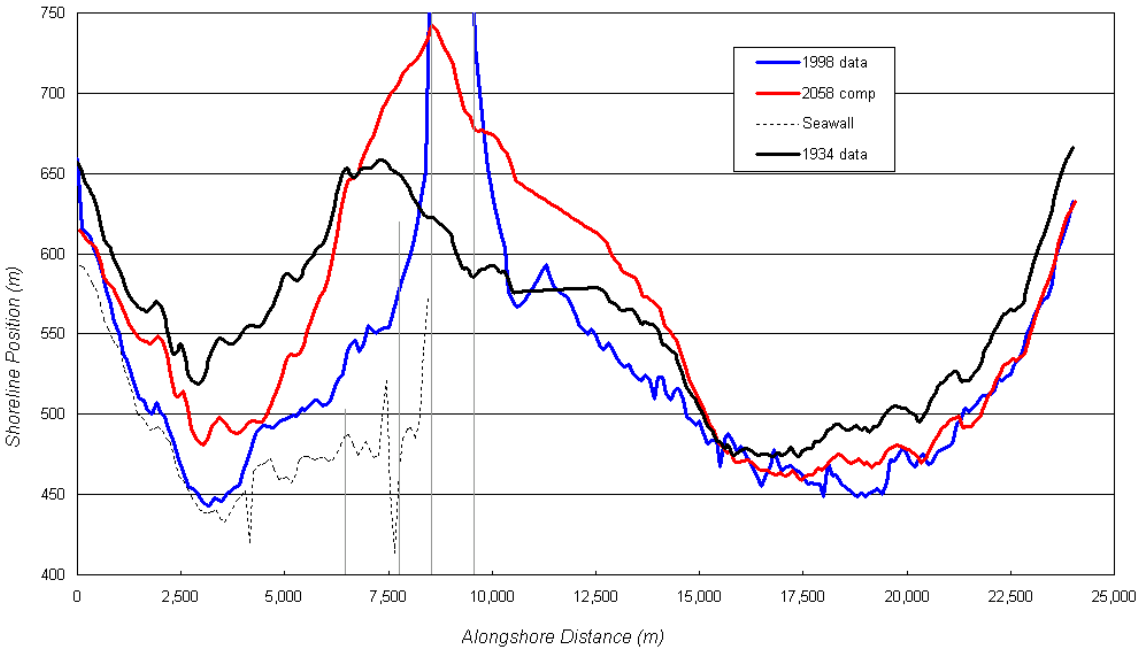

Figure 6-11. Forecast final shoreline position if breakwaters were removed in 1998.

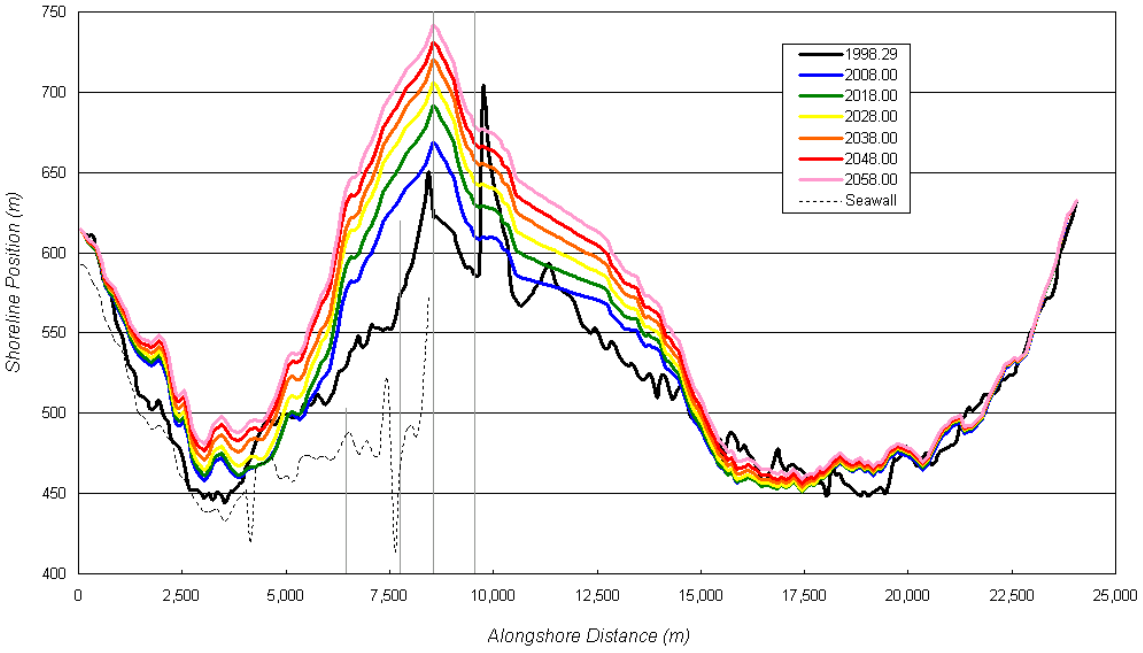

Figure 6-12. Forecast shoreline evolution if breakwaters were removed in 1998.

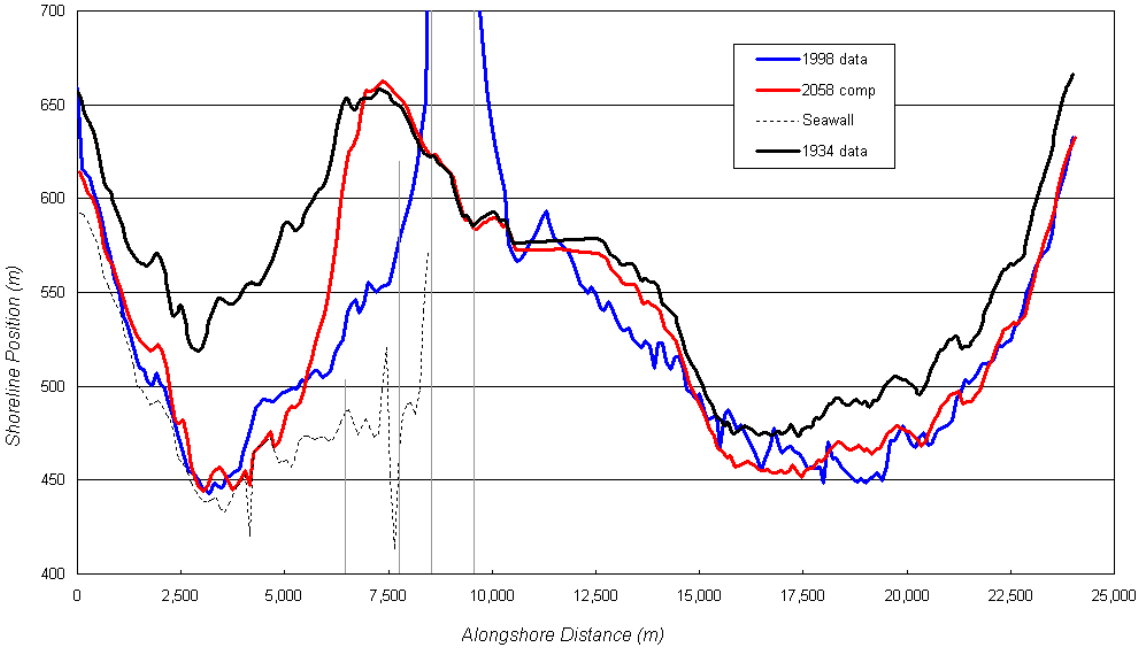

Figure 6-13. Forecast final shoreline position if breakwaters never existed.

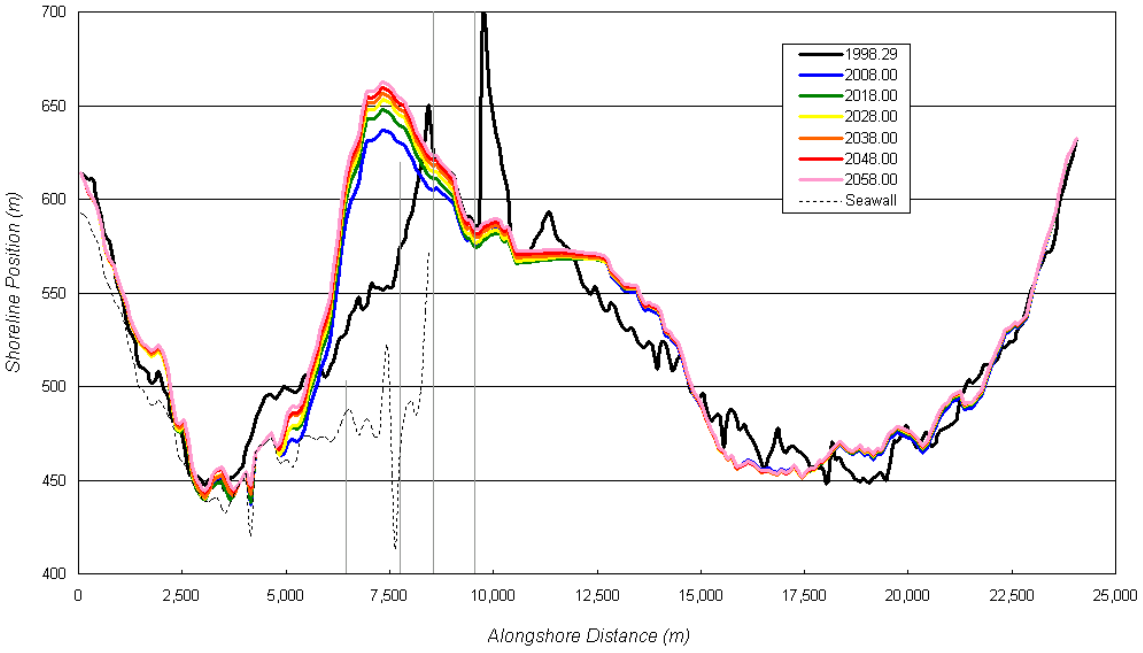

Figure 6-14. Forecast shoreline evolution if breakwaters never existed.

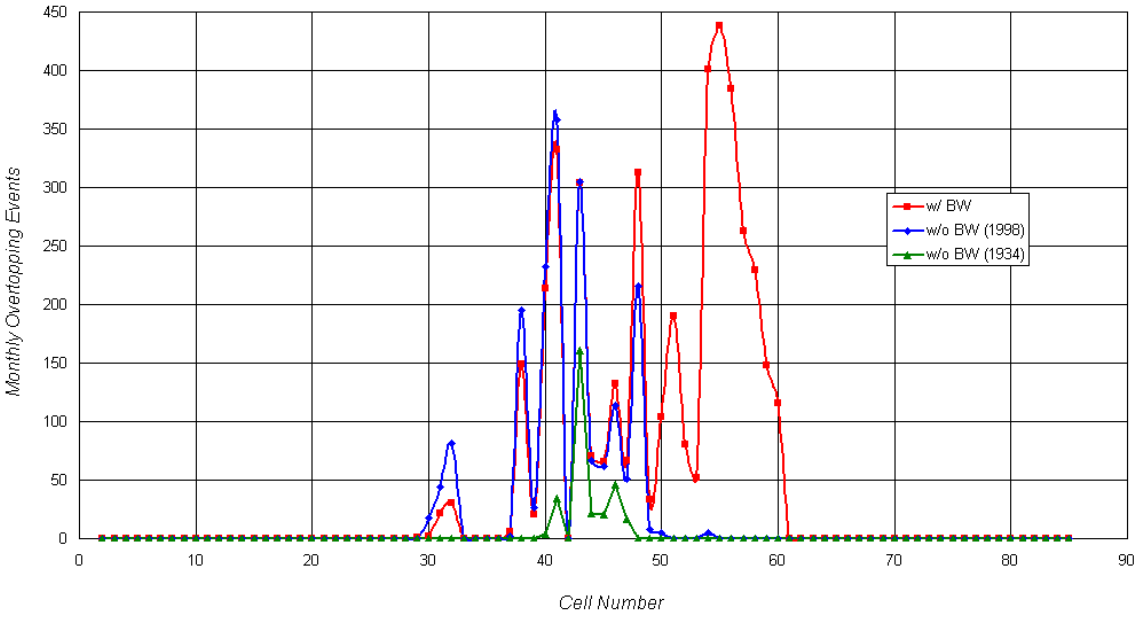

Figure 6-15. Forecast monthly overtopping events with breakwaters, removing breakwaters in 1998, and if breakwaters never existed.

CHAPTER 7
CONCLUSIONS

Our objective was to estimate the shoreline impacts attributable to Oceanside Harbor. To accomplish this, the shoreline characteristics within the project area were defined. Since the Oceanside and Carlsbad coastlines are almost entirely armored by seawalls, a seawall algorithm was added to the DNR model and then calibrated. Run-up, bore propagation, and force calculations were also added to the DNR model. Simulations were made for the time period from 1934 to 1998 to calibrate the model. Then two 60-year forecast cases were examined to estimate the future impacts of the harbor: 1) With breakwaters, and 2) Without breakwaters.

To model the shoreline, it was necessary to correctly specify the variables that define the project area. Most of the coastline characteristics (including the historical shoreline positions, beach nourishments, by-passing/dredging rates, river sediment contributions, and structures) have been studied and documented. For these, the published results defined the input. Other input parameters needed to be simulated, including the background erosion rates and local wave angles. The wave input file included derived values for the wave heights based on historical buoy data and simulated values for the wave direction. These simulated wave angle values were necessary to correctly define the local incoming wave angles. Finally, several parameters were the result of calibration and sensitive analyses, including the offshore loss coefficient and the nourishment fill factor.

A seawall algorithm for the DNR model was developed and examples were presented to verify the model. To incorporate the seawall routine into the DNR model, which normally tracks the shoreline position, adjustments were made that allowed the model to track the change in sediment volume along a seawall. The algorithm then calculates the shoreline position from the change in volume assuming an equilibrium profile and the incorporated reduced transport seaward of the seawall. The verification of the seawall algorithm provides insight on how the routine interacts with the nourishment and groin subroutines.

Once the characteristic site input data were gathered and the DNR model modified to accommodate seawalls and calculate the run-up, bore propagation, and forces; the impact of the harbor breakwaters was examined. Two forecast simulations were made that spanned 60 years into the future. One included the breakwaters, by-passing, and nourishments and the other one did not. Results for the with-breakwater condition show that if the current natural processes and human practices continue into the future, the shoreline will erode back to the seawall causing progressively more overtopping and damage events along the Oceanside coastline. Results for the without-breakwater conditions shows the shoreline equilibrating to a final shoreline position that is similar to the shape of the 1934 measured shoreline.

LIST OF REFERENCES

Boswell, M.K. (2004), "***Closure Depth and Beach Profiles for Southern California Beaches***", University of Florida Master of Science Report, Department of Civil and Coastal Engineering, 41 pp.

Brownlie, W.R., and B.D. Taylor (1981), "***Sediment Management of Southern California Mountains, Coastal Plains, and Shorelines – Part C, Coastal Sediment Delivery by Major Rivers in Southern California***", California Institute of Technology, Environmental Quality Laboratory Report No. 17 – C, Pasadena, California, 314 pp.

CIRIA/CUR (1991), "***Manual on the Use of Rock in Coastal Shoreline Engineering***", CIRIA Special Publication 83/CUR Report 154, A.A. Balkema Publishers, pp. 246-252.

Coastal Frontiers Corporation (2003), "***SANDAG 2002 Regional Beach Monitoring Program – Annual Report***", Chatsworth, CA, 105 pp. + app.

Cox, J.C, and J. Machemehl (1986), "***Overload Bore Propagation Due to an Overtopping Wave***", Journal of Waterway, Port, Coastal, and Ocean Engineering, Volume 112, No. 1.

Dean, R.G. (2001), "***Beach Nourishment: Theory and Practice***" Advance Series on Ocean Engineering, World Scientific Publishing Co, Singapore.

Dean, R.G., and R.A. Dalrymple (2002), "***Coastal Processes with Engineering Applications***," Cambridge University Press, Cambridge, 475 pp.

Dean, R.G., and J. Grant (1989), "***Development of Methodology for Thirty-Year Shoreline Projections in the Vicinity of Beach Nourishment Projects***", University of Florida Master of Science Thesis, Department of Coastal and Oceanographic Engineering Department, Gainesville, FL, 153 pp.

Hales, L.Z. (1978), "***Coastal Processes Study of the Oceanside, California Littoral Cell, Final Report***", U.S. Army Corp of Engineers, Waterways Experiment Station, Misc. Paper H-78–8, Vicksburg, MS, 464 pp.

Inman, D.L., and S.A. Jenkins (1983), "***Oceanographic Report for Oceanside Beach Facilities***", prepared for the city of Oceanside, 206 pp.

Marine Advisors (1960), "***Design Waves for Proposed Small Craft Harbor at Oceanside, California***" prepared for the U.S. Army Corp of Engineers, Los Angeles District, La Jolla, CA.

Ramsden, J.D., and F. Raichlen (1990), "***Forces on Vertical Wall Caused by Incident Bores***", Journal of Waterway, Port, Coastal, and Ocean Engineering, Volume 116, No. 5.

Ruggerio, P. and W.G. McDougal (2001), "***An Analytic Model for the Prediction of Wave Setup, Longshore Currents and Sediment Transport on Beaches with Seawalls***", Coastal Engineering: An International Journal for Coastal, Harbour and Ocean Engineers, Volume 43, pp. 161-182.

Shoreline Protection Manual (1984), 4th Edition, Volumes I and II, U.S. Army Corp of Engineers, Waterway Experiment Station, Government Printing Office, Washington, DC.

Simons, Li and Associates (1985), "***Analysis of the Impact of Dams on Delivery of Sediment From the Santa Margarita River, California***". U.S. Bureau of Reclamation, Lower Colorado Region, Boulder City, Nevada.

Simons, Li and Associates (1988), "***River Sediment Discharge Study, San Diego Region***", U.S. Army Corps of Engineers, Los Angeles District, Coast of California Storm and Tidal Waves Study (CCSTWS) Report No. 88-3, 4 Volumes.

Tekmarine, Inc. (1987), "***Oceanside Littoral Cell, Preliminary Sediment Budget Report***", U.S. Army Corp of Engineers, Los Angeles District, Coast of California Storm and Tidal Waves Study (CCSTWS) Report No. 87-4, 36 pp. + Appendices.

U.S. Army Corps of Engineers (USACE), Los Angeles District (1984), "***Geomorphology Framework Report, Dana Point to the Mexican Border***", Coast of California Storm and Tidal Wave Study (CCSTWS) Report No. 84-4, 75+ pp.

U.S. Army Corps of Engineers (USACE), Los Angeles District (1991a), "***State of the Coast Report, San Diego Region: Chapter 6, Sources, Transport Modes, and Sinks of Sediments***", Coast of California Storm and Tidal Wave Study (CCSTWS) Volume 1 – Main Report.

U.S. Army Corps of Engineers (USACE), Los Angeles District (1991b), "***State of the Coast Report, San Diego Region: Chapter 7, Application of Beach Change Models***", Coast of California Storm and Tidal Wave Study (CCSTWS) Volume 1 – Main Report.

U.S. Army Corps of Engineers (USACE), Los Angeles District (1994a), "***Oceanside Shoreline, Oceanside, San Diego County California: Chapter 2.0 The Study Area***", Reconnaissance Report, Main Report.

U.S. Army Corps of Engineers (USACE), Los Angeles District (1994b), "***Oceanside Shoreline, Oceanside, San Diego County California: Coastal Engineering Appendix***," Reconnaissance Report, Economic Appendix, Environmental Evaluation, Real Estate Appendix.

BIOGRAPHICAL SKETCH

Gabriel Alejandro Perdomo graduated from Dr. Phillips High School, in Orlando, in May 1996. He was accepted to the University of Florida (UF) and began his undergraduate studies in Civil Engineering in August 1996. During his undergraduate studies, Gabriel Perdomo worked under the supervision of Dr. Kurt Gurley, studying the effects of hurricane-force winds on structures. In May 2001, he graduated with a Bachelor of Science degree in civil engineering, with an emphasis on structural engineering. In August 2001, Gabriel Perdomo began graduate studies at UF in structural engineering, but changed his degree program in January 2002 to coastal engineering. In July 2002, he began work on a project (with William G. McDougal and Robert G. Dean) that focused on modeling the Oceanside, CA coastline to determine the effects of Oceanside Harbor on the beaches downcoast. On completing the project, Gabriel Perdomo graduated from the coastal engineering program at UF with a Master of Science degree in May 2004.